JOURNAL OF BIOMOLECULAR STRUCTURE AND DYNAMICS
https://doi.org/10.1080/07391102.2020.1835725

Exploring nature's bounty: identification of *Withania somnifera* as a promising source of therapeutic agents against COVID-19 by virtual screening and *in silico* evaluation

Aditi Srivastava[a], Sahabjada Siddiqui[b], Rumana Ahmad[a], Sudhir Mehrotra[c], Bilal Ahmad[d] and A. N. Srivastava[e]

[a]Department of Biochemistry, Era's Lucknow Medical College and Hospital, Era University, Lucknow, UP, India; [b]Department of Biotechnology, Era's Lucknow Medical College and Hospital, Era University, Lucknow, UP, India; [c]Department of Biochemistry, University of Lucknow, Lucknow, UP, India; [d]Research Cell, Era's Lucknow Medical College and Hospital, Era University, Lucknow, UP, India; [e]Department of Pathology, Era's Lucknow Medical College and Hospital, Era University, Lucknow, UP, India

Communicated by Ramaswamy H. Sarma

ABSTRACT

Coronaviruses are etiological agents of extreme human and animal infection resulting in abnormalities primarily in the respiratory tract. Presently, there is no defined COVID-19 intervention and clinical trials of prospective therapeutic agents are still in the nascent stage. *Withania somnifera* (L.) Dunal (WS), is an important medicinal plant in Ayurveda. The present study aimed to evaluate the antiviral potential of selected WS phytoconstituents against the novel SARS-CoV-2 target proteins and human ACE2 receptor using *in silico* methods. Most of the phytoconstituents displayed good absorption and transport kinetics and were also found to display no associated mutagenic or adverse effect(s). Molecular docking analyses revealed that most of the WS phytoconstituents exhibited potent binding to human ACE2 receptor, SAR-CoV and SARS-CoV-2 spike glycoproteins as well as the two main SARS-CoV-2 proteases. Most of the phytoconstituents were predicted to undergo Phase-I metabolism prior to excretion. All phytoconstituents had favorable bioactivity scores with respect to various receptor proteins and target enzymes. SAR analysis revealed that the number of oxygen atoms in the withanolide backbone and structural rearrangements were crucial for effective binding. Molecular simulation analyses of SARS-CoV-2 spike protein and papain-like protease with Withanolides A and B, respectively, displayed a stability profile at 300 K and constant RMSDs of protein side chains and Cα atoms throughout the simulation run time. In a nutshell, WS phytoconstituents warrant further investigations *in vitro* and *in vivo* to unravel their molecular mechanism(s) and modes of action for their future development as novel antiviral agents against COVID-19.

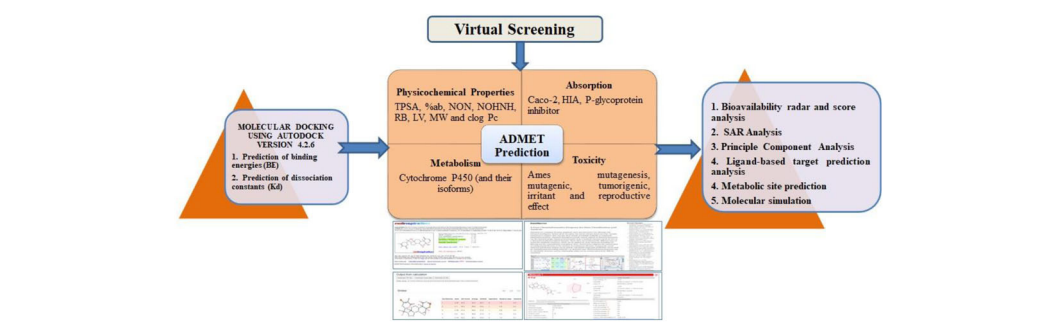

ARTICLE HISTORY
Received 19 June 2020
Accepted 2 October 2020

KEYWORDS
Withanolides; phytomedicine; SARS-CoV-2 target proteins; molecular docking; molecular chemoinformatics

1. Introduction

As per the World Health Organization (WHO), viral diseases are on the rise posing serious public health concerns. Over the last twenty years, numerous viral epidemics such as the Severe Acute Respiratory Syndrome (SARS) in 2002–2003, H1N1 influenza in 2009 and Middle East Respiratory Syndrome (MERS) in 2012 have been reported. Wuhan, the sprawling capital of Central China's Hubei province very recently witnessed 'pneumonia of unknown etiology' that

CONTACT Rumana Ahmad rumana_ahmad@yahoo.co.in; rahmad@erauniversity.in Department of Biochemistry, Era's Lucknow Medical College and Hospital, Era University, Sarfarazganj, Hardoi Road, Lucknow, UP 226003, India

Supplemental data for this article can be accessed online at https://doi.org/10.1080/07391102.2020.1835725

was first reported to the WHO Country Office in China on December 31, 2019. The causal agent coronavirus belonging to the family coronaviridae are enveloped viruses which are divided into four genera (α, β, γ, and δ). The SARS-CoV-2 virus (formerly designated as COVID-19) belonging to the class of β-coronaviruses is supposed to have evolved from bats and thereafter, spread like wildfire worldwide. A total of 43,825,003 confirmed cases of COVID-19 and 1,165,289 deaths have been registered round the globe, whereas in India the confirmed cases has reached to 7,946,429 with 119,535 deaths as of October 27, 2020 (https://www.worldometers.info/coronavirus/country/india/).

Coronaviruses are a large family of single stranded RNA (ssRNA) viruses ranging from 60 to 140 nm in diameter. Under the electron microscope, they appear to possess spike like projections present on the surface giving it a crown like appearance, hence named 'coronaviruses' (Richman et al., 2016). SARS-CoV-2 virus spreads faster than its two predecessors (SARS-CoV and MERS-CoV), but has a lower fatality rate though it is highly contagious. Coronavirus possesses four main structural proteins : Spike (S) protein, membrane (M) protein, envelope (E) protein and nucleocapsid (N) protein (Bosch et al., 2003). Published literature has tracked the onset of symptoms which include a pandemic of cases with pneumonia, unexplained lower respiratory tract infections and multi-organ dysfunction. On the other hand, many reported cases are asymptomatic. SARS-CoV-2 has become one of the major disease pathogens in emerging outbreaks.

Intense co-operative worldwide efforts and aggressive isolation measures have more or less led to a progressive decline in the number of incidents. The political and health authorities are making an extraordinary effort to halt the shock wave which is seriously challenging the health system globally. Currently, therapeutic options are limited and preventive attempts to minimize social transmission are our best defence weapons. Researchers are working diligently to find novel and/or repurposed therapeutic options to prevent and treat this global pandemic. In this process, they have laid down three strategies , the first includes testing of existing broad-spectrum antiviral drugs (Chan et al., 2013), the second strategy is to use molecular dynamics tools to screen for natural molecules effective as therapeutic and preventive drugs (de Wilde et al., 2014; Dyalla et al., 2014), and third strategy includes the direct utilization of genomic information and pathological symptoms of different mutated coronaviruses to develop new targeted drugs from scratch (Zumla et al., 2016).

Till date, research has identified more than 30 therapeutic agents, including natural products, allopathic drugs and traditional Chinese medicines which could potentially be effective against COVID-19. For initial treatment of COVID-19, the People's Republic of China National Health Commission (NHC) has included antiviral agents including interferon α (IFN-α), lopinavir/ritonavir, chloroquine phosphate, ribavirin and arbidol in the revised edition of the guidelines for the prevention, diagnosis and treatment of novel coronavirus-induced pneumonia. Combinations of protease inhibitor(s) lopinavir/ritonavir for the treatment of COVID-19 infected patients have been evaluated which have been used previously to treat HIV patients (Liu et al., 2020). In several animal models, including non-human primates (Fouchier et al., 2003; Kuiken et al., 2003; McAuliffe et al., 2004; Rowe et al., 2004), ferrets (Martina et al., 2003), mice (Glass et al., 2004; Hogan et al., 2004) and Syrians hamsters (Roberts et al., 2005), experimental infections with SARS-CoV have been found to cause severe respiratory tract infections.

Several antiviral therapies have been identified for human pathogenic CoVs including synthetic inhibitors of neuraminidase, nucleoside analogs, remdesivir, tenofovir disoproxil (TDF), umifenovir (arbidol) and lamivudine (3TC) (Li et al., 2005). Studies involving identification of cellular receptors that facilitate the binding and entry of human associated coronaviruses have been done. Angiotensin I-converting enzyme 2 (ACE2) is a membrane bound aminopeptidase expressed in renal, cardiovascular, vascular and testicular tissue, as well as the small intestine (Donoghue et al., 2000; Hamming et al., 2004; Harmer et al., 2002). It has been shown to be a co-receptor for viral entry of SARS-CoV-2 with increasing evidence that it has a significant role in SARS-CoV-2 pathogenesis. Therefore, targeting the human ACE2 receptor might block the entry and the subsequent pathophysiology of the virus and is one of the premises of the present study (Zhou et al., 2020). SARS-CoV-2 entry into host cells is mediated by transmembrane spike(S) like glycoprotein that causes neutralization of antibodies, facilitates the projection of homotrimers from the viral surface, binds to human ACE2 receptor, and finally mediates membrane fusion and transport (Tortorici & Veesler, 2019). Spike (S) protein initially cleaves itself into two functional subunits (S_1 and S_2) which remain non-covalently bound to each other in a prefusion conformation. The S_1 subunit is responsible for binding to ACE2, whereas S_2 subunit has role in viral and host cell membrane fusion (Belouzard et al., 2009; Bosch et al., 2003; Burkard et al., 2014; Kirchdoerfer et al., 2016).

SARS-CoV-2 also encodes a non-structural replicase polyprotein that is processed by viral proteases *viz*. the primary viral proteinase (3CL-pro) and the papain-like protease (PL-pro). 3CL-pro (Nsp5) regulates viral replication and cleavage of Nsp4 to Nsp16 (Ziebuhr et al., 2000). This main protease is another attractive therapeutic target (Anand et al., 2003; Liu et al., 2020). PL-pro, another crucial non-structural protein, is a virally encoded cysteine protease which has a role in N-terminal processing of viral polyproteins causing release of Nsp1, Nsp2 and Nsp3 which are essential for viral replication to proceed in a correct manner (Chen et al., 2020; Harcourt et al., 2004). Recently, the structure of two critical non-structural proteins in complex Nsp10/Nsp16 has been reported. The complex is responsible for the modification of genetic material of virus in order to camouflage it with host cell DNA. This permits viral evasion and escape from the immune cells of the host, thereby perpetuating infection. Thus, targeting the Nsp10/Nsp16 complex might help in the effective combat and eradication of COVID-19 infection (https://www.anl.gov/article/new-drug-target-found-for-covid19).

In the past decade, hundreds of drugs were withdrawn from the market as a result of their failure to either exhibit

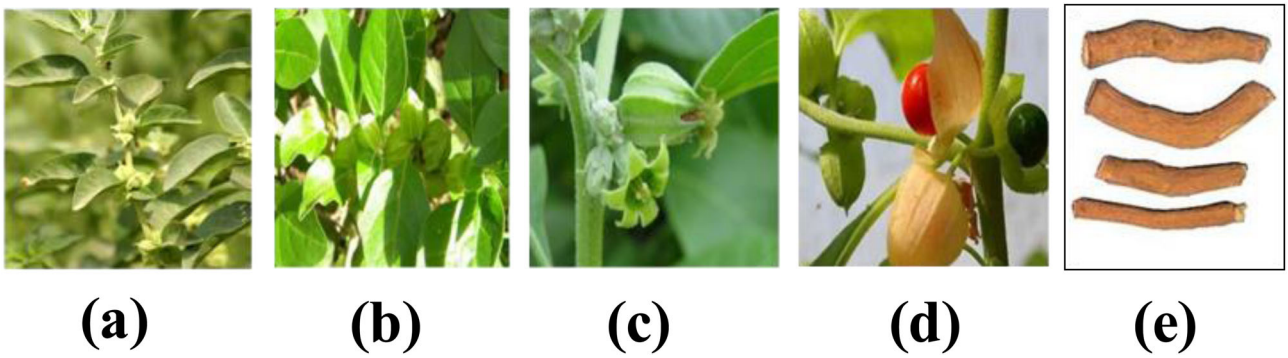

Figure 1. (a) *Withania somnifera* (L.) Dunal Habit (b) Leaves (c) Flower (d) Fruit (e) Stem (Image courtesy naturesalive.wordpress.com, www.nmpb.nic.in, www.flowersofindia.net, Jain et al. (2012), https://stock.adobe.com/in/search?k=ashwagandha).

the desired biological activity or due to their unexpected toxicity and adverse side effects in clinical trials. These poor outcomes may be attributed due to lack of a planned and systematic approach to rational drug design and discovery leading to losses that place a heavy burden on the poor economic sections of the society in particular and the third world countries in general. In the post genomic era, *in silico* prediction of chemical leads has a significant role in drug discovery, which has proven to be more time and cost effective (Xu et al., 2012). Clinical studies of various drug like properties are very time consuming and expensive. Therefore, computational techniques come is as helpful and handy before going for the expensive *in vitro*, *in vivo* studies and clinical trials. Computational techniques can filter and predict the druglikeness, absorption, distribution, metabolism, excretion, and toxicity (ADMET) criteria of a prospective drug candidate (Cheng et al., 2012). In this context, Ayurveda, the Indian traditional system of medicine encompassing a plethora of medicinal plants and their phytoconstituents(s) with proven diverse pharmacological activities, has remained largely unexplored. Thus, Ayurveda offers a staggering array of natural products and prospective therapeutic agents for evaluation against the causal agent of the ongoing global pandemic.

Withania somnifera (WS), commonly known as 'Indian Ginseng' and 'Ashwagandha' in Hindi, belongs to family Solanaceae (Figure 1) and holds an important position in Ayurveda owing to its broad therapeutic spectrum and a plethora of pharmacological activities including anti-spasmodic, anti-arthritic, anti-inflammatory, sedative, nerve soothing, hypotensive, antioxidant, immunomodulatory, anti-stress and anti-tumor (Jain et al., 2012).

The plant comprises 29 natural secondary metabolites commonly called as 'withanolides' extracted from leaves, stems, roots, and flowers which are known for their potent anti-tumor effect (Table 1). Some previous studies have reported the anti-influenza properties of active constituents of WS against H1N1 influenza and antiviral activity of withanone from WS against novel coronavirus (Balakrishnan et al., 2014; Cai et al., 2015; Varshney et al., 2020). However, still, not much is known regarding the antiviral activity of WS phytoconstituents. Therefore, one of the main aims of the present study was to evaluate the antiviral activity of WS phytoconstituents against major target proteins of SARS-CoV-2, the causal agent of the ongoing pandemic.

Withanolides, including withanolides A, B, D, E, anaferine, withaferin A, withasomnine, withanone and viscosalactone B (Table 1) are responsible for various pharmacological activities as detailed above (Jain et al., 2012; Misra et al., 2008). They belong to chemical classes of alkaloids and steroidal lactones.

Agents that can preferentially bind to ACE2 receptor can be thought of as promising 'preventive' agents against SARS-CoV-2 infection. Alternately, agents that bind to main viral proteins can interfere and/or block crucial stages in the viral life cycle such as viral entry, replication, membrane fusion and hence, can function as promising therapeutic agents. The present paper attempts to highlight the preventive/therapeutic potential of withanolides from WS as promising antiviral agents to augment our limited armamentarium of drugs available against SARS-CoV-2 to effectively combat COVID-19.

All the standard reference drugs used in the study like losartan, procainamide, cinacalcet, arbidol, hydroxychloroquine, oberadilol and poziotinib are FDA-approved drugs that were chosen for their specific binding to proteins selected for the study *viz*. human ACE2 receptor, SARS-CoV and SARS-CoV-2 target proteins (Spike S glycoprotein, protease) as referenced in literature (Arya et al., 2020; Liu et al., 2020, Wu et al., 2020). Since there is no available literature on Nsp10/Nsp16 complex, two randomly selected reference drugs were chosen against it in binding studies.

2. Materials and methods

2.1. Selection and preparation of ligands

The present study was carried out at Molecular Chemoinformatics Section, Cell and Tissue Culture Lab, Dept. of Biochemistry, Era's Lucknow Medical College and Hospital, Era University, Lucknow. The ligands (WS phytoconstituents) selected for the study were first evaluated for their ability to obey Lipinski's rule of five (Lipinski et al., 1997) using Molinspiration server. Lipinski's rules are used to determine the drug like characteristics of a compound with properties that would make it a potential drug for humans. PubChem database was used to access the 3D structures of the WS phytoconstituents and reference drugs. Prior to docking,

Table 1. List of withanolides from *Withania somnifera*.

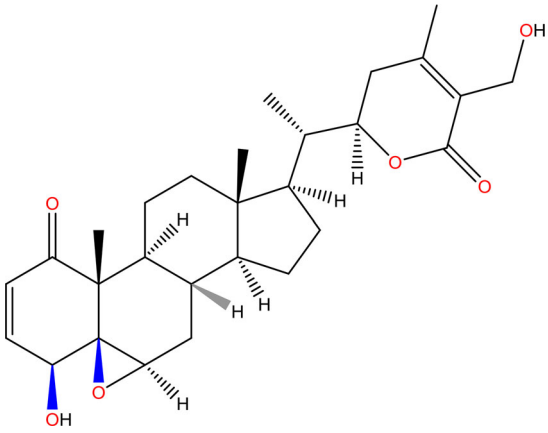

Withaferin A
PubChem CID: 265237
Molecular Formula: $C_{28}H_{38}O_6$
Chemical Class: Steroidal Lactone

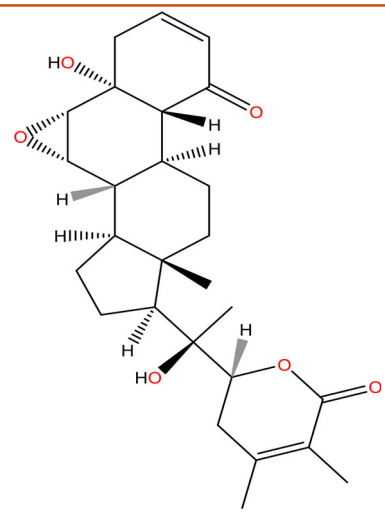

Withanolide A
PubChem CID: 11294368
Molecular Formula: $C_{28}H_{38}O_6$
Chemical Class: Steroidal Lactone

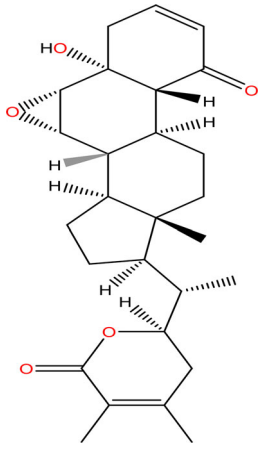

Withanolide B
PubChem CID: 14236711
Molecular Formula: $C_{28}H_{38}O_5$
Chemical Class: Steroidal Lactone

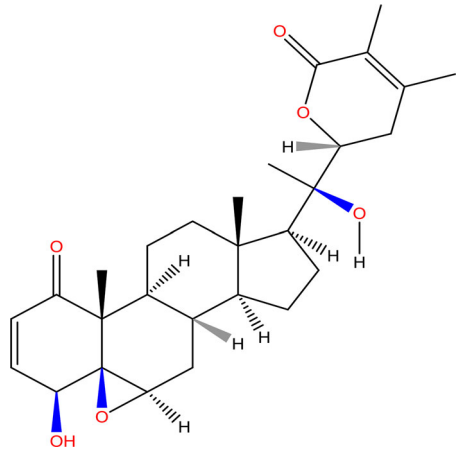

Withanolide D
PubChem CID: 161671
Molecular Formula: $C_{28}H_{38}O_6$
Chemical Class: Steroidal Lactone

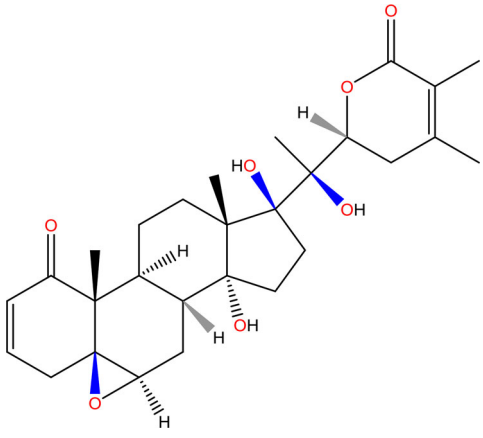

Withanolide E
PubChem CID: 301751
Molecular Formula: $C_{28}H_{38}O_7$
Chemical Class: Steroidal Lactone

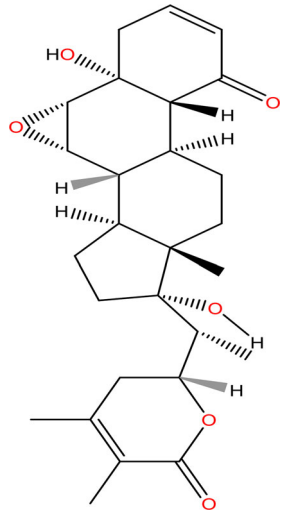

Withanone
PubChem CID: 21679027
Molecular Formula: $C_{28}H_{38}O_6$
Chemical Class: Steroidal Lactone

(*continued*)

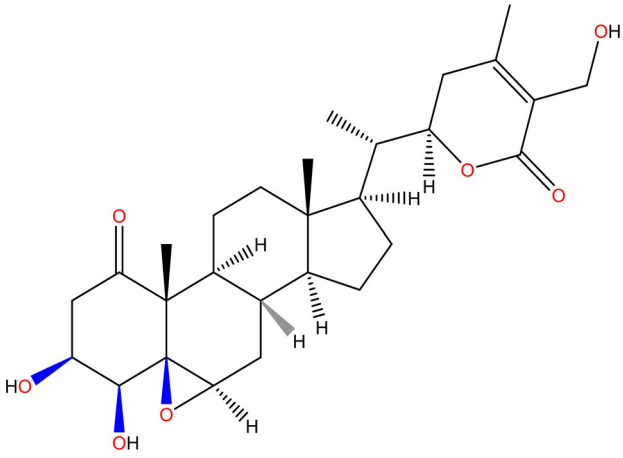

Viscosalactone B
PubChem CID: 57403080
Molecular Formula: $C_{28}H_{40}O_7$
Chemical Class: Steroidal Lactone

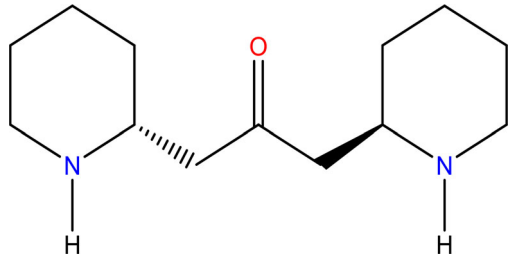

Anaferine
PubChem CID: 443143
Molecular Formula: $C_{13}H_{24}N_2O$
Chemical Class: Piperidine Alkaloid

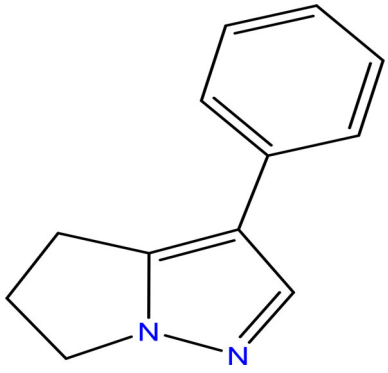

Withasomnine
PubChem CID: 442877
Molecular Formula: $C_{12}H_{12}N_2$
Chemical Class: Pyrazole Alkaloid

energy minimization of ligands was carried out using Merck Molecular Force Field (MMFF94) in order to achieve a better relaxation in the arrangement of atoms.

The PubChem IDs of the reference drugs and selected ligands were as follows: arbidol (CID-131411), losartan (CID-3961), procainamide (CID-4913), cinacalcet (CID-156419), oberadilol (CID-3047798), poziotinib (CID-25127713), hydroxychloroquine (CID-3652), anaferine (CID-443143), withanolide A (CID-11294368), withanolide B (CID-14236711), withanolide D (CID-161671), withanolide E (CID-301751), withaferin A (CID-265237), withasomnine (CID-442877), withanone (CID-21679027) and viscosalactone B (CID-57403080).

Prior to docking, the protonation states of the ligands were determined at pH 7.4 using Protoss, a fully automated hydrogen prediction online tool for protein–ligand complexes (https://proteins.plus/).

2.2. Prediction of activity spectra for substances (PASS) analysis

PASS is an online web tool hosted at http://195.178.207.233/PASS/index.html (Ahmad, 2019). Based on the structure–activity relationship with a known chemical entity, PASS analysis server predicts biological activities of chemical compounds. The tool predicts the pharmacological behavior, mechanism of action and side effects such as mutagenicity, carcinogenicity, embryotoxicity and teratogenicity. In the present study, PASS analysis was performed using OSIRIS Property Explorer version 4.5.1. (http://www.openmolecules.org/propertyexplorer/index.html)

2.2.1. Lipinski's rule of five

The druglikeness of WS phytoconstituents was also assessed using Lipinski's rule of five (Ertl et al., 2000; Lipinski et al., 1997; Veber et al., 2002). The parameters of druglikeness such as MW $\leq$500, logP $\leq$5, number of hydrogen bond donors (NOHNH) $\leq$5 and hydrogen bond acceptor sites (NON)$\leq$10, topological polar surface area (TPSA) ($\leq$140 Å^2), and number of rotatable bonds ($\leq$10) were determined. In the present study, the druglikeness of selected WS phytoconstituents was analyzed using Molinspiration (http://www.molinspiration.com/cgi-bin/properties) and compared to that of standard reference drugs.

2.2.2. Veber rule

For oral bioavailability, membrane permeability is an important factor. Polar surface area and number of rotatable bonds are two critical considerations for a compound to behave as a potential drug candidate. With a reduction in polar surface area, permeation increases and with the increase in number of rotatable bonds permeation decreases significantly (Veber et al., 2002). The following two criteria should be met by a potential drug candidate in order to obey Veber rules:

1. $\leq$10 rotatable bonds;
2. Polar surface area $\leq$140Å^2 (or 12 or fewer H-bond donors and acceptors).

2.2.3. Ghose filter

Receptor binding, cellular uptake and bioavailability of drug molecules is strongly influenced by molecular lipophilicity and molar refractivity. Both of them signify hydrophobic and dispersive (van der Waals) interactions (Ghose & Crippen, 1987) of a drug molecule and are employed in 3D-QSAR studies to evaluate the drug-like character of molecules under study (Viswanadhan et al., 1990, 1991). The following are the qualifying parameters for a putative drug candidate as per Ghose filter:

1. clogP range between -0.4 and 5.6, with an average value of 2.52;
2. MW range between 160 and 480, with an average value of 357;
3. Molar refractivity range between 40 and 130, with an average value of 97;
4. Total number of atoms between 20 and 70, with an average value of 48.

The above parameters should be kept in mind for testing hypothetically proposed compounds before any *in vitro* and *in vivo* experimentation (Ghose, 1987; Ghose et al., 1999).

2.2.4. Leadlikeness

According to Teague et al. (1999) compounds with MW in the range 250–350, a XLOGP3 value of $<$3.5 and $<$7 rotatable bonds satisfy the criteria for leadlikeness.

2.2.5. Egan rule

It is defined as compounds having TPSA $>$ 131.6 Å or log $p > 5.88$ have drug-like character and properties (Egan et al., 2000).

2.2.6. Muegge rule

It states that compounds having MW between 200 and 600, XLogP between -2 and 5, TPSA $<$ 150, no. of rings $<$ 7, no. of carbon atoms $>$4, no. of heteroatoms $>$ 1, no. of rotatable bonds $<$ 15, no. of H-bond acceptors $<$ 10, no. of H-bond donors $<$ 5 are found to obey Muegge rule and behave as potential drugs (Muegge et al., 2001).

2.3. Pharmacokinetic (PK) parameters prediction

Drug discovery process requires early prediction of ADMET properties of candidate drug molecules. The fate of a therapeutic drug in an organism can be predicted conveniently by employing a user-friendly interface of SwissADME (http://www.swissadme.ch.). The server predicts important properties like lipophilicity (LIPO), flexibility (FLEX), TPSA, size, unsaturation (INSATU), insolubility (INSOLU) and bioavailability. Another online program admetSAR v1.0 (http://lmmd.ecust.edu.cn/admetsar2/) calculates and predicts physicochemical properties like lipophilicity (LIPO) of a query compound (XLOGP3) by using a known logP value of a reference compound as a starting point (Teague et al., 1999). The percentage of *sp*-hybridized carbons in the overall carbon count (Fraction Csp3) in the saturation percentage should be at least 0.25 (Tian et al., 2015). For solubility, log S (calculated with the ESOL model) should not exceed 6 (Delaney, 2004). admetSAR is also used to predict physiological and biochemical properties of a prospective drug candidate like human intestinal absorption (HIA), blood–brain barrier (BBB) permeability, Caco-2 penetration, P-glycoprotein inhibitor, Ames test-based mutagenesis, subcellular localization, biodegradation and acute oral toxicity.

2.4. Selection and preparation of protein targets

The available X-ray crystal structures of human ACE2 receptor, SARS-CoV and SARS-CoV-2 protein targets were downloaded from Protein Data Bank in PDB format (http://www.rcsb.org/pdb). Before docking analyses, the protein structures were subjected to refinement and energy minimization. The refinement involved the addition of missing atoms, polar hydrogen atoms and Kollman charges to the residues and removal of crystallographic water-molecules. These structures were visualized in Accelrys Biovia Discovery Studio 2017 R2 (Biovia, San Diego, CA, USA).

The PDB IDs of the target proteins were as follows: Angiotensin converting enzyme (PDB ID: 1O8A), SARS-CoV spike glycoprotein (PDB ID: 5WRG), SARS-CoV-2 spike glycoprotein (PDB ID: 6VXX), SARS-CoV-2 main protease (PDB ID: 6LU7), SARS-CoV main protease (3CL-pro) structure (PDB ID: IP9U), papain like protease of SARS-CoV-2 (PDB ID: 6W9C), Nsp-10/Nsp-16 complex from SARS-CoV-2 (PDB ID: 6W75), SARS-CoV-2 spike receptor-binding domain (PDB ID: 6M0J) and SARS-CoV-2 spike receptor-binding domain (RBD) bound with ACE2 (PDB ID: 6M0J).

The identification of protein ligand-binding sites was carried out using online server Metapocket 2.0 (http://metapocket.eml.org) which combines prediction of sites from four methods *viz*. LIGSITE csc, PASS, Q-SiteFinder and SURFNET to improve the prediction. The active site residues of enzymes 3CL-pro, PL-pro of SARS-CoV, SARS-CoV-2 and human ACE2 were found from review of literature (Báez-Santos et al., 2015; Chen et al., 2020; Guy et al., 2005; Zhang et al., 2020).

2.5. Molecular docking studies

2.5.1. AutoDock

Molecular docking of selected phytoconstituents of WS against human ACE2 receptor, SARS-CoV and SARS-CoV-2 target proteins was performed using AutoDock 4.0/ADT version 4.2.6 program (Morris et al., 1998) and further validated using two additional softwares *viz*. AutoDock vina and iGEMDOCK version 2.1 in order to investigate binding kinetics and binding modes to the refined proteins. Grid spacing was set at 0.375 Å and the grid points in the *X*, *Y* and *Z* axes were set to $60 \times 60 \times 60$. The quest was based on the Lamarckian genetic algorithm (Miyamoto & Kollman, 1992; Oprea et al., 2001) and the binding energies of the results were subjected to further analysis.

Molecular docking computation and visualization of binding interactions of withanolide analogs to human ACE2 receptor and selected SARS-CoV and SARS-CoV-2 protein targets was done using Accelrys Biovia Discovery Studio version 2017 R2. The best possible orientation of the ligand(s) in the protein binding pocket was selected for analysis on the basis of lowest binding energy (BE) and dissociation constant (K_d).

2.5.2. AutoDock Vina

AutoDock Vina is a free platform designed to be significantly faster than AutoDock 4, yet at the same time more accurate in predictions of binding pockets. It calculates grid maps and clusters automatically, in contrast to AutoDock 4 and as a result of multithreading on multicore machines, faster results are obtained (Trott & Olson, 2010).

2.5.3. iGEMDOCK

Institute of Bioinformatics in Taiwan's National Chiao Tung University developed iGEMDOCK version 2.1, a graphical, user-friendly and automated software for integrated docking, screening and post-analysis (Yang & Chen, 2004). Binding sites for a particular ligand were established with the help of the software. iGEMDOCK employs a generic evolutionary method (GA) in order to calculate ligand conformation and orientation with respect to the target protein binding site. The parameters selected for GA were as follows: population size = 200, generations = 70, solution number = 2 and docking feature as 'standard docking'. Once a set of poses is generated, the software recalculates the energy of each pose and the interaction data represents the individual as well as overall energy. Best fit is selected, representing the total energy *viz*. vdW (van der Waals energy), H-bond (hydrogen bonding energy) and Elect (electrostatic energy) of the predicted pose at the protein binding site.

2.6. Bioactivity score (BAS) prediction

Bioactivity score values also predict the overall druglikeness of a compound. Molinspiration version 2016.10 was used to predict the drug score of WS phytoconstituents with respect to several human receptors (Proudfoot, 2002). As a general rule, the higher the bioactivity score, the greater is the probability of the compound under investigation for being active.

2.7. Toxicity risk prediction

Toxicity prediction was done using OSIRIS Property Explorer version 4.5.1. (Information Management Drug Discovery, Actelion Ltd, Allschwil, Switzerland) in order to identify possible side effects of WS phytoconstituents (Khan et al., 2018).

2.8. Swiss Target Prediction

Computational approaches are key players in narrowing down the dataset of potential drug targets and suggesting alternative targets for known molecules. Molecular insight of the bioactive molecules and their mode of actions are important for understanding the observed phenotypes, prediction and optimization of existing compounds. Swiss Target Prediction (http://www.swisstargetprediction.ch.) is an online web-based interface which helps in finding bioactive molecules having similar configuration with related or similar biochemical targets (Campillos et al., 2008). The primary goal of the tool is to identify biochemical targets of molecules which are known to be bioactive. In the present study, Swiss Target Prediction online server was used for predicting the percentage proportion activity of each selected WS phytoconstituent with known intracellular targets like kinases, nuclear receptors, transcription factors, phosphodiesterases, oxidoreductases, cytochrome P450, voltage gated-ion channels, hydrolases, phosphatases, G-protein coupled receptors and primary active transporters.

2.9. Prediction of cytochrome P450 mediated sites of metabolism (SOM)

Most of the FDA-approved drugs are known to be metabolized by a ubiquitous protein family of heme-thiolate enzymes known as cytochrome P450s (CYPs). Regioselectivity-WebPredictor (http://reccr.chem.rpi.edu/Software/RS-WebPredicto/) is an algorithm for accurate prediction of isozyme-specific cytochrome P450 (CYP)-mediated sites of metabolism (SOM) on drug like molecules (Nebert & Russell, 2002). This is the very first repository that makes metabolic predictions for nine isozymes (1A2, 2A6, 2B6, 2C8, 2C9, 2C19, 2D6, 2E1 and 3A4) available to the public and uses models trained on the largest set of CYP substrate and metabolite data (Zaretzki et al., 2013).

2.10. Principal component analysis (PCA)

The process of drug discovery has come to involve a critical concept known as 'Chemical space' which is defined as a multidimensional space projection of the number of property descriptors calculated for each chemical entity. PCA is a method to visualize chemical space in lower dimensions in order to identify and underline dominant patterns of drug like entities. The term PCA was first coined by Karl Pearson

Table 2. PASS analysis of WS phytoconstituents *versus* FDA-approved standard reference drugs (Losartan, Procainamide, Cinacalcet, Arbidol, Hydroxychloroquine, Oberadilol, Poziotinib).

Physicochemical properties									
		Lipinski's rule of 5 parameters							
S. No.	Ligands	% Absorption (>50%)[a]	Topological polar surface area (Å)^2 (TPSA)[b] (<160 Å)	MW (<500)	clog P[c] (<5)	Hydrogen bond donors (NOHNH) (≤5)	Hydrogen bond acceptors (NON) ≤10)	Number of rotatable bonds (≤10)	Lipinski's violation (LV)
1.	Withaferin A	75.76	96.36	470.61	2.49	2	6	3	0
2.	Withanolide A	75.76	96.36	470.61	2.56	2	6	2	0
3.	Withanolide B	82.74	76.13	454.61	3.42	1	5	2	0
4.	Withanolide D	75.76	96.36	470.61	2.56	2	6	2	0
5.	Withanolide E	68.78	116.59	486.61	1.77	3	7	2	0
6.	Withanone	75.76	96.36	470.61	2.60	2	6	2	0
7.	Viscosalactone B	68.78	116.59	488.62	1.92	3	7	3	0
8.	Anaferine	94.81	41.12	224.35	1.47	2	3	4	0
9.	Withasomnine	102.85	17.83	184.24	2.65	0	2	1	0
10.	Losartan	77.09	92.5	422.9	3.95	2	5	8	0
11.	Procainamide	88.85	58.4	235.33	0.93	2	3	6	0
12.	Cinacalcet	104.86	12	357.4	5.65	1	4	6	1
13.	Arbidol	81.4	80	477.4	4.17	1	5	8	0
14.	Hydroxychloroquine	92.31	48.38	335.88	3.08	2	4	9	0
15.	Oberadilol	67.95	119	484	2.80	4	7	10	0
16.	Poziotinib	82.57	76.6	491.3	5.29	1	7	6	1

Rule: [a]Percentage absorption was calculated as: % absorption = 109 – [0.345 × topological polar surface area].
[b]Topological polar surface area (defined as a sum of surfaces of polar atoms in a molecule).
[c]Logarithm of compound partition coefficient between *n*-octanol and water.

in 1901 and is an application of linear algebra (Ahmad, 2019, Khan et al., 2018).

Osiris Property Explorer 4.5.1 was used for defining and visualizing multivariate datasets of prospective drug candidates from WS and standard reference drugs through comparison of properties like TPSA, percent absorption, MW, hydrogen bond donor, hydrogen bond acceptor, number of rotatable bonds, Lipinski's violations, leadlikeness and BAS. PCA helps in reducing the dimensionality of the dataset and increases interpretability. It does so by creating new uncorrelated variables which maximize the variance successively. Another added advantage of PCA is a 3D visualization in chemical space of how 'drug-like' are the molecules under study to known standard drugs in terms of their proximity to them in 3D chemical space.

2.11. Molecular dynamics (MD) simulation

2.11.1. Playmolecule open server

Two of the WS phytoconstituents *viz*. withanolides A and B showing significant binding to selected viral target proteins were subjected to molecular dynamics simulation studies with SARS CoV-2 spike receptor binding domain (PDB ID: 6M0J) and SARS CoV-2 papain like protease (PDB ID: 6W9C), respectively. The playmolecule web platform (https://www.playmolecule.com/SimpleRun/) is publicly available at www.playmolecule.org and uses high-throughput molecular dynamics (HTMD), a python-based framework in order to perform simple molecular-simulation-based drug discovery (Raimondas et al., 2019; Rossell et al., 2017). The MD simulation was run for 3 ns for both SARS-Cov-2 glycoprotein–withanolide A complex and SARS CoV-2 papain like protease-withanolide B complex at 300 K.

2.11.2. Ligand and receptor molecular dynamics (LARMD) online server

The MD simulation analyses of SARS-CoV spike glycoprotein (PDB ID: 5WRG) with withanolide B and SARS-CoV-2 main protease (PDB ID: 6LU7) with withanolide A were performed using Ligand and Receptor Molecular Dynamics (LARMD, http://chemyang.ccnu.edu.cn/ccb/server/LARMD/; http://agroda.gzu.edu.cn:9999/ccb/server/LARMD/). It is an online bioinformatics tool to investigate and visualize ligand-driven protein dynamics. LARMD comprises of three computational modules out of which Int_mod, which aids in the investigation of protein fluctuation, was implemented (Yang et al., 2019).

3. Results

3.1. Virtual screening of prospective antiviral candidates from WS phytoconstituents on the basis of physicochemical parameters and Lipinski's rule of five (PASS analysis)

In the drug discovery context, it is generally believed that an orally active drug candidate cannot have more than one violation of Lipinski's criteria otherwise it might compromise its bioavailability (Balakrishnan et al., 2014).

Based on Lipinski's rule of five, WS phytoconstituents were previously screened and selected for their drug like properties (Table 2). As is evident from Table 2, none of the selected WS phytoconstituents exhibited Lipinski's violation. Interestingly, standard reference drugs cinacalcet and poziotinib displayed 1 violation each of Lipinski's rule of five.

WS phytoconstituents were further analyzed using additional filters *viz*. Ghose, Veber, Egan, Muegge and Leadlikeness filters (Table 3). The selected phytoconstituents

Table 3. Drug-like character of WS phytoconstituents *versus* FDA-approved standard reference drugs (Losartan, Procainamide, Cinacalcet, Arbidol, Hydroxychloroquine, Oberadilol, Poziotinib).

S. No.	Ligands	GNo. of vio.[a]	VNo. of vio.[b]	ENo. of vio.[c]	MNo. of vio.[d]	Leadlikeness
1.	Withaferin A	1	0	0	0	2
2.	Withanolide A	1	0	0	0	1
3.	Withanolide B	1	0	0	0	2
4.	Withanolide D	1	0	0	0	1
5.	Withanolide E	2	0	0	0	1
6.	Withanone	1	0	0	0	1
7.	Viscosalactone B	1	0	0	0	1
8.	Anaferine	0	0	0	0	1
9.	Withasomnine	0	0	0	0	1
10.	Losartan	0	0	0	0	3
11.	Procainamide	0	0	0	0	1
12.	Cinacalcet	1	0	1	2	2
13.	Arbidol	0	0	0	0	3
14.	Hydroxychloroquine	0	0	0	0	2
15.	Oberadilol	2	0	0	0	2
16.	Poziotinib	2	0	0	1	2

Rule: [a]Ghose filter.
[b]Veber filter.
[c]Egan (Pharmacial) filter.
[d]Muegge (Bayer) filter.

showed no violations of Veber, Egan and Muegge filters thereby indicating their drug-like character. The drug cinacalcet showed 1 and 2 violations of Egan and Muegge filters, respectively, whereas drug poziotinib exhibited 1 violation of Muegge filter.

3.2. admetSAR analysis of selected WS phytoconstituents

Good ADME and toxicity properties are as critical as therapeutic properties. Human intestinal absorption (HIA), Caco-2 cell permeability, Blood–brain barrier (BBB) penetration, and Ames test were calculated for the chosen phytoconstituents and reference drugs using admetSAR version 1.0 (Table 4).

3.2.1. Human intestinal absorption (HIA)

An orally administered drug is absorbed primarily in the intestine. All WS phytoconstituents and standard reference drugs exhibited positive results, thereby indicating their absorption and assimilation in human intestine.

3.2.2. Caco-2 permeability

Caco-2 is a human colon epithelial cancer cell line and is used as a model for human intestinal assimilation of drugs and other compounds. In the present study, whereas anaferine and withasomnine exhibited positive results indicating Caco-2 permeability, the remaining seven WS phytoconstituents displayed negative results. In case of standard reference drugs, procainamide, cinacalcet, arbidol and hydroxychloroquine displayed good permeability characteristics for Caco-2 (Table 4).

3.2.3. Blood–brain barrier (BBB) penetration

An important consideration for drug candidates is their ability to cross the BBB. All of the chosen WS phytoconstituents displayed positive results for BBB penetration except withanolide E. In case of standard reference drugs, only losartan displayed inability to penetrate the BBB (Table 4).

3.2.4. Ames test

In the present study, none of the chosen WS phytoconstituents were predicted to have any mutagenic effect in contrast to standard reference drugs arbidol and hydroxychloroquine which tested positive for their ability to induce mutations (Table 4).

3.3. Docking studies of WS phytoconstituents with respect to selected target proteins

Docking studies of the selected WS phytoconstituents were carried out with human ACE2 receptor, SARS-CoV and SARS-CoV-2 specific proteins. The catalytically active sites of SARS-CoV-2 specific proteins were targeted in order to obtain the binding energy involved in the complex formation and to discover the molecular mechanisms responsible for specific inhibition of targets. Tables 5–11 summarize the predicted binding energies and dissociation constants (K_d) of WS phytoconstituents with respect to specific human ACE2 receptor, SAR-CoV and SARS-CoV-2 spike glycoproteins as well as the two main SARS-CoV-2 proteases *viz*. 3CL-pro and PL-pro. The binding sites of the WS phytoconstituents on the selected viral target proteins as well as the interacting amino acids were predicted to be almost the same by the three molecular docking softwares (Tables 5–11). The common interacting amino acids between the three softwares have been written in italicized form in Tables 5–11. As is evident from Tables 5–11, most of the WS phytoconstituents exhibited potent binding kinetics to the above-mentioned proteins. Docking analyses using AutoDock 4.0/ADT version 4.2.6 program revealed that the binding affinities of the WS phytoconstituents for the human ACE2 receptor decreased in the order withanolide B > withanolide A > withanolide E > viscosalactone B > withaferin A > anaferine > withanolide

Table 4. admetSAR prediction of selected WS phytoconstituents *versus* FDA-approved standard reference drugs (Losartan, Procainamide, Cinacalcet, Arbidol, Hydroxychloroquine, Oberadilol, Poziotinib).

	Human intestinal absorption (HIA)		Caco-2 permeability		P-glycoprotein inhibitor		Blood–brain barrier penetration (BBB)		Ames mutagenesis		Subcellular localization		Biodegradation		Acute oral
Ligands	±	*p* value	±	*p* value	±	*p* value	±	*p* value	±	*p* value	±	*p* value	±	*p* value	toxicity (kg/mol)
Withaferin A	+	0.9729	−	0.6673	+	0.6132	+	0.9537	−	0.6900	Mitochondria	0.7714	−	0.8750	3.276
Withanolide A	+	0.9829	−	0.6006	+	0.6554	+	0.8333	−	0.8700	Mitochondria	0.6830	−	0.8000	5.165
Withanolide B	+	0.9829	−	0.5605	+	0.7494	+	0.9128	−	0.8000	Mitochondria	0.6784	−	0.8750	4.099
Withanolide D	+	0.9750	−	0.6274	−	0.4303	+	0.8345	−	0.7800	Mitochondria	0.7352	−	0.8250	3.66
Withanolide E	+	0.9640	−	0.6455	−	0.4399	−	0.5510	−	0.7100	Mitochondria	0.6273	−	0.9250	5.292
Withanone	+	0.9829	−	0.6472	+	0.6845	+	0.8333	−	0.8300	Mitochondria	0.6830	−	0.8500	4.775
Viscosalactone B	+	0.9480	−	0.7386	−	0.4906	+	0.9214	−	0.7500	Mitochondria	0.7598	−	0.8250	3.059
Anaferine	+	0.9064	+	0.5418	−	0.9112	+	0.9929	−	0.7300	Mitochondria	0.7672	−	0.7000	2.517
Withasomnine	+	0.9932	+	0.9586	−	0.9813	+	0.9966	−	0.9100	Mitochondria	0.5372	−	0.8750	2.41
Losartan	+	0.9883	−	0.9373	+	0.8124	−	0.9930	−	0.5200	Mitochondria	0.7540	−	0.9250	3.322
Procainamide	+	0.9795	+	0.9185	−	0.9721	+	0.9707	−	0.5900	Lysosomes	0.8295	−	0.6000	2.59
Cinacalcet	+	0.9911	+	0.7035	+	0.5803	+	0.9974	−	0.5000	Lysosomes	0.9070	−	1.0000	3.492
Arbidol	+	0.9684	+	0.6814	+	0.6810	+	0.9739	+	0.5300	Lysosomes	0.5338	−	0.9000	2.753
Hydroxychloroquine	+	0.9934	+	0.5313	−	0.7900	+	0.9878	+	0.6400	Lysosomes	0.8067	−	0.8500	2.665
Oberadilol	+	0.9820	−	0.7895	+	0.7739	+	0.9693	−	0.6300	Mitochondria	0.8157	−	0.7250	3.747
Poziotinib	+	0.9852	−	0.6765	+	0.8852	+	0.9900	−	0.5600	Mitochondria	0.5163	−	0.9000	3.121

D > withanone > withasomnine. Withanolide B exhibited a 1000× stronger binding to human ACE2 receptor (Table 5; BE: −10.21 kcal/mol, K_d: 32.78 nM) as compared to standard reference drugs, arbidol (Table 5; BE: −6.69 kcal/mol, K_d: 12.47 μM) and losartan (Table 5; BE: –6.72 kcal/mol, K_d: 11.86 μM). Withanolide B also exhibited potent binding to papain like protease of SARS-CoV-2 (Table 8; BE −10.3 kcal/mol, K_d: 28.32 nM) as compared to procainamide (Table 8; BE −5.03 kcal/mol, K_d: 206.96 μM) and cinacalcet (Table 8; BE −6.44 kcal/mol, K_d: 19.17 μM).

Withasomnine was found to bind near or at the active site of SARS-Co-V main protease 3CL-pro (PDB ID: 1P9U; Table 9), whereas anaferine was found to interact with the active site residues Cys145, Glu166, Ser144, Met165, His163, His164, Gln189, Asp187, Arg188, Met49 and His41 present at the active site of SARS-CoV-2 main protease 3CL-pro (PDB ID: 6LU7; Table 10). The 3CL-pro active site has been found to be evolutionarily conserved between SARS-CoV and SARS-CoV-2 (Báez-Santos et al., 2015; Chen et al., 2020; Guy et al., 2005; Zhang et al., 2020). In the same manner, the other seven phytoconstituents also displayed potent binding to the active site of SARS-CoV-2 3CL-pro except viscosalactone B as predicted by AutoDock vina and iGEMDOCK. The active site residues have been written in bold in Tables 9 and 10. As far as viral PL-pro and human ACE2 are concerned, WS phytoconstituents displayed allosteric binding to these enzymes.

On the other hand, withanolide A displayed strong binding to SARS-CoV spike glycoprotein (Table 6; BE: −9.78 kcal/mol, K_d: 67.23 nM), SARS-CoV-2 spike glycoprotein (Table 7; BE: −7.18 kcal/mol, K_d: 5.48 μM), SARS-CoV 3CL-pro main protease (Table 9; BE: –8.93 kcal/mol, K_d: 285.01 nM) and SARS-CoV-2 Nsp10/Nsp-16 complex (Table 11; BE: −10.38 kcal/mol, K_d: 24.67 nM). Interestingly, withanolide A exhibited almost 1000× times stronger binding to SARS-CoV main protease as compared to standard reference drugs arbidol (Table 6; BE: −4.91 kcal/mol, K_d: 251.65 μM) and hydroxychloroquine (Table 6; BE: −5.25 kcal/mol, K_d: 142.18 μM). The same binding profile was observed for withanolide A with respect to SARS-CoV-2 spike glycoprotein as compared to standard reference drugs arbidol (Table 7; BE: −3.14 kcal/mol, K_d: 4.99 mM) and hydroxychloroquine (Table 7; BE: −2.48 kcal/mol, K_d: 15.11 mM). Withanolide A also displayed a 1000× stronger binding to Nsp-10/Nsp-16 complex from SARS-CoV-2 in comparison to losartan (Table 11; BE: −6.49 kcal/mol, K_d: 17.54 μM) and hydroxychloroquine (Table 11; BE: −4.93 kcal/mol, K_d: 244.14 μM)

Withanone also displayed significant binding to SARS-Cov-2 main protease (Table 10; BE: −6.14 kcal/mol, K_d: 31.77 μM) in comparison to standard reference drug oberadilol (Table 10; BE: −2.23 kcal/mol, K_d: 23.18 mM). The best docking poses of the WS phytoconstituents with respect to the human ACE2 receptor and viral target proteins have been depicted in Table 12 (Tables 12.1–12.7). Binding studies on WS constituents to unbound spike receptor-binding domain (RBD) of SARS-CoV-2 (PDB ID: 6M0J) and binding of WS phytoconstituents with SARS-CoV-2 spike receptor-binding

Table 5. Binding energies of WS phytoconstituents with human ACE2 receptor (PDB ID: 1O8A) in comparison to the FDA approved standard reference drugs (Arbidol and Losartan).

		AutoDock v4.2.6			AutoDock vina			iGEMDOCK v2.1				
S. No.	Ligands	BE (kcal/mol)	K_d	Interacting amino acids	BE (kcal/mol)	K_d	Interacting amino acids	TE (kcal/mol)	VDW	HB	EI	Interacting amino acids
1.	Withaferin A	−8.44	647.61 nM	Glu123, Met223, Trp220, Pro519, *Arg522*, Ser517, *Val518, Glu411*, His410, *Ser355, Ala356*, His387, Phe391, Glu403	−10.4	23.67 nM	His353, *Val518*, His513, Tyr523, *Glu411, Arg522,* Phe512, *Ala356, Ser355*, Ser516, Glu143, Asn70, Asn66, Tyr69, Leu140, Leu139, Leu81, Asn85, Tyr62, Asn136, Arg124	−111.33	−90.07	−21.26	0	Ser284, Tyr287, Val291, Asp288, Asn285, Glu376, Leu375, Asn374, Thr302, Thr301, Asp300, Met299, Ser298, Pro297, Pro294, Ala296
2.	Withanolide A	−10.13	37.44 nM	Asp453, Thr282, Gln281, Phe457, Glu376, Val379, Val380, Asp415, His383, Glu384, Ala354, *His353, His387, Glu411, His513, Phe512, Tyr523*	−10.6	15.57 nM	His410, Ala353, *His387*, Trp357, Phe391, Asn66, Asn70, Ser516, Glu143, *Phe512,* Val518, *His353, Ser355, His513, Tyr523, Glu411,* Arg522	−98.26	−78.36	−19.90	0	Leu375, Lys449, Tyr287, Ser298, Met299, Asp300, Thr301, Thr302
3.	Withanolide B	−10.21	32.78 nM	Phe391, *His387, Ala356,* His383, *Ser355,* Ala354, *His353,* Glu403, Gly404, His410, *Glu411,* Pro407, *Tyr523, Arg522, Phe512, His513,* Met223	−10.7	10.60 nM	Asn85, Tyr62, Arg124, Asn66, *Phe512, His353,* Val518, *His513, Tyr523, Arg522, Glu411*, Leu81, Leu140, Leu139, Tyr69, Glu143, Asn70, Ser516, *Ser355, Ala356, His387*	−97.61	−86.31	−11.29	0	Thr226, Glu225, Pro227, Tyr224, Leu229, Ser222, Arg221, Asp218, Tyr213, Asn211, Asp121, Gln120, Lys117
4.	Withanolide D	−8.23	934.88 nM	*Phe391, Ala356, Ser355, His387, Glu384, Ala354, His353, Glu411, Tyr523, Val518,* His383, Val380	−11.3	600 pM	*Glu411, Tyr523,* Arg522, His410, *Phe391, Ala356, His387, Asn66, Asn70, Tyr69,* Trp357, *Glu143,* Val351, Ser516, *Phe512, His353,Val518, Ser355*	−101.56	−82.00	−19.56	0	Arg124, Leu140, Leu81, *Glu143, Asn66, Asn70, Tyr69, His353, Ala354, Ser355,* Ala356, *Glu384, His387, Glu411, Tyr523, Val518,* His513, *Phe512*
5.	Withanolide E	−9.75	71.2 nM	*Phe391*, His410, His387, Glu411, Arg522, Tyr523, *Val518,* His513, *Phe512, His353,* Ala354, *Ser355, Glu384, Ala356,* Lys368, *Asn70*	−10.6	15.45 nM	Arg124, Leu140, Leu139, Leu81, *Asn70,* Tyr69, Glu143, Ser516, Val351, Trp357, *Phe512, His353, Ser355, Ala356, Glu384,* His387, *Phe391, Val518,* Tyr62, Asn66	−104.39	−90.97	−13.41	0	Glu239, Arg235, Leu236, Asp232, Ser228, Thr226, Pro575, Trp574, Pro585, Asn586, Met587
6.	Withanone	−8.12	1.12 μM	Ser422, Phe527, Lys454, Tyr523, Val379, His383, Glu384, Val380, His513, Gln281, Thr282, *Ser284,* Phe457, Asp453	−10.2	31.56 nM	Lys449, *Val291, Pro297, Ser298, Asp300, Met299, Ser284, Asn285*, Asn374, Glu376, *Thr302, Leu375, Thr301, Tyr287,* Asp288	−100.15	−79.22	−20.92	0	Asn374, *Leu375, Thr302, Thr301, Asp300, Met299, Ser298, Pro297,* Ala296, Pro294, *Val291, Tyr287, Asn285*
7.	Viscosalactone B	−8.83	339.1 nM	*Ala356, His387, Ser355, Glu384, Ala354, His353, His513, Phe512, Tyr523,* Thr282, Asp453, Ser284, Glu376, Val379, Val380, *His383, Glu411*	−11.1	760 pM	*Tyr62,* Asn85, *Asn136, Leu81, Glu143, Leu139, Leu140, Asn66,Asn70, Phe512, Ala356, Ser355, Ala354, His353, Tyr523, His383, His387, Glu411,* Arg522, Val518, Arg124	−119.88	−92.25	−27.63	0	*Tyr62, Leu81,Asn136, Asn66,* Tyr69, *Leu139, Leu140, Glu143,* Ser516, *Asn70, His513, His353, Ala354, Tyr523, Ser355, Ala356, Trp357, His387, Glu411, Glu384, His383*
8.	Anaferine	−8.25	890.86 nM	*Glu411, Tyr523, His383, His387, Glu384,* Val380, *Ala356, Ser355, Ala354, His353*	−6.7	12.50 μM	*His383, His387, Ala354, Glu384, Ser355, Ala356,* Val518, His513, Phe512, *His353, Tyr523,* Tyr520, Gln281, Phe457, Phe527	−77.85	−74.35	−3.5	0	Phe570, Met223, Asn406, Glu403, Gly404, Pro407, His410, Phe391, *Glu411, His387*
9.	Withasomnine	−4.99	218.08 μM	Tyr523, His513, Val380, His383, Glu384, His387, Ala356, *Ser355,* Ala354, His353	−6.7	12.59 μM	Phe291, Tyr394, His410, Arg522, Gly404, Pro407, Glu403, Met223, Phe570, Asn406	−74.24	−64.10	−10.14	0	Leu122, Thr92, Ala125, Arg124, Ala89, Ile88, Asn85, Asn136, Trp59
10.	Arbidol	−6.69	12.47 μM	*Ala354, His353,* Glu162, Lys511, Trp279, Gln281, Thr282, Phe457, Asp453, *Tyr523,* Lys454, Phe527, Asp415, His383, Val380, Glu384	−8.3	880.23 nM	Phe570, Met223, Asn406, Gly404, Glu403, Arg402, Tyr394, Tyr360, *Phe391*, Asp358, *Trp357, Ala356,His387, His410, Glu411,* Arg522, Pro407	−86.22	−73.55	−12.67	0	*Phe391, His410, Glu411, His387, Trp357, Ala356, Ser355, Ala354, His353,* Asn66, Ala63, Tyr62, Val518, *Tyr523*
11.	Losartan	−6.72	11.86 μM	*Asn406, Met223, Arg522, Pro407, Gly404, Glu403, His410, Glu411, Tyr523, Phe391, His387, Ala356, Val518*	−9.4	129.59 nM	*Met223, Pro519, Arg522, His410, His387, Tyr523, Glu411, Ser355, Val518, Ala356,* Asp358, Tyr360, *Phe391, Gly404, Glu403, Asn406*, Pro407	−101.28	−85.24	−16.04	0	Asp121, Leu122, Thr92, Trp220, Glu123, Arg124, Ala89, Ile88, Pro519, Tyr62, Ser517, Tyr135, Ile204

Table 6. Binding energies of WS phytoconstituents with SARS-CoV spike glycoprotein (PDB ID: 5WRG) in comparison to the FDA approved standard reference drugs (Arbidol and Hydroxychloroquine).

		AutoDock v4.2.6			AutoDock vina			iGEMDOCK v2.1				
S. No.	Ligands	BE (kcal/mol)	K_d	Interacting amino acids	BE (kcal/mol)	K_d	Interacting amino acids	TE (kcal/mol)	VDW	HB	EI	Interacting amino acids
1.	Withaferin A	−8.39	702.21 nM	Ile979, Leu983, Thr980, Gly981, Gln984, Tyr738, Leu983, Gln984, Thr980	−10.3	28.30 nM	Lys715, Ala753, Ala754, Asp757, Arg761, Leu846, Arg758, Pro651, Ile652, Leu843, Leu597, Gln599, Ala633, Val581, Tyr300, Thr302	−104.25	−83.69	−20.56	0	Arg453, Glu452, Asp454, Ser456, Arg449, Arg441, Val458, Pro459, Arg444, His445, Phe460, Pro466, Gly464, Ser461, Lys465
2.	Withanolide A	−9.78	67.23 nM	Gln984,Leu983, Thr980, Gly981, Arg977, Phe952, Tyr738	−10.5	19.50 nM	*Ile299, Ala754, Ser750, Thr302,* Ala753, Val581, Leu843, Gln599*, Ile652,* Arg758, *Lys715,* Gly653, Asp757, Tyr300, Arg761, *Pro651,* Leu846	−97.67	−85.32	−12.35	0	*Ile652, Pro651, Thr302,* Tyr300, *Ile299,* Gln301, *Ser750, Ala754,* Arg747, Gly751, *Lys715*
3.	Withanolide B	−9.4	129.59 nM	*Gln984, Thr980, Leu983, Gly981, Arg977, Phe952, Tyr738, Asp976*	−10.4	23.67 nM	Ser950, Asn951, *Gly981, Arg977,Thr980, Asp976,* Asp976, *Phe952,Gln984*, Leu983, Gln947, Phe741, Ser985, *Tyr738*	−100.62	−94.31	−6.32	0	Lys715, Asp757, Ala753, Arg761, Arg758, Ala754, Leu846, Gly653, Ile652, Pro651, Tyr300
4.	Withanolide D	−9.1	212.78 nM	Thr980, Gly981, Leu983, Tyr738, Phe952, Gln984, Asp976, Ile979	−10.7	11.45 nM	Ile299, Ala754, Pro651, Arg758, Arg761, Asp757, Leu846, Leu597, Lys715, Val581, Ile652, Ala633, Gln599, Leu843, Tyr300, Ser750, Ala753, Thr302	−103.3	−84.53	−18.77	0	Ala926,Leu927, Ser924, Gly928, Thr925, Gln931, Asn935, Lys297, Asp296, Ile295, Glu294, Val290
5.	Withanolide E	−7.13	5.93 μM	Thr980, Gly981, Gln984, Arg977, Tyr738, Leu983	−9.5	99.21 nM	*Lys715, Ala753, Ser750, Pro844, Thr302, Leu843, Ala633,Gln599, Ile652, Leu597, Val581, Ile299, Pro651, Ile650, Tyr300, Ala754*	−99.34	−93.84	−5.49	0	*Leu597,Ala633, Gln599, Ile652, Val581, Pro651, Thr302, Ile650,* Tyr300, *Ile299, Pro844, Leu843, Lys715, Ser750, Ala753, Ala754*
6.	Withanone	−6.49	17.46 μM	Thr980, Gly981, Gln984, Leu983, Phe741,Tyr738	−9.5	99.56 nM	*Arg747,* Gly751, Ala754, Pro651, Ile652, Lys715, Gln599, Val581, Tyr200, Leu843, Ala753, Thr302, Ser750, Ile299, Gln939, Gln301	−104.09	−85.03	−19.07	0	Leu810, Ala938, Asn942, Lys946, Thr943, Gln744, *Arg747,* Thr743, Ser289, Gln301, Val290, Lys291
7.	Viscosalactone B	−7.6	2.69 μM	Gln987, Gln984, Leu983, Thr980, Asp976, Phe952, Gly981, Gln984, Thr988	−10.2	32.60 nM	Leu994, Ile995, Glu999, Ala998, Ile752, Arg1001, Ala997, Glu755, Gln936, Asp932, Ile299, Asp296, Tyr300, Gln301, Gln939, Arg747, Ala748, Gly751, Arg996	−121.82	−89.39	−32.43	0	Arg563, Arg315, Phe551, Gln550, Asn530, Gly531, Asn505, Leu504, Leu503, Ser380, Phe379, Cys378, Arg965, Asn530, Gly551
8.	Anaferine	−6.94	8.16 μM	*Gln947, Phe741, Ser985, Gln984,* Gly981, Tyr738, Phe952, Leu983, Thr980, Ile979, Asp976	−7.0	6.40 μM	Arg747, Thr943, Gln744, Thr988, *Gln987, Phe741, Gln947, Ser985,* Tyr989, Leu944, Ala940, Gln992	−84.12	−69.13	−14.99	0	Arg965, Leu374, Lys373, Tyr352, Cys378, Leu503, Phe501, Met417, Val369, Ser370
9.	Withasomnine	−5.87	49.69 μM	Gln947, Phe741, Ser985, Gln984, Gly981, Leu983, Phe952, Asn951, Tyr738, Ser950	−7.1	6.25 μM	Leu963, Ser728, Cys725, Val958, Leu948, Phe558, Asp557, Phe837, Asn960, Thr535, Thr533, Asp727, Leu959	−80.03	−72.43	−7.60	0	Cys278, Phe262, Met263, Val276, Cys288, Lys287, Ser292
10.	Arbidol	−4.91	251.65 μM	Phe952, Gln947, Gly739, Phe741, Tyr738. Gly981, Arg977, Thr980, Asp976, Thr980, Leu983, Gln984	−7.7	2.20 μM	Ala754, Ser750, Asn746, Arg747, Thr302, Gln599, Gln301, Val581, Tyr300	−83.02	−78.02	−5	0	Leu859, Pro1035, Phe1034, Ser1033, Cys1014, Val1015, Gln883, Leu1016, Pro879, Gly862
11.	Hydroxychloroquine	−5.25	142.18 μM	Gln984, Leu983, Thr980, Ile979,Ser985, Gly981, Phe741, Gln947, Tyr738, Phe952	−7.0	7.0 μM	Ala753, Ser750, Pro651, Lys715, Leu843, Gly653, Ile652, Val581, Tyr300, Thr302, Gln599, Leu597, Ile299, Ala754	−76.22	−68.13	−8.09	0	Lys1027, Gly1026, Val1022, Ser1012, Val1015, Gln766, Lys768

Table 7. Binding energies of WS phytoconstituents with SARS-CoV-2 spike glycoprotein (PDB ID:6VXX) in comparison to FDA approved standard reference drugs (Arbidol and Hydroxychloroquine).

		AutoDock v4.2.6			AutoDock vina			iGEMDOCK v2.1				
S. No.	Ligands	BE (kcal/mol)	K_d	Interacting amino acids	BE (kcal/mol)	K_d	Interacting amino acids	TE (kcal/mol)	VDW	HB	EI	Interacting amino acids
1.	Withaferin A	−6.11	33.39 μM	Leu303, Tyr313, Thr302, Gln314, Thr315, Ser316, Asn317, Arg319	−8.6	447.56 nM	Gln218, Phe59, Gly219, Phe220, Thr33, Asp287, Phe58, Val289, Ser297, Lys300, Asp294, Leu296, Asn606, Leu293	−84.45	−66.52	17.93	0	Thr430, Asp428, Phe515, Ser514, Glu516, Tyr396, Arg355, Phe464
2.	Withanolide A	−7.18	5.48 μM	Glu309, Tyr313, Thr302, Leu303, Lys304, Gln957	−8.4	650.76 nM	Leu977, Cys743, Val976, Asn978, Leu966, Ser975, Ser967, Arg44, Ser45, Val47, Asn856, Arg1000, Tyr741, Ile742	−83.67	−61.91	−21.76	0	Arg273, Pro272, Cys291, Thr274, Cys301, Gln52, Lys304, Ser50, Thr301, Thr315, Ala292, Glu298
3.	Withanolide B	−6.81	10.26 μM	Gln31, Tyr313, Thr302, Leu303, Lys304, Gln957, Asn960, Lys964	−8.0	771.67 nM	Arg319, Thr572, Thr573, Asp571, Arg567, Leu546, Thr547, Gly548, Phe541, Thr549, Pro589, Cys590, Phe592, Arg319	−86.89	−78.89	−7.9	0	Asn556, Ile584, Leu582, Arg577, Lys557, Lys558, Phe559, Leu560, Pro561
4.	Withanolide D	−6.9	8.68 μM	Gln957, *Thr961,* Lys964, *Gln965, Ser967,* Ser968, Leu303, Lys304, Thr302	−8.7	398. 84 nM	Val976, Arg1000, Phe855, Ser975, Lys854, Val963, Asn856, *Ser967,* Leu966, Asn978, Leu977, Asp745, Met740, Gly744, Tyr741	−82.91	−69.68	−13.23	0	Gln954, Ala958, *Thr961,* Leu962, Arg1014, Glu1017, Ile1013, Gln1010, Tyr1007, Thr1006, Ser1003, *Gln965*
5.	Withanolide E	−6.94	8.17 μM	Gln957, Lys964, Lys304, Leu303, Thr302	−8.0	771.57 nM	Asn30, Phe59, Thr33, Phe58, Phe306, Val289, Ala288, Lys300, Ser297, Leu296, Leu293, Asp294	−91.24	−82.26	−8.98	0	Glu340, Gly339, Phe338, Cys336, Ala363, Asp364, Val362, Leu335
6.	Withanone	−7.15	5.75 μM	Gln309, Ser305, Leu303, Lys304, Thr302, *Lys964,* Gln957	−8.0	771.87 nM	Asn978, Val963, *Lys964,* Ser967, Asn856, Ser975, Val976, Leu966, Tyr741, Leu977, Arg1000, Gly744	−84.14	−69.21	−14.92	0	Pro793, Pro792, Thr791, Lys790, Pro897, Thr883, Ile896, Gln895
7.	Viscosalactone B	−6.02	38.89 μM	Gln957, Ser305, Lys304, Leu303, Thr302, Thr315, Gln31, Ser316, Asn317	−8.2	935.88 nM	Asn856, Gly744, Arg1000, Val976, Ser975, Ser967, Leu966, Asn978, Leu977	−98.52	−80.77	−17.75	0	Phe86, Asn87, Ile235, Asp88, Asn234, Pro272, Ile233, Leu54, Asn196, Asp53, Gln52, Ile197, Gly199, Asp198
8.	Anaferine	−3.86	1.47 mM	Tyr313, Glu309, Leu303, Lys304, Gln957	−5.0	213.05 μM	Ser967, Ser975, Val976, Leu977, Arg1000, Asn978, Gly744, Asp745, Met740, Phe855, Tyr741, Leu966, Asn856, Val963, Lys964	−72.56	−58.62	−13.94	0	Lys933, Ser929, Ile934, Ala930, Gln926, Thr719, Ser721, Ile720, Val722
9.	Withasomnine	−4.51	494.91 μM	Ser316, Thr315, Glu298, Cys291, Thr302, Cys301, Thr274, Lys304, Ser50	−6.2	29.91 μM	Ser1003, Leu962, Tyr1007, Gln957, Arg1014, Gln1010, Ala958, Thr1006, Gln965, Thr961	−73.49	−65.71	−7.78	0	Glu1111, Gln1113, Thr1105, Gln1106, Val1104, Thr912, Asn1119, Glu1092
10.	Arbidol	−3.14	4.99 mM	Glu309, Tyr313, Gln314, Leu303, Thr302, Gln957, Thr961, Lys964	−5.8	56.89 μM	Phe59, Thr33, Phe220, Thr286, Asp287, Ala288, Val289, Asp290, Leu293, Asp294, Leu296, Ser297, Lys300	−78.93	−72.29	−6.64	0	Thr618, Glu619, Gln644, Asn616, Val615, Asp614, Phe592, Cys590, Pro589, Thr589
11.	Hydroxychloroquine	−2.48	15.11 mM	Ser50, Cys301, Glu298, Thr302, Thr315, Ser316	−6.1	35.2 μM	Asp294, Leu296, Leu293, Ser297, Lys300, Val289, Asp287, Phe306, Thr33, Asn606, Thr602	−72.42	−62.92	−9.5	0	Val722, Thr724, Ile726, Ile934, Ser937, Leu938, Thr941, Ala944, Ser943, Ile726

Table 8. Binding energies of WS phytoconstituents with papain like protease of SARS-CoV-2 (PDB ID: 6W9C) in comparison to the FDA approved standard reference drugs (Procainamide and Cinacalcet).

		AutoDock v4.2.6			AutoDock vina			iGEMDOCK v2.1				
S. No.	Ligands	BE (kcal/mol)	K_d	Interacting amino acids	BE (kcal/mol)	K_d	Interacting amino acids	TE (kcal/mol)	VDW	HB	EI	Interacting amino acids
1.	Withaferin A	−8.74	393.84 nM	*Asn109, Leu162, Gly160, Gln269, Glu161, Val159, His89, Thr158*	−9.8	61.88 nM	*His89, Val159, Gly160, Glu161,Leu162, Gln269, Asn109, Thr158*	−101.80	−86.23	−15.57	0	Trp106, Ala107, Asn267, Asp108, *Leu162,* Gly163, Lys157, Asp164, Glu167, Tyr264, Pro248, Pro247
2.	Withanolide A	−10.19	34.04 nM	*Gln269, Asn109, Leu162, Glu161, Gly160, Val159, Thr158*	−10.2	32.78 nM	Asp286, Asn267, Asp164, Tyr264, Tyr273, Pro248, Gly163, *Leu162,* Lys157, Asp108, Ala107, Trp106, Gly266, Ala288, Lys105, Tyr268, Leu289	−103.61	−84.71	−18.90	0	*Asn109, Val159, Thr158, Glu161, Gly160, Gln269, Leu162*
3.	Withanolide B	−10.3	28.32 nM	*Gln269, Asn109, Leu162, Glu161, Gly160, Val159, His89, Thr158*	−10.4	22.51 nM	*His89, Thr158, Gly160, Asn109,Gln269, Leu162, Val159*	−104.57	−96.14	−8.43	0	*Thr158, Leu162, Glu161, Gly160, His89,* Asp108, Ser85, Ala86, Gly160, *Val159, Asn109*
4.	Withanolide D	−9.56	98.21 nM	*Gly160, Glu161, Asn109, Gln269,* Cys270, *Leu162,* Cys160, *Val159, Thr158, His89*	−10.1	38.9 nM	*Thr158, His89, Glu161, Gly160, Asn109, Gln269, Leu162, Val159*	−99.07	−91.72	−7.35	0	Pro59, Ala68, Arg65, Phe69, Thr74, Thr75, Pro77, Ile44, Lys45, Pro46, Met23, His47, Asn48
5.	Withanolide E	−9.05	231.88 nM	*Asn109, Gln269, Leu162, Gly160, Asp108, Glu161, His89*	−10.6	15.57 nM	*Asp108, Thr158, Glu161, Val159, His89, Gly160, Leu162, Asn109, Gln269*	−107.44	−76.48	−30.96	0	*Thr158, Asn109, Gly160, Glu161, Leu162, Asp108, Val159, His89*
6.	Withanone	−9.09	218.4 nM	*Val159, Gly160, Glu161, Asn109, Leu162, Gln269, Gln269*	−10.1	38.83 nM	Trp106, Glu167, Ala107, Trp93, Lys92, *His89,* Asp108, Lys157, Asp164, Tyr264, Gly163, Tyr273, Val165, Thr301, Pro248	−109.36	−87.06	−22.31	0	*Asn109,* Thr158, *Gly160, Gln269,Glu161, Leu162, Val159,His89*
7.	Viscosalactone B	−9.02	243.41 nM	Ser85, Ala86, *His89, Va159, Gly160, Asp108, Asn109,* Gln269, *Leu162,Glu161*	−9.7	70.23 nM	Lys92, *His89, Val159,* Trp93, *Asp108, Leu162,* Gly163, Tyr273, Tyr264, Pro248, Pro247, Thr301, Asp164, Lys105, Glu167, *Trp106, Ala107, Glu161,* Lys157	−102.08	−86.12	−15.96	0	*Leu162, Glu161, Gly160, Val159,* Thr158,*Asn109, Asp108, Ala107, Trp106*
8.	Anaferine	−6.43	19.24 μM	Gly160, Asp108, Ala107, Trp93, Leu162, Glu161, Lys157	−6.0	39.69 μM	Thr301, Tyr273, Tyr264, Trp106, Asp164, Pro248, Pro247, Met208, Arg166	−75.28	−68.35	−6.93	0	Ala68, Thr74, Phe79, Asp76, Pro77, Lys43, Arg65, Pro59, Leu58
9.	Withasomnine	−5.56	84.41 μM	Asn109, Gln269, Cys270, Leu162, Gly160, Cys270	−7.2	4.50 μM	*Asp76, Pro59,* Phe79, *Leu80,* Thr74, Ala68, *Thr75, Arg65, Pro77, Leu58*	−69.24	−69.24	0	0	*Asp76, Pro77, Thr75, Leu80, Leu58, Pro59, Arg65*
10.	Procainamide	−5.03	206.96 μM	*Glu161, Asn109, Leu162, Asp108, Gly160, Gln269, Cys270*	−6.3	24.06 μM	*Asn109, Gln269, Leu162,* Val159, His89, *Asp108, Glu161, Gly160*	−76.81	−66.66	−10.15	0	*Leu162, Glu161, Gly160, Gln269,Asp108, Asn109,Cys270*
11.	Cinacalcet	−6.44	19.17 μM	*Val159, Asp108, Gly160, Glu161, Leu162, His89, Val159*	−8.8	344.50 nM	*Gly160, Asn109, Leu162, Gln269, Cys270, Glu161, Asp108*	−81.40	−81.40	0	0	Thr158, *Leu162, Glu161, Gly160, His89,* Ser85, Ala86, *Asn109, Val159,* Asn108

Table 9. Binding energies of WS phytoconstituents with SARS–CoV main protease/3CL-pro (PBB ID: 1P9U) in comparison to the FDA approved standard reference drugs (Oberadilol and Poziotinib).

		AutoDock v4.2.6			AutoDock vina			iGEMDOCK v2.1				
S. No.	Ligands	BE (kcal/mol)	K_d	Interacting amino acids	BE (kcal/mol)	K_d	Interacting amino acids	TE (kcal/mol)	VDW	HB	EI	Interacting amino acids
1.	Withaferin A	−7.56	2.87 μM	Thr47, Leu164, Pro188, Gln187, Glu165, Ser189, Met190, Gln191, Leu192, Asn168, Gly167, Leu166	−9.4	129.60 nM	Gly126, Leu3, Cys284, Glu286, Arg4, Phe287, Lys5, Tyr280, Ser282, Ser279, Lys136	−116.60	−96.85	−19.75	0	Thr288, Thr290, Glu291, Arg294, Val299, Thr143, Tyr117, Cys116, Gly122, Ala115, Ser123, Gln8, Val150, Leu151, Glu152, Met6, Ser110
2.	Withanolide A	−8.93	285.01 nM	Gly182, Gly183, Tyr184, Glu185, Leu192, Gln191, Met190, Ser189, Gln187, Val50	−10.9	345 nM	Leu3, Arg4, *Glu286,* Tyr280, Phe287, Lys5, *Cys284, Lys136,* Ser279	−100.1	−84.54	−15.56	0	Phe272, Gly271, Leu268, Lys270, Asn269, Ser282, Leu283, *Cys284,* Asp285, *Glu286, Lys136,* Met198, Asn196
3.	Withanolide B	−8.12	1.12 μM	Glu185, Gly183, Gly182, Tyr184, Ser189, Met190, Gln191, Leu192	−9.7	72.23 nM	Lys270, Arg267, Leu268, Trp217, Phe218, Arg275, Gln256, Arg216, Thr254, Gly214	−104.12	−93.39	−10.74	0	Gly154, Asn153, Leu151, Glu152, Gly122, Tyr117, Ser123, Ala115, Thr143, Met6, Ser138, Ile140, Gln295, Arg294, Gly298
4.	Withanolide D	−7.68	2.34 μM	Gly182, Tyr184, Glu185, Ser189, Met190, Gln191, Leu192, Glu193	−9.3	145.58 nM	Glu54, Asn52, Tyr53, Arg40, Tyr81, Met57, Gln132, Ser131, Arg80, Val197, Thr239, Gly83	−111.44	−98.83	−12.61	0	Gly154, Asn153, Leu151, Glu152, Gln8, Gly122, Ser123,Cys116, Tyr117, Ala115, Thr143, Ile140, Ser138, Gln295, Met6, Arg294
5.	Withanolide E	−7.72	2.19 μM	Glu185, Tyr184, Gly182, *Gln132,* Glu193, Gly194, Leu192, Gln191, Met190, Ser189	−9.0	240.98 nM	Lys82, Gly83, Lys234, Ser131, *Gln132,* Ala107, Glu54, Tyr81, Arg80, Met57, Val197, Arg40, Thr239, Glu240	−104.61	−85.73	−18.88	0	Met6, Asn112, Ser110, Gln8, Val150, Glu152, Glu109, Thr288, Glu291, Gln295, Thr290, Arg294
6.	Withanone	−7.41	3.7 μM	Glu193, Leu192, Gln191, Met190, Ser189, Glu185, Tyr184, Gly183, Gly182, Gln132	−9.1	212.78 nM	Thr254, Arg216, Trp217, Arg275, Phe218, Lys260, Gln256, Leu268, Arg267, Lys270	−109.22	−100.63	−8.59	0	Arg294, Gln295, Ile140, Glu291, Glu152, Gly122, Ala115, Ser123, Met6, Gln8, Ala7, Ser110, Phe111, Val150, Asn112, Tyr149
7.	Viscosalactone B	−7.34	4.14 μM	Leu192, Gly167, Leu166, Glu165, Leu164, Gln191, Met190, Ser189, Pro188, Gln187	−9.5	107.69 nM	*Lys5, Phe287, Glu286, Lys136,* Met198, Asp285, *Cys284,* Leu283, Ser282, *Arg4, Leu278, Ser279, Tyr280, Leu3*	−100.67	−85.43	−15.24	0	Tyr125, Met6, Gly126, *Lys5, Arg4, Leu3, Lys136, Leu278, Ser279, Tyr280, Cys284, Glu286, Phe287*
8.	Anaferine	−6.19	29.14 μM	Gly183, Glu185, Tyr184, Gly182, Gln191, Leu192, Glu193, Gln132	−6.8	10.34 μM	Arg294, Gln295, Glu291, Gln8, Ser110, *Lys5, Gly126,* Ala7, Met6, Ser123, Gly122	−74.07	−60.38	−13.68	0	Tyr280, Leu3, Arg4, *Lys5,Gly126,* Tyr125, Val124
9.	Withasomnine	−6.06	36.09 μM	Tyr53, Ile51, Ser189, Gln191, Gln187, Pro188, Asp186, Thr47, **His41,** Leu164, Glu165	−7.1	6.20 μM	Arg294, Met6, Gln295, Glu291, Lys5, Asn112, Phe111, Gln8, Val150, Ser110, Leu151	−71.58	−63.14	−8.44	0	Ala79, Val60, Gly194, Met57, Ser58, Glu193, Gln132, Val197, Arg80, Thr195
10.	Oberadilol	−4.54	469.45 μM	Glu185, Tyr184, Gly183, Gly182, Gln132, Glu193, Leu192, Gln191, Met190, Ser189	−8.7	401.24 nM	Glu54, Tyr53, Arg40, Gly83, Val197, Arg80, Ser131, Thr239, Ala107, Glu240, Lys234, Lys82, Tyr81	−95.18	−81.58	−13.60	0	Trp217, Arg267, Leu268, Lys270, Phe272, Gly271, Gly273, Gly274, Arg275, Val219
11.	Poziotinib	−6.41	20.18 μM	Thr195, Gly194, Glu193, Leu192, *Gln191,* Met159, Tyr184, Gly182, Gln132	−8.4	710.54 nM	Met190, Gly167, Leu166, Ser189, Glu165, Ala141, Ile140, Phe139, Cys144, Thr47, **His41,** Pro188, Leu164, Gln187, *Gln191*	−103.87	−94.39	−9.49	0	Arg275, Gly274, Gly273, Trp217, Thr220, Asn221, Gly271, Lys270, Thr222, Arg267, Leu263

Table 10. Binding energies of WS phytoconstituents with SARS-CoV-2 main protease/3CL-pro (PDB ID: 6LU7) in comparison to the FDA approved standard reference drugs (Oberadilol and Poziotinib).

		AutoDock v4.2.6			AutoDock vina			iGEMDOCK v2.1				
S. No.	Ligands	BE (kcal/mol)	K_d	Interacting amino acids	BE (kcal/mol)	*Kd*	Interacting amino acids	TE (kcal/mol)	VDW	HB	EI	Interacting amino acids
1.	Withaferin A	−2.85	8.21 mM	Tyr126, Gln127, Gly138, Va171, Gly170, Lys137, Lys5	−8.4	670.89 nM	Arg105, Ile106, Val104, Ser158, Phe294, Phe112, Phe8, Thr111, Asp295, Asn151, Gln110, Thr292, Gln107	−98.51	−78.64	−19.87	0	Gly143, **Ser144, Cys145, His163, Met165, Glu166, Gln189, Thr190,** Asn142, Leu141, Phe140
2.	Withanolide A	−5.26	139.0 μM	Lys5, Gln127, Tyr126, Val125, Ser139, *Lys137*, Glu288, Glu290	−8.5	592.38 nM	Asp289, Thr199, Glu290, Arg131, *Lys137,* Tyr239, Leu272, Leu287, Leu286, Met276, Gly275	−91.61	−70.18	−21.43	0	Gly179, Asn180, Phe181, Asn84, Cys85, Arg40, Phe185, Tyr54, Asn53, Pro52, **Arg188**
3.	Withanolide B	−5.67	69.79 μM	Ser139, Gly138, *Lys137,* Cys128, *Glu290,* Gln127, Tyr126, Val125	−8.3	845.65 nM	Leu287, Tyr239, Tyr237, Leu272, Leu286, Asn238, Thr199, Asp289, Glu288, Arg131, *Glu290, Lys137*	−89.17	−72.53	−16.64	0	**His163, His164, Met165, Cys145, Ser144,** Phe140, Leu141, Asp142, Gly143, Thr25, Met149, Thr45, Ser46, Thr24
4.	Withanolide D	−5.55	85.19 μM	Tyr126, Gln127, Gly138, Ser139, His172, Gly170, *Lys137,* Lys5	−8.7	424.04 nM	Tyr239, Leu287, Val204, Leu272, Tyr237, Asn238, Arg131, *Lys137,* Thr199, Leu286, Asp289	−104.35	−85.29	−19.06	0	Thr26, Leu27, **Cys145,** Gly143, **Ser144, His164,** Asn142, **Met165, Glu166,** Pro168, Thr190, **Gln189, Arg188, Met49,His41**
5.	Withanolide E	−5.2	154.68 μM	Tyr126, Gln127, Lys5, Glu290, *Lys137,* Gly138, Ser139	−8.1	1.16 μM	Asn238, Asp289, Arg131, *Lys137,* Thr199, Leu286, Leu287, Tyr239, Leu272, Tyr237	−97.42	−70.98	−26.44	0	Arg131,Asn133, Ala194, Gly195, Asp289, Asp197, Thr196, Thr199, Thr198, Asn238
6.	Withanone	−6.14	31.77 μM	Val125, Tyr126, Gln127, Cys128, Ser139, Gly138, *Lys137,* Ala129, Glu290	−8.4	707.34 nM	Leu286, Tyr239, *Lys137,* Asp197, Arg131, Thr198, Thr199, Asn238, Tyr237, Met276, Gly275, Leu272, Leu271, Leu287	−100.18	−88.69	−11.49	0	Thr24, Thr25, Thr26, **His41**, Gly143, **Cys145, Ser144, His164, His163,** His172, Phe140, **Glu166,** Leu141, Asn142, **Met49,** Ser46
7.	Viscosalactone B	−4.86	274.4 μM	Val104, Asn151, Phe8, Arg298, Gln127, Asp295, Phe294, Thr111, Thr292, Gln110, Gln107, Ile106, Arg105	−8.2	969.04 nM	*Gly278,* Lys137, Asp289, Arg131, *Tyr239, Thr199, Leu287, Leu286,* Leu272, *Gly275, Met276, Asn274,* Asn277	−97.17	−67.45	−29.72	0	*Tyr239,* Asn238, Tyr237, *Thr199, Leu287, Leu286,* Ala285, *Gly278, Asn277, Met276,Gly275*
8.	Anaferine	−5.13	174.99 μM	Glu290, Cys128, Lys5, Gln127, Tyr126, Lys137	−5.7	66.02 μM	***Cys145,*** Asn142, *Leu141, Phe140,* ***Glu166, Ser144,*** *His172,* ***Met165,*** **His164, Gln189, Asp187, Arg188, Met49, His41**	−76.27	−67.75	−8.52	0	Thr25, Thr26, Leu27, ***Cys145,*** **His163,** ***Met165, Glu166,*** *His172, Phe140, Leu141,* ***Ser144,*** Gly143
9.	Withasomnine	−5.22	149.2 μM	Ser158, *Ile152, Asp153, Asn151, Thr111,* Asp295, *Phe294,* Thr292, *Gln110*	−6.2	28.68 μM	*Ile152,* Phe8, Val104, Ile106, *Gln110, Thr111, Asn151, Asp153, Phe294*	−71.96	−60.03	−11.94	0	**His41, His163, His164, Met165, Cys145, Ser144,** His172, **Glu166,** Phe140, Leu141
10.	Oberadilol	−2.23	23.18 mM	*Lys137,* Glu290, Gln127, Tyr126, Lys5	−6.9	9.00 μM	Leu286, Tyr239, *Lys137,* Asp197, Arg131, Thr198, Thr199, Asn238, Tyr237, Met276, Gly275, Leu272, Leu271, Leu287	−100.96	−94.41	−6.55	0	**His163, Cys145, His164, Met165,** Asn142, **Glu166,** Leu141, **Leu167,** Pro168, **Gln189, Met49, Asp187, His41**
11.	Poziotinib	−4.49	513.87 μM	Tyr126, Gln127, Cys128, Lys5, Ala129, Glu290, *Lys137,* Gly138, Ser139	7.7	2.20 μM	Gly278, Ala285, Gly275, Tyr237, Leu272, Asn238, Tyr239, Thr199, Asp289, Arg131, Leu286, *Lys137,* Leu287, Met276	−111.32	−96.66	−14.66	0	**His41, Cys145, His164, Asp187, Arg188, Met165, Gln189, Glu166, Thr190, Ala191, Gln192,** Pro168, Phe140, Leu141, Asn142

Table 11. Binding energies of WS phytoconstituents with Nsp-10/Nsp-16 complex from SARS-CoV-2 (PDB ID: 6W75) in comparison to the FDA approved standard reference drugs (Losartan and Hydroxychloroquine).

		AutoDock v4.2.6			AutoDock vina			iGEMDOCK v2.1				
S. No.	Ligands	BE (kcal/mol)	K_d	Interacting amino acids	BE (kcal/mol)	K_d	Interacting amino acids	TE (kcal/mol)	VDW	HB	EI	Interacting amino acids
1.	Withaferin A	−9.33	144.58 nM	Asp6906, Asn7095, Ser6907, Thr6908, Leu7093, Leu6909, Val7092, Ser7089, Ser7090, Val7092	−10.0	40.98 nM	*Lys6968, Glu7001, Ser6999, Thr6970, Ser7000, Asn6996, Lys6844, Asn6841, Tyr6930, Gly6871, Asp6928,* Pro6932, *Ser6872,* Met6929, Gly6869, Leu6898, Asp6897, Asn6899	−99.04	−82.04	−17	0	Tyr6828, *Ser6999, Ser7000, Thr6970, Glu7001, Asn6996, Lys6844, Lys6968, Asn6841, Asp6928, Tyr6930, Gly6871, Ser6872*
2.	Withanolide A	−10.38	24.67 nM	Ala6905, Asp6906, Lys4346, Ser6907, Thr6908, Leu6909, Ile6910, Ser7090, Leu7093, Val7092, Ser7090	−10.4	23.67 nM	*Pro6932,* Tyr6930, *Asn6899, Asp6931, Leu6898, Asp6897, Met6929, Gly6869,* Ser6872, *Gly6871,* Asn6841, Lys6844, Lys6968, Glu7001, Thr6970, Ser6999	−101.39	−78.76	−22.63	0	*Gly6871, Gly6869, Asn6899, Asp6897, Leu6898,* Asp6912, Cys6913, Phe6947, *Asp6931,* Lys6933, *Pro6932, Met6929,* Asp6928
3.	Withanolide B	−10.09	39.9 nM	Lys4346, Cys4330, His4333, Val6902, Ser6903, Phe6901, Asp6900, Thr6908, Ile6910, Leu6909, Val7092, Ser7090	−11.0	1.98 nM	Lys6844, Asn6841, Asp6928, Lys6968, Tyr6930, Gly6871, Gly6869, Asp6931, Leu6898, Cys6913, Met6929, Phe6947, Asp6897, Asn6899, Ser6872, Pro6932	−103.08	−95.57	−7.51	0	Val4274, Ile4334, Asp4335, Ile4334, Cys4332, Arg4331, Thr4292, Ile4291, Pro4290, Gln4289, Ala4271, Phe4272, Ala4273
4.	Withanolide D	−9.58	94.36 nM	Val7092, Ser7089, Ser7090, Asp7091, Leu6909, Thr6908, Ser6907, *Asp6906, Lys4346*	−10.5	27.89 nM	Lys6844, Asn6841, Asp6928, Ser6872, Tyr6930, Gly6871, Met6929, Gly6869, Leu6898, Asp6897, Asp6899, Pro6932, Asp6931, Lys6968, Thr6970, Glu7001, Ser6999	−110.77	−85.34	−25.43	0	Gly4341, Phe4342, Cys4343, *Asp6906, Lys4346,* Gly4347, Lys4348, Val4310, Arg6884, Thr6889, Gly6890, Asn7096
5.	Withanolide E	−8.96	272.55 nM	*His4333*, Phe6901, Val6902, Leu6909, Ser6903, Thr6908, Lys4346, Ser6907, Asp6906, Val7092	−9.8	62.56 nM	*His4333,* Cys4332, Phe4272, Thr4292, Ile4291, Ala4271, Gln4289, Asn4293, Arg4331, Val6876, Lys6874, Gly6875, Val6902	−104.92	−92.21	−12.72	0	Tyr7020, Leu6820, Glu6821, Lys6822, Asp6942, Trp6974, Asn6941, Glu6940, Glu6971, His6972, Lys6939
6.	Withanone	−10.17	34.9 nM	Cys4330, His4333, Val6901, Asp6900, Phe6901, Thr6908, *Ile6910, Leu6909, Ser7090, Val7092*	−9.8	63.56 nM	*Val7092,* Asp7091, Thr6915, Leu7093, Asp6912, Gly6911, Leu6898, Ser7089, *Ile6910, Leu6909,Ser7090*	−105.42	−91.03	−14.39	0	Ala4273, Cys4332, Val4274, Ile4334, Ala4276, Asp4335, Pro4337, Tyr4329, His4336, Asn4338, Pro4339
7.	Viscosalactone B	−9.03	238.8 nM	*Asp6900,* Leu7093, *Val7092,* Gly6911, Asp7091, *Ser7090, Ile6910, Leu6909, Thr6908,* Ser6907, Asp6906	−9.9	57.78 nM	His4336, *Ile4334, Asp4335, Tyr4329,* Cys4330, His4333, Val6902, *Ile6910, Asp6900, Val7092, Leu6909,* Ser7089, *Ser7090, Thr6908*	−119.11	−103.53	−15.58	0	Thr4292, Ile4291, Pro4290, Gln4289, Tyr4283, Ala4271, Phe4272, Arg4331, Cys4332, *Ile4334, Asp4335, Tyr4329,* Val4274, Ala4273
8.	Anaferine	−7.1	6.25 μM	Asp4335, Asp6900, Phe6901, Ile6910, Thr6908	−6.3	22.67 nM	Leu6819, Tyr7020, Val7021, Asp7018, Leu6820, Met6818, Arg6817	−86.35	−74.35	−12	0	Gly6911, Asp6912, Cys6913, Phe6947, Leu6898, Asp6897, Gly6871, Gly6869, Met6929, Tyr6930, Asp6928, Phe6947
9.	Withasomnine	−6.06	36.03 μM	Val7092, Asp7091, Ser7090, Ile6910, Leu6909, Ser7089	−8.0	1.23 μM	Tyr7020, Leu6820, Met6818, Leu6819, Ala7024, Arg6817, Val7021, Asp7018	−74.52	−65.96	−8.56	0	Thr4292,Arg4331, Ile4291, Pro4290, Gln4289, Tyr4283, Phe4272, Ala4271,
10.	Losartan	−6.49	17.54 μM	Thr6908, Leu6909, Ile6910, Asp6900, Ser7090, Ser7089, Val7092	−8.3	780.68 nM	Ala4273, Val4274, Asp4335, His4333, Ala4271, Ile4334, Pro4290, Gln4289, Thr4292, Ile4291, Cys4332, Phe4272, Arg4331, Gly6875, Lys6874, Val6876	−104.17	−75.33	−28.84	0	Gln6957, Gln6956, Glu7062, Lys6958, Lys6921, Ile7080, Leu6959, Leu6961, Tyr7009, Ile6955, His6984
11.	Hydroxychloroquine	−4.93	244.14 μM	Thr6908, Ile6910, Ser6907, Leu6909, Ser7090, Ser7089, Val7092	−6.7	11.70 μM	*Gly6869, Gly6871,* Asn6841, *Tyr6930, Pro6932, Ser6872,* Asp6873, *Asn6899, Asp6897,Leu6898, Met6929*	−80.22	−69.44	−10.78	0	Lys6968, Asp6928, *Gly6871, Gly6869, Met6929, Asp6897,A sn6899, Leu6898, Tyr6930, Pro6932, Ser6872*

Table 12. Best docking poses of human and viral target proteins with selected WS phytoconstituents.

Ligands	AutoDock v4.2.6	AutoDock vina	iGEMDOCK v2.1

12.1. Best docking poses of WS phytoconstituents with human ACE2 receptor (PDB ID: 1O8A) in comparison to the FDA approved standard reference drugs (Arbidol and Losartan)

Withaferin A

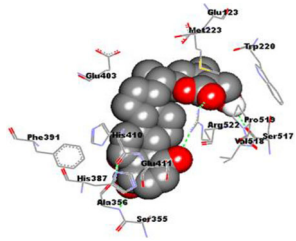
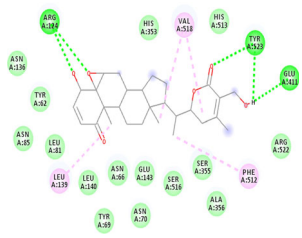
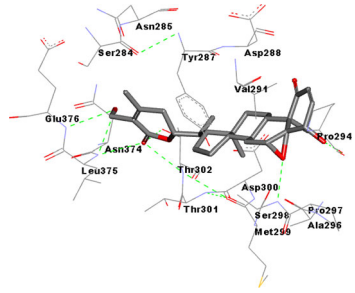

Withanolide A

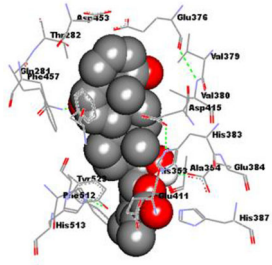
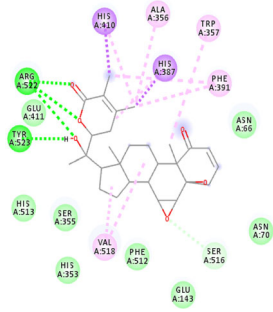
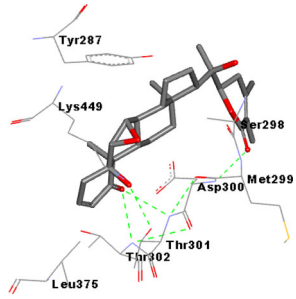

Withanolide B

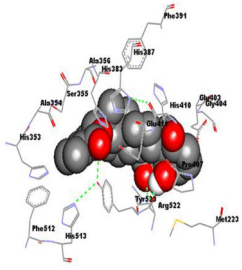
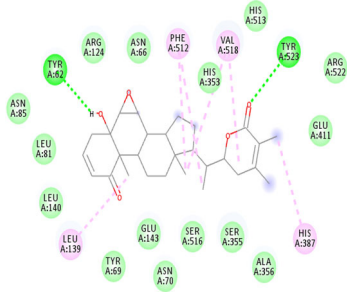
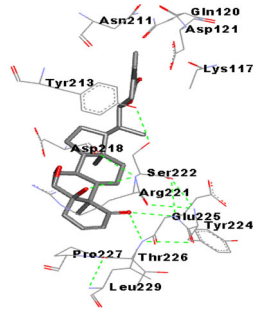

Withanolide D

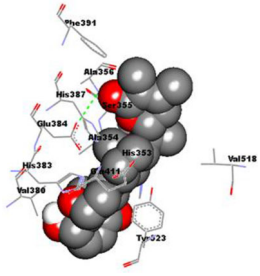
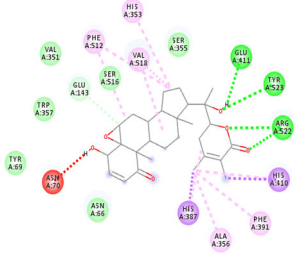
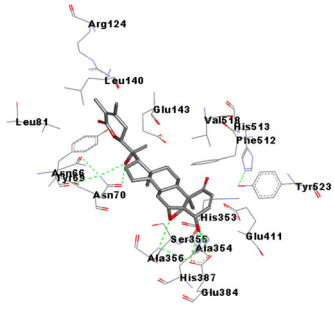

Withanolide E

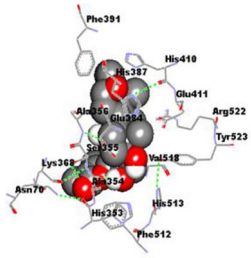
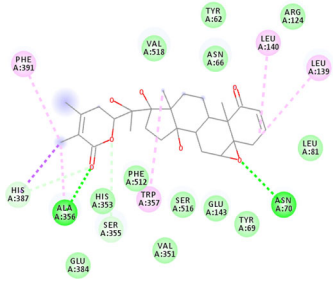
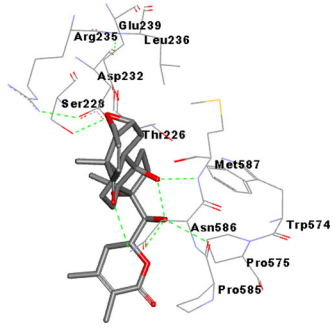

(*continued*)

Table 12. Continued.

Ligands	AutoDock v4.2.6	AutoDock vina	iGEMDOCK v2.1
Withanone	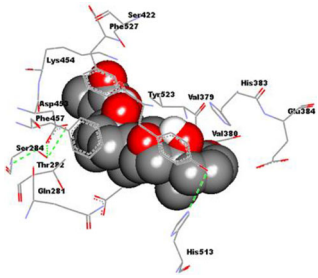	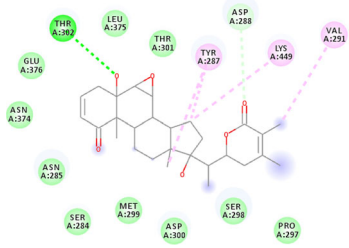	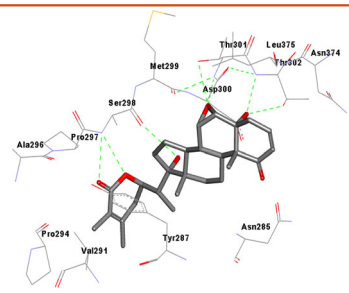
Viscosalactone B	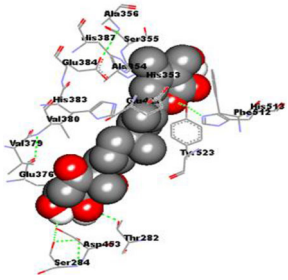	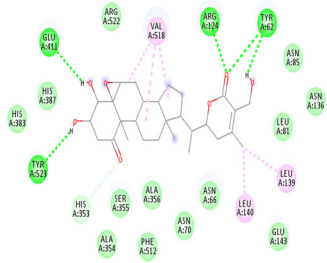	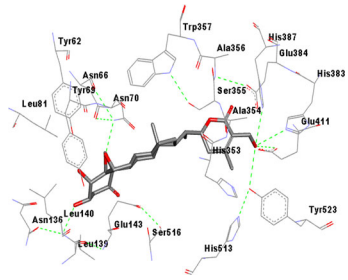
Anaferine	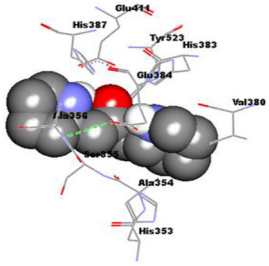	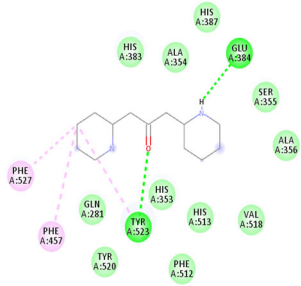	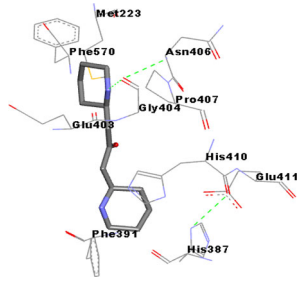
Withasomnine	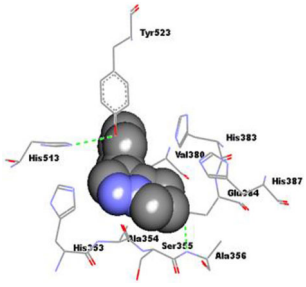	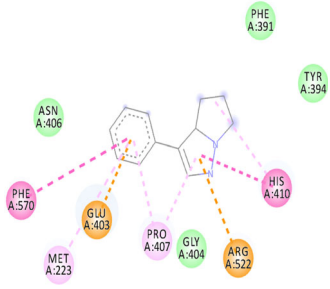	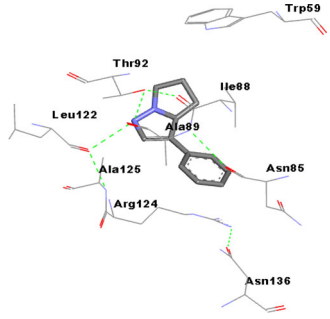
Arbidol	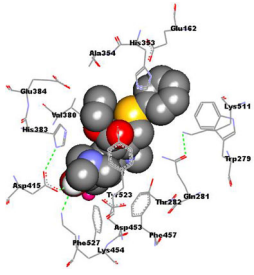	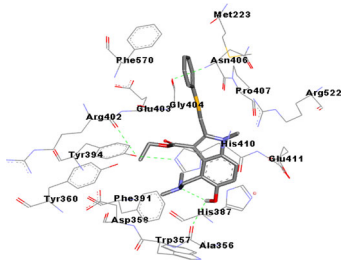	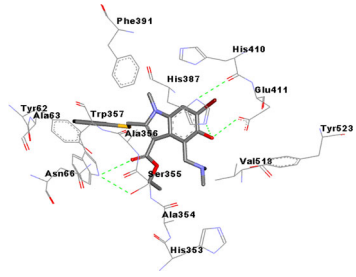

(*continued*)

Table 12. Continued.

Ligands	AutoDock v4.2.6	AutoDock vina	iGEMDOCK v2.1
Losartan	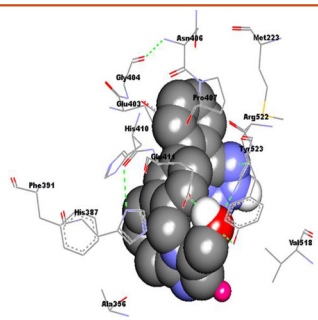	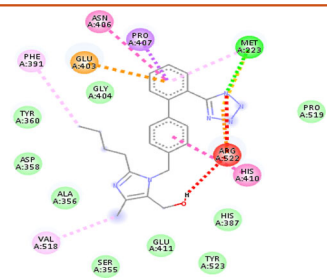	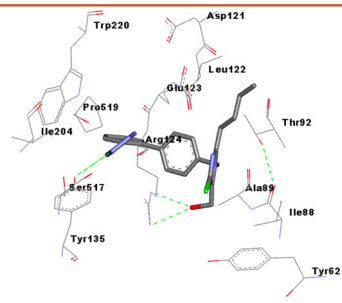

12.2. Best docking poses of WS phytoconstituents with SARS-CoV spike glycoprotein (PDB ID: 5WRG) in comparison to the FDA approved standard reference drugs (Arbidol and Hydroxychloroquine)

Withaferin A	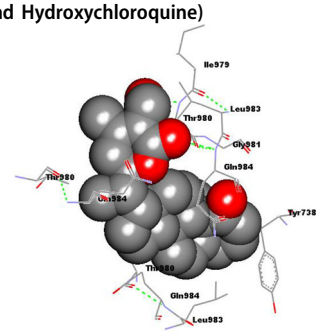	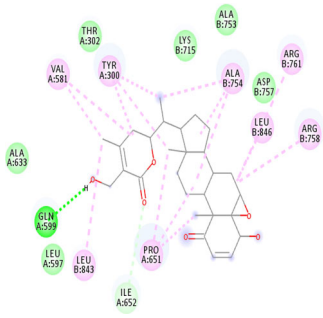	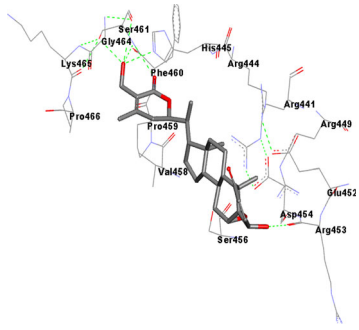
Withanolide A	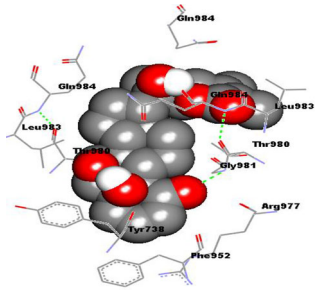	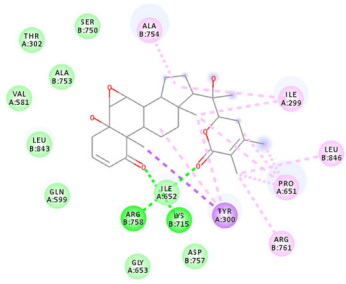	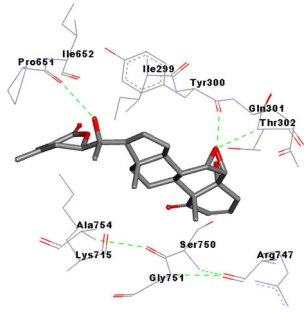
Withanolide B	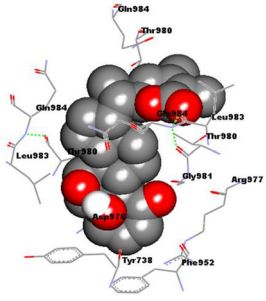	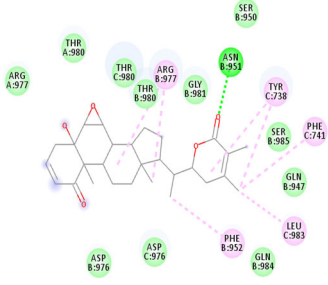	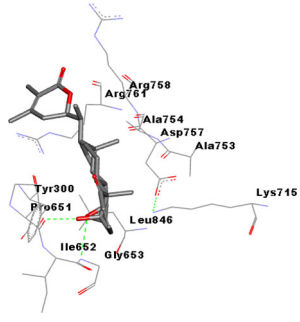
Withanolide D	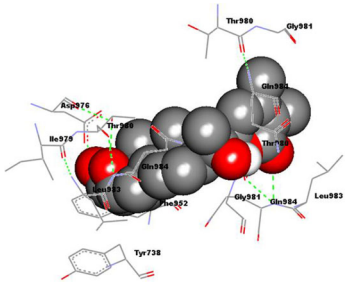	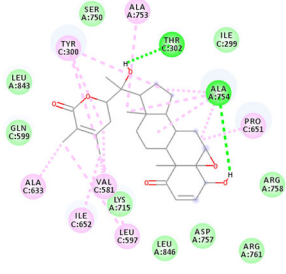	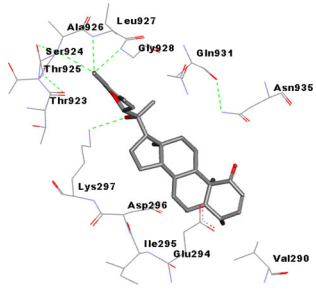

(*continued*)

Table 12. Continued.

Ligands	AutoDock v4.2.6	AutoDock vina	iGEMDOCK v2.1
Withanolide E	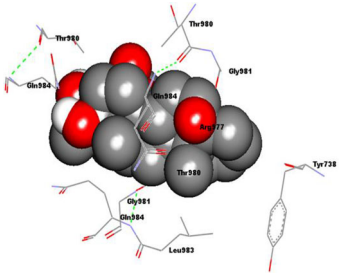	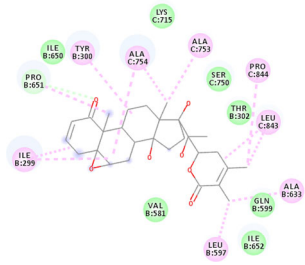	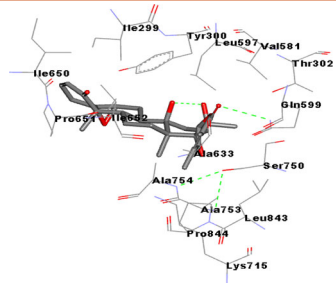
Withanone	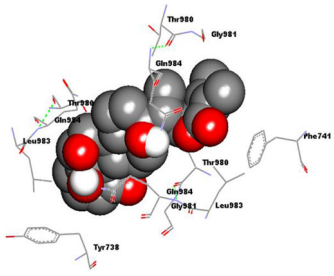	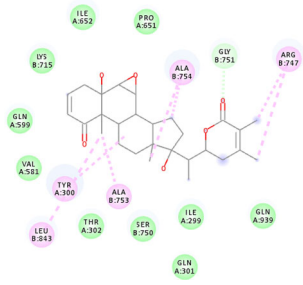	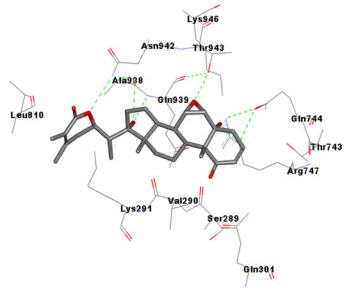
Viscosalactone B	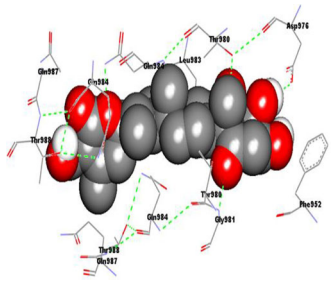	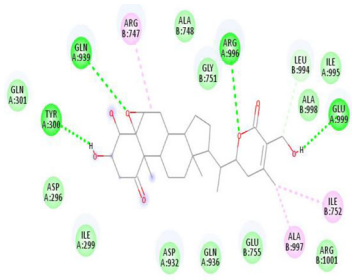	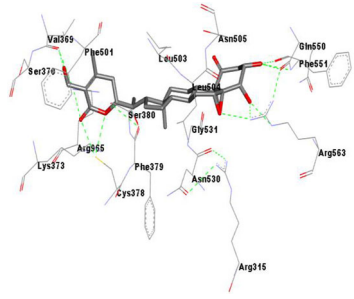
Anaferine	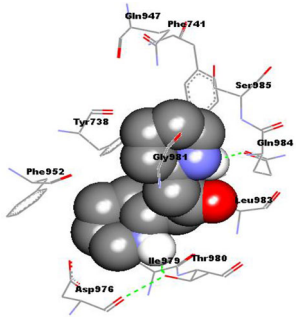	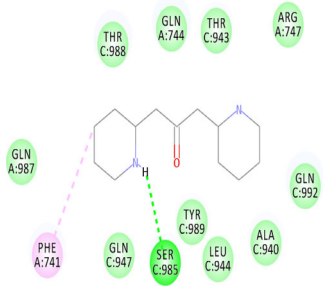	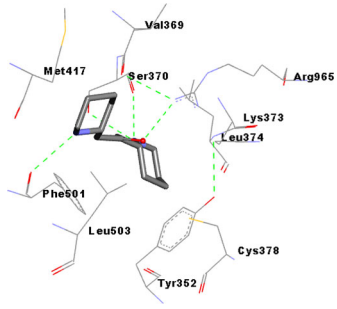
Withasomnine	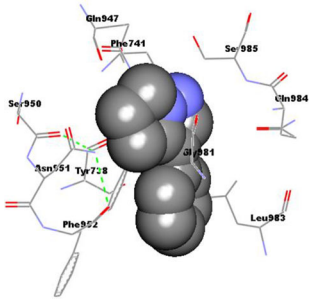	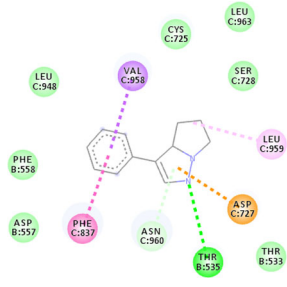	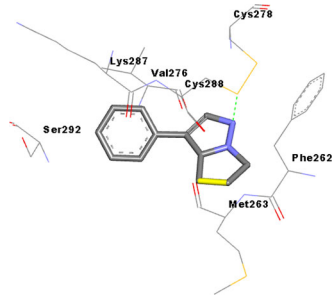

(*continued*)

Table 12. Continued.

Ligands	AutoDock v4.2.6	AutoDock vina	iGEMDOCK v2.1
Arbidol	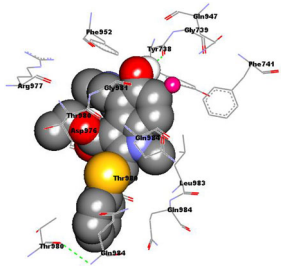	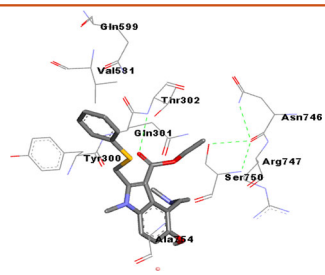	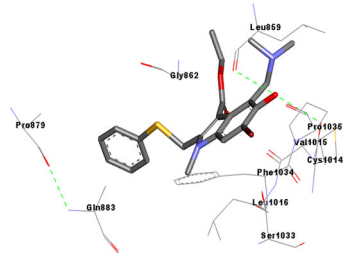
Hydroxychloroquine	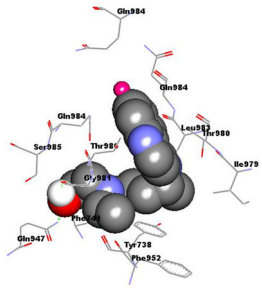	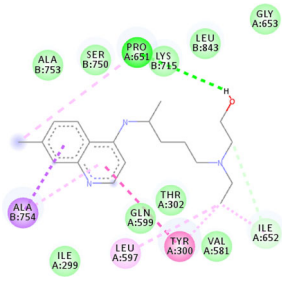	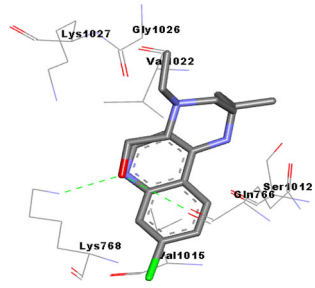

12.3. Best docking poses of WS phytoconstituents with SARS-CoV-2 spike glycoprotein (PDB ID: 6VXX) in comparison to FDA approved standard reference drugs (Arbidol and Hydroxychloroquine)

Withaferin A	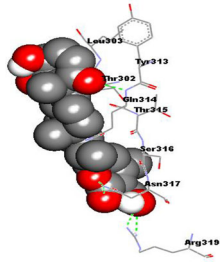	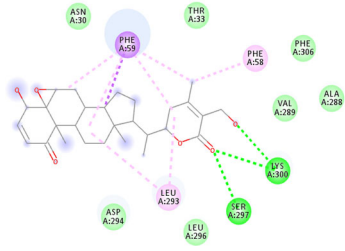	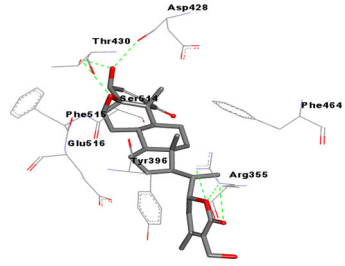
Withanolide A	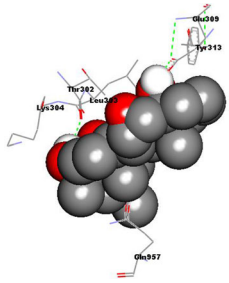	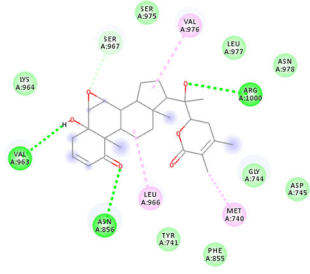	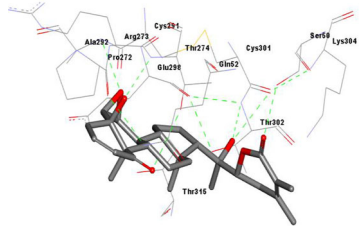
Withanolide B	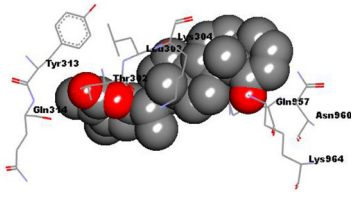	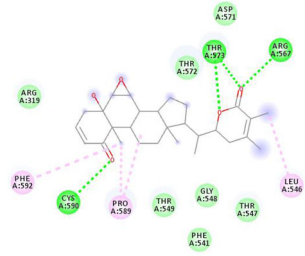	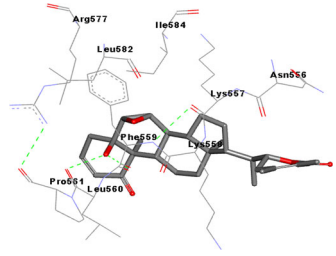
Withanolide D	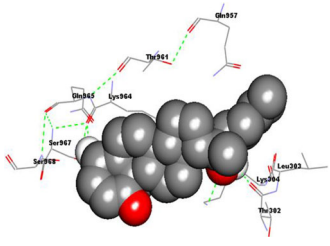	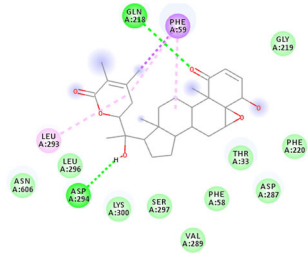	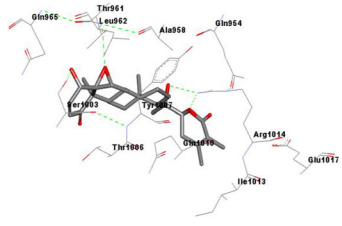

(*continued*)

Table 12. Continued.

Ligands	AutoDock v4.2.6	AutoDock vina	iGEMDOCK v2.1
Withanolide E	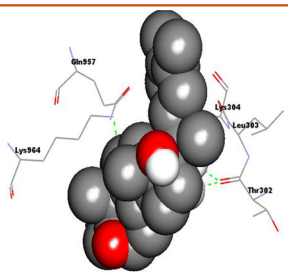	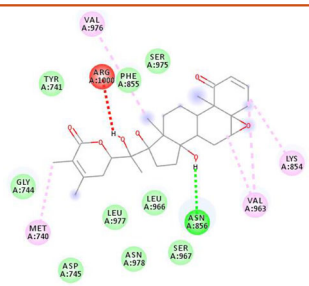	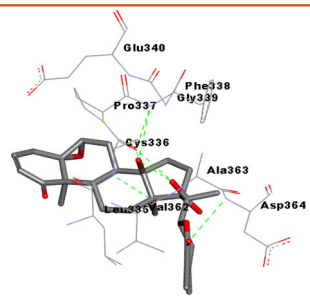
Withanone	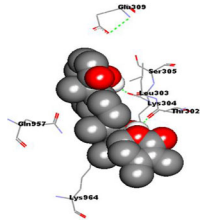	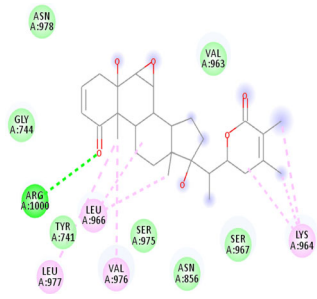	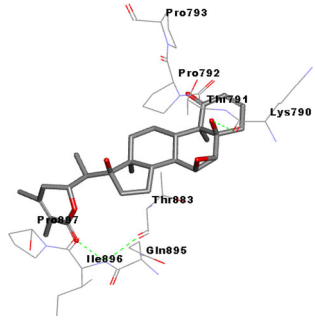
Viscosalactone B	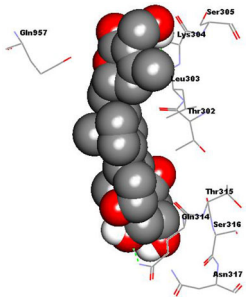	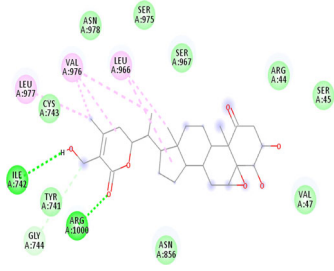	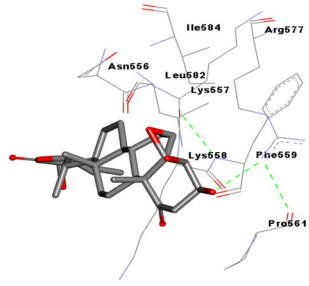
Anaferine	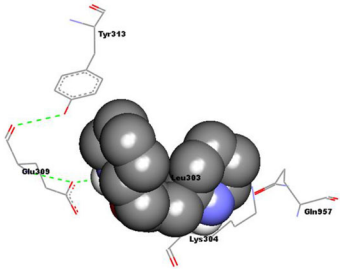	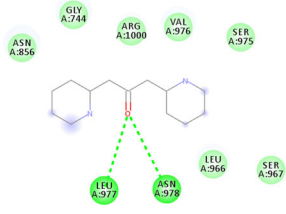	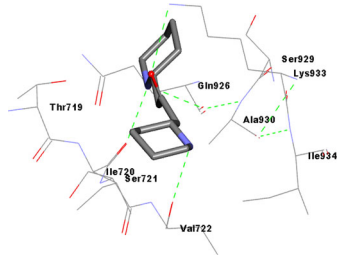
Withasomnine	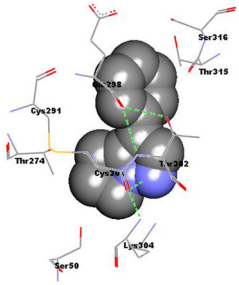	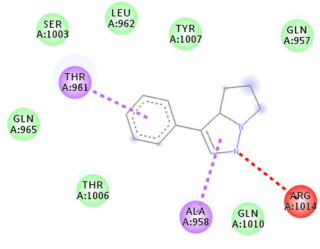	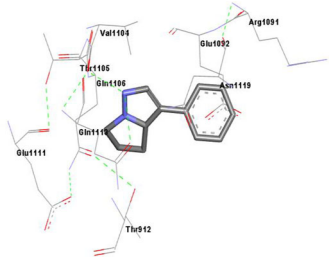

(*continued*)

Table 12. Continued.

Ligands	AutoDock v4.2.6	AutoDock vina	iGEMDOCK v2.1
Arbidol	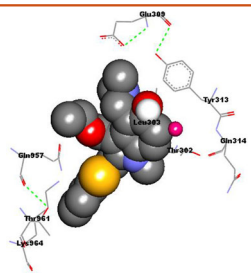	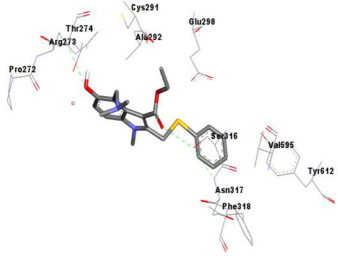	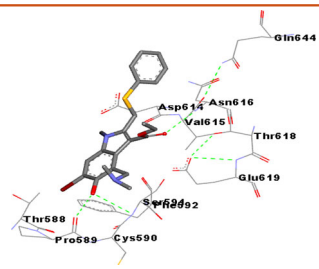
Hydroxychloroquine	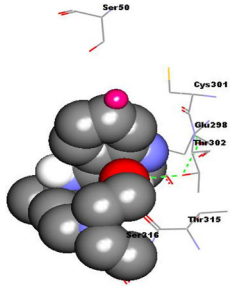	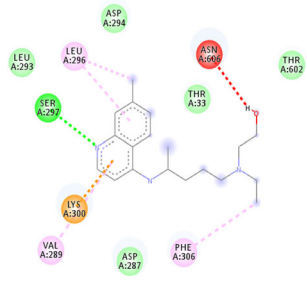	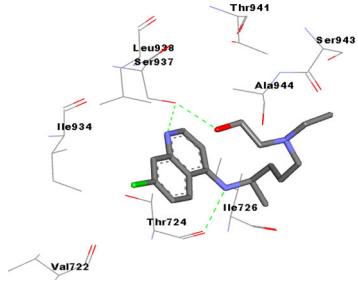

12.4. Best docking poses of WS phytoconstituents with papain like protease of SARS-CoV-2 (PDB ID: 6W9C) in comparison to the FDA approved standard reference drugs (Procainamide and Cinacalcet)

Withaferin A	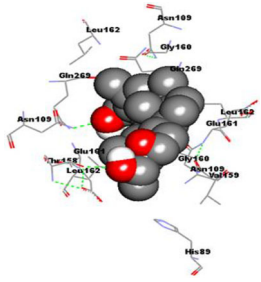	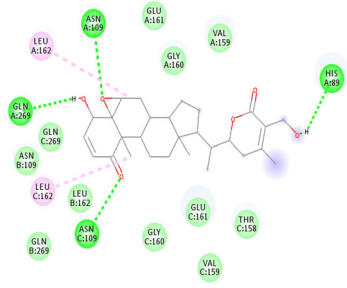	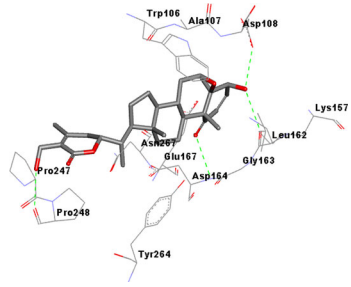
Withanolide A	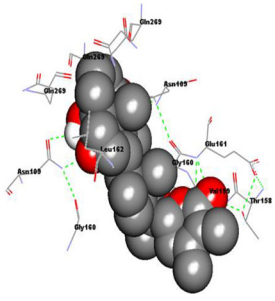	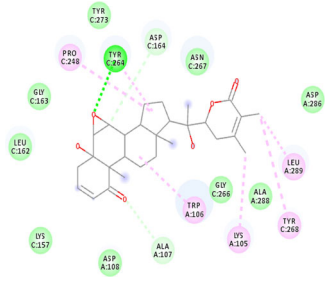	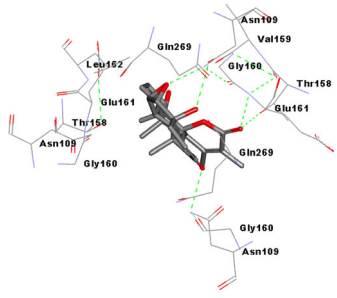
Withanolide B	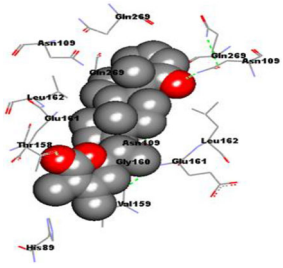	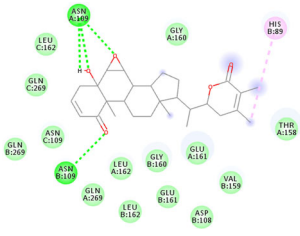	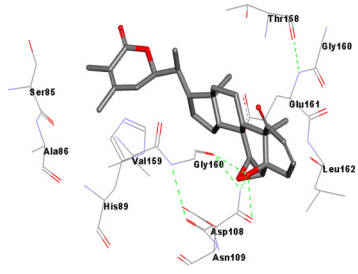

(*continued*)

Table 12. Continued.

Ligands	AutoDock v4.2.6	AutoDock vina	iGEMDOCK v2.1
Withanolide D	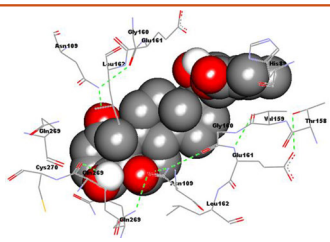	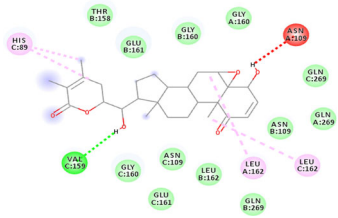	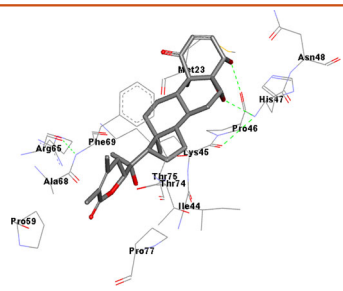
Withanolide E	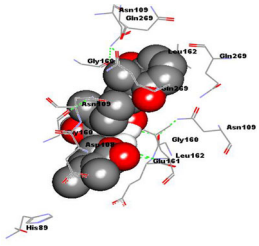	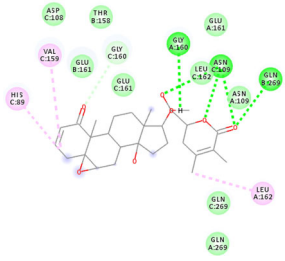	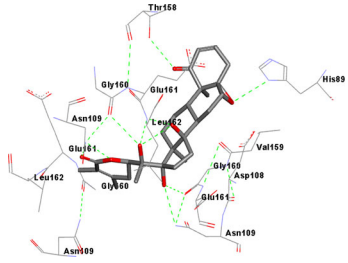
Withanone	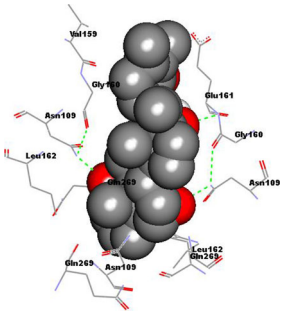	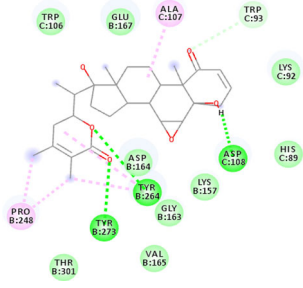	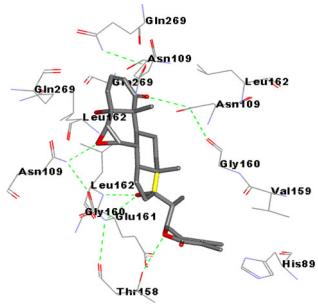
Viscosalactone B	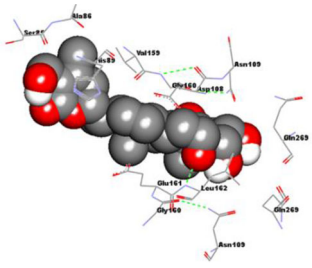	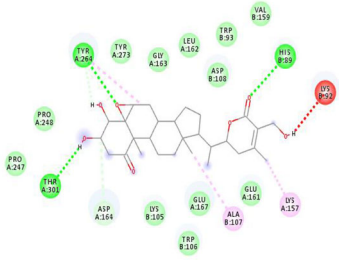	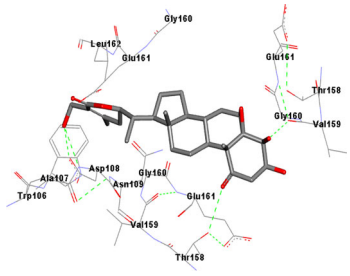
Anaferine	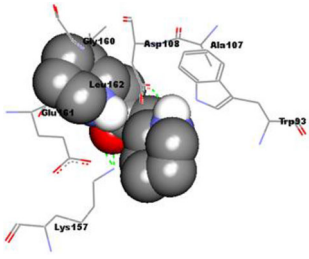	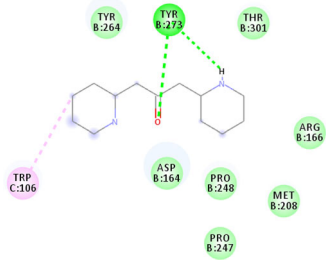	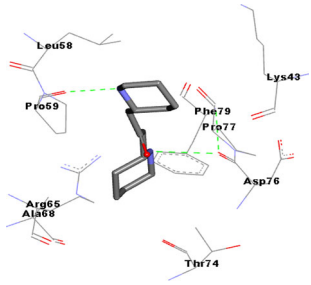
Withasomnine	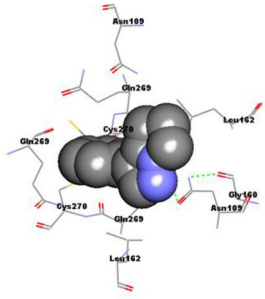	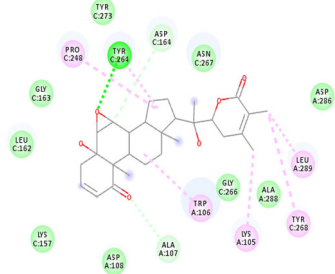	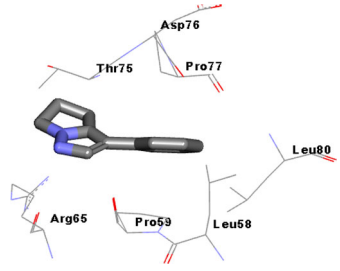

(*continued*)

Table 12. Continued.

Ligands	AutoDock v4.2.6	AutoDock vina	iGEMDOCK v2.1
Procainamide	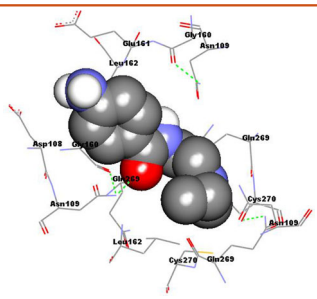	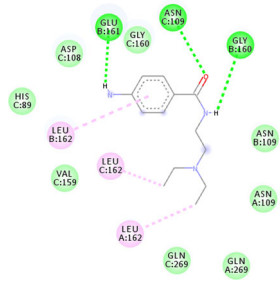	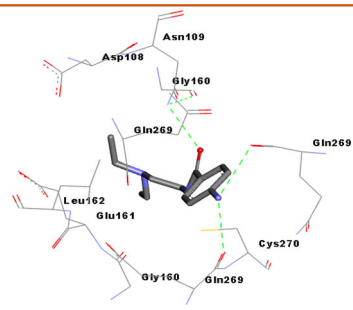
Cinacalcet	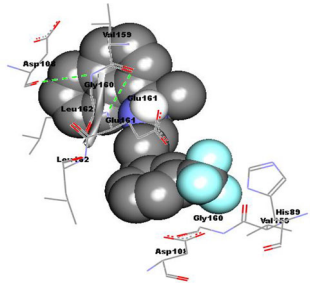	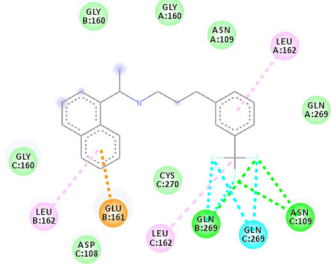	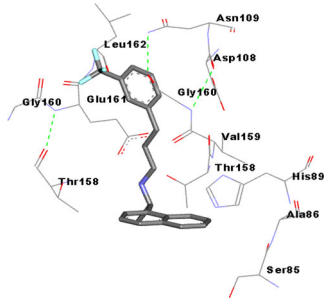

12.5. Best docking poses of WS phytoconstituents with SARS-CoV main protease/3CL-pro (PBB ID: 1P9U) in comparison to the FDA approved standard reference drugs (Oberadilol and Poziotinib)

Withaferin A	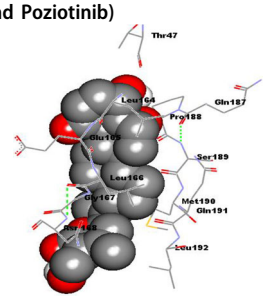	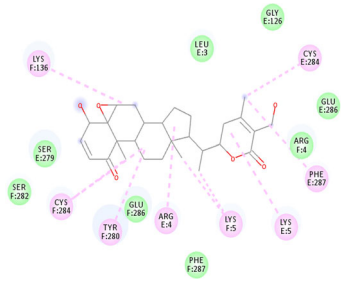	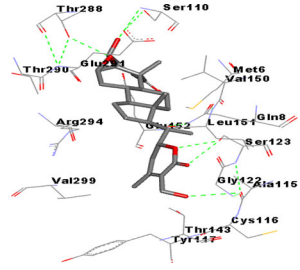
Withanolide A	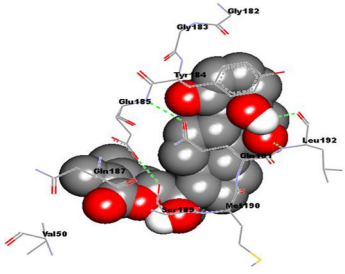	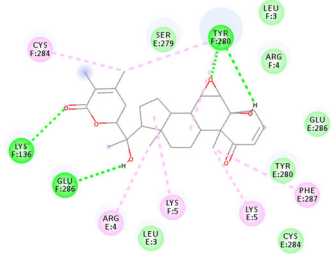	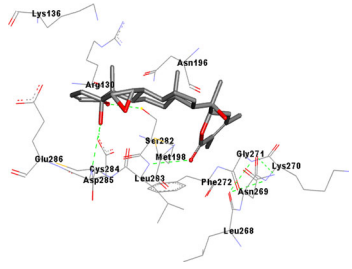
Withanolide B	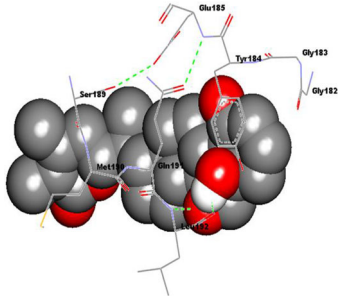	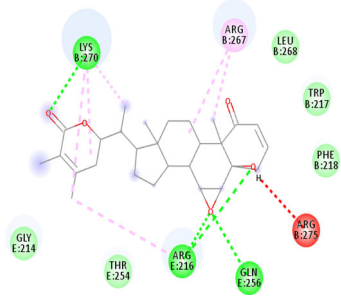	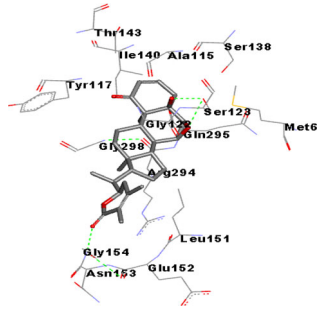

(*continued*)

Table 12. Continued.

Ligands	AutoDock v4.2.6	AutoDock vina	iGEMDOCK v2.1
Withanolide D	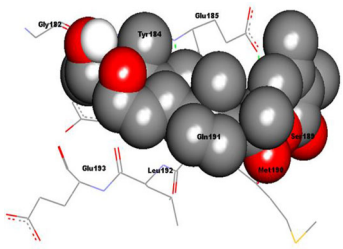	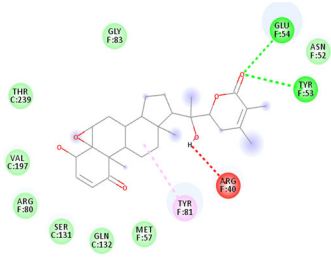	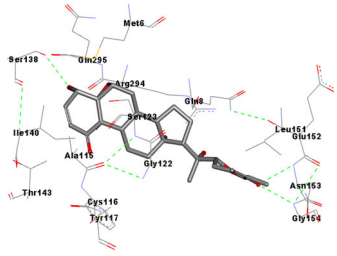
Withanolide E	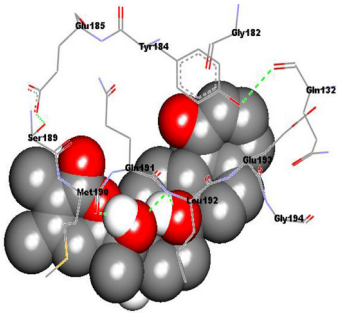	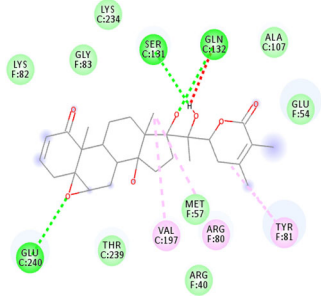	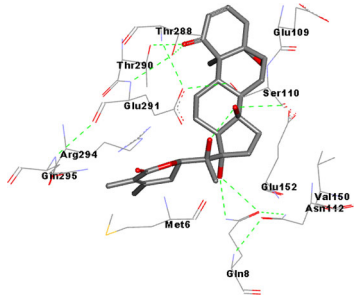
Withanone	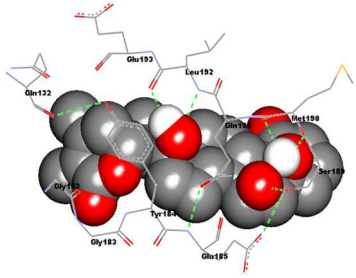	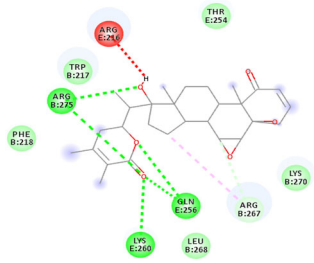	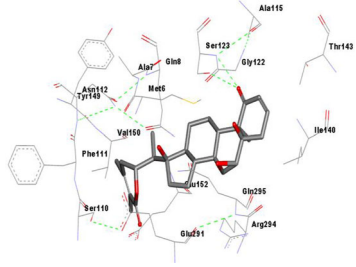
Viscosalactone B	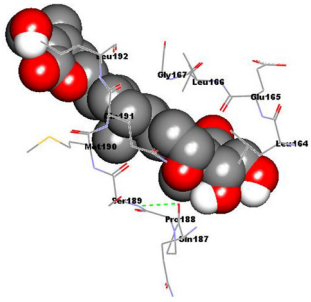	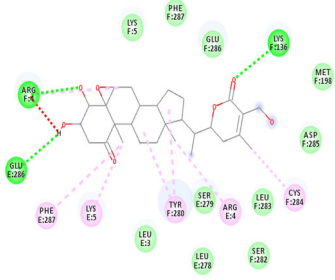	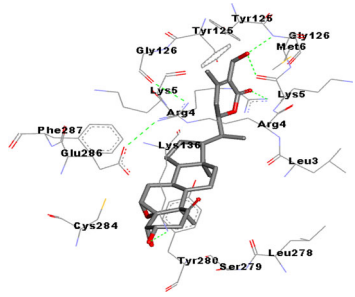
Anaferine	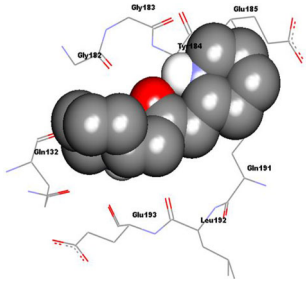	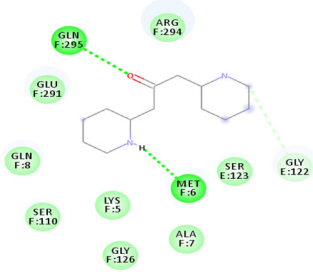	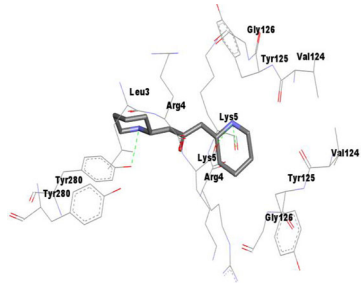

(*continued*)

Table 12. Continued.

Ligands	AutoDock v4.2.6	AutoDock vina	iGEMDOCK v2.1
Withasomnine	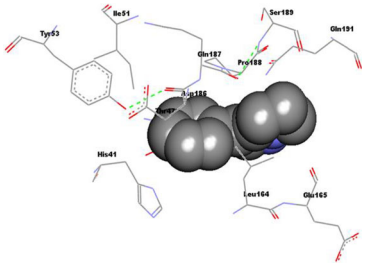	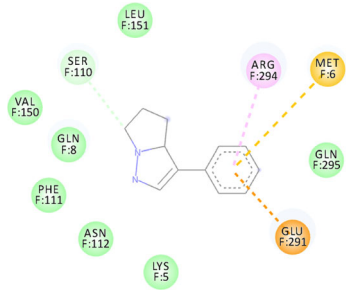	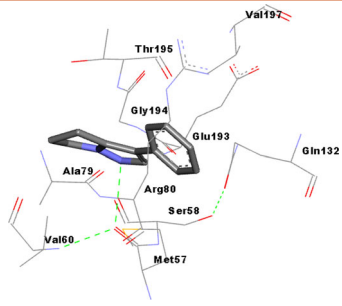
Oberadilol	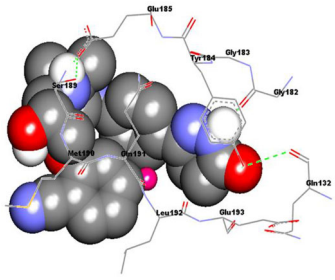	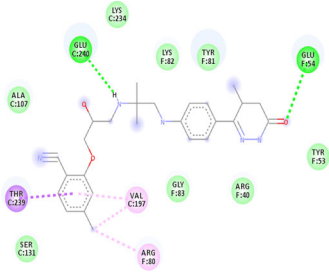	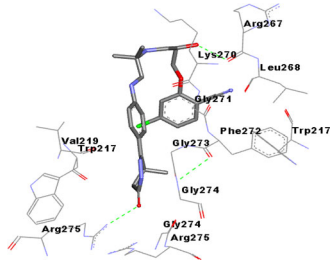
Poziotinib	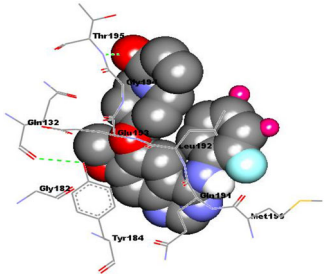	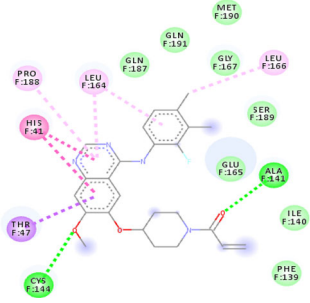	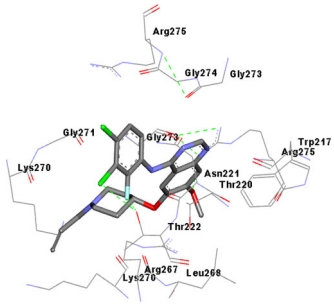

12.6. Best docking poses of WS phytoconstituents with SARS-CoV-2 main protease/3CL-pro (PDB ID: 6LU7) in comparison to the FDA approved standard reference drugs (Oberadilol and Poziotinib)

Withaferin A	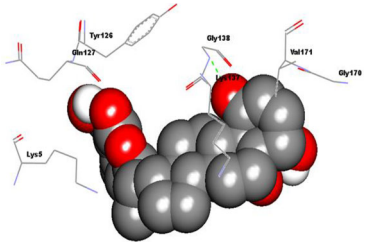	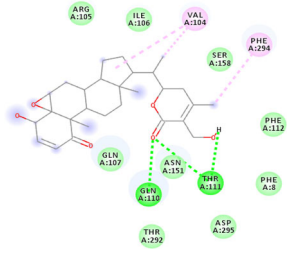	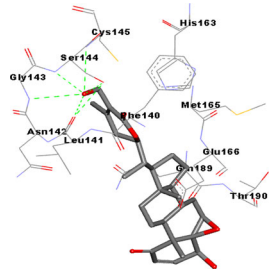
Withanolide A	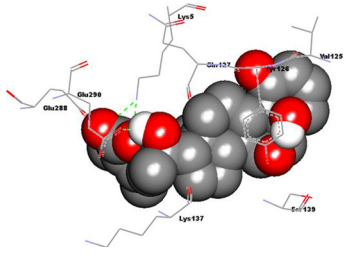	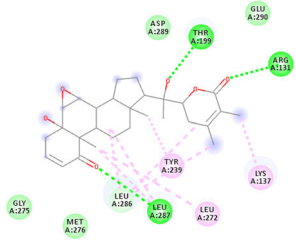	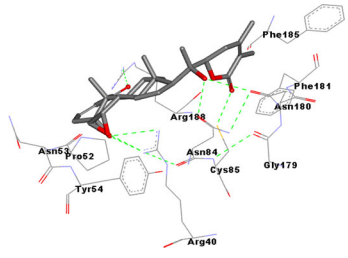

(*continued*)

Table 12. Continued.

Ligands	AutoDock v4.2.6	AutoDock vina	iGEMDOCK v2.1
Withanolide B	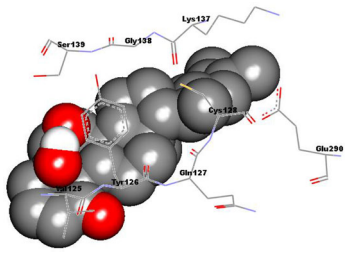	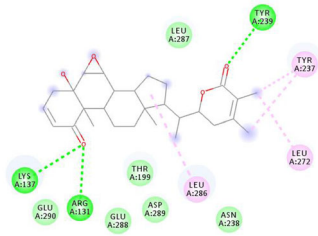	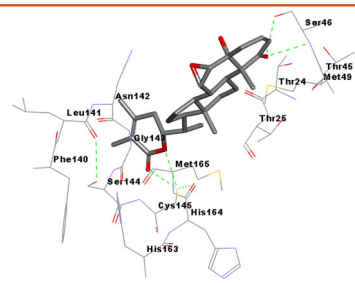
Withanolide D	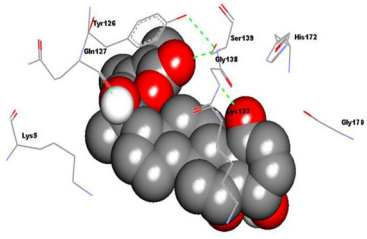	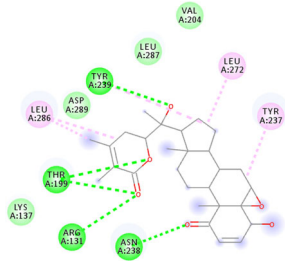	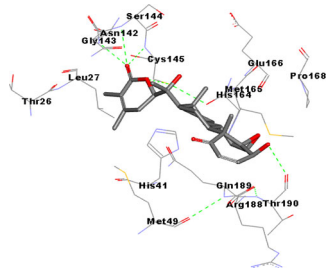
Withanolide E	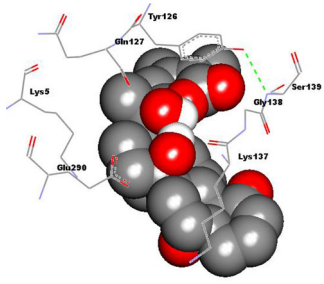	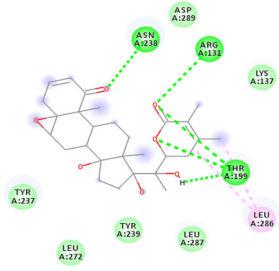	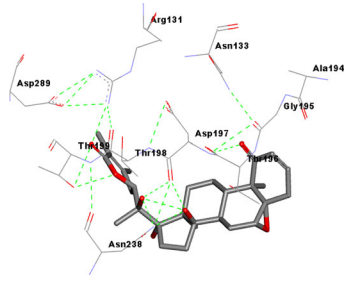
Withanone	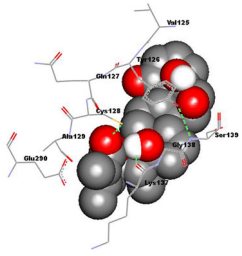	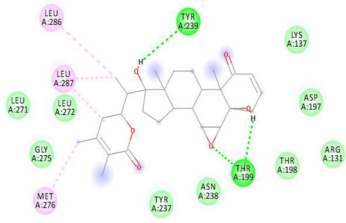	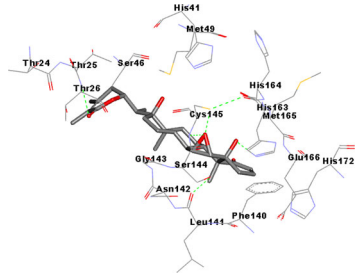
Viscosalactone B	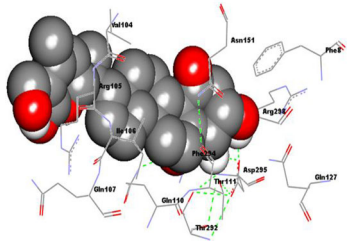	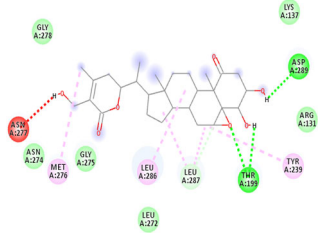	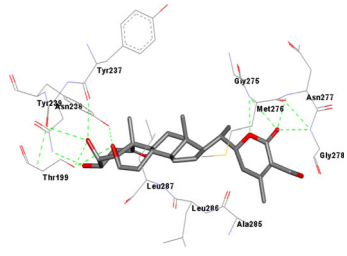
Anaferine	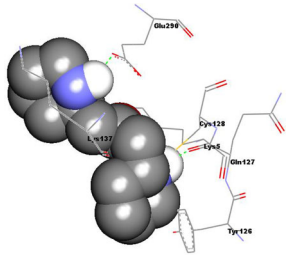	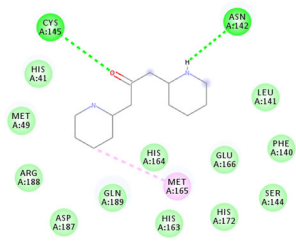	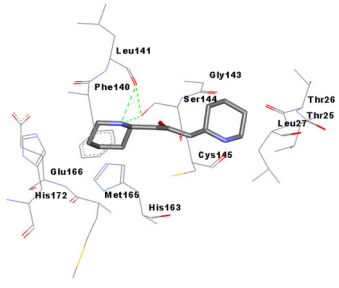

(*continued*)

Table 12. Continued.

Ligands	AutoDock v4.2.6	AutoDock vina	iGEMDOCK v2.1
Withasomnine	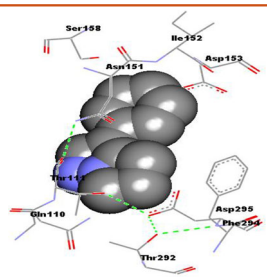	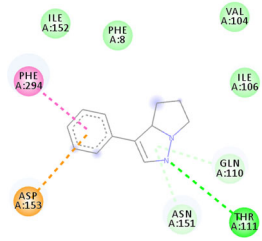	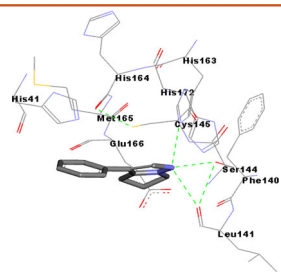
Oberadilol	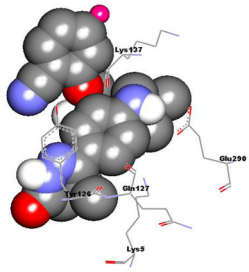	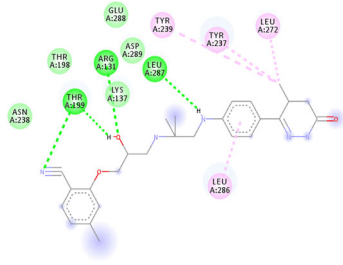	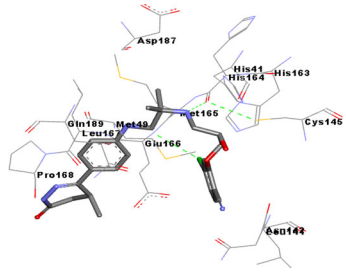
Poziotinib	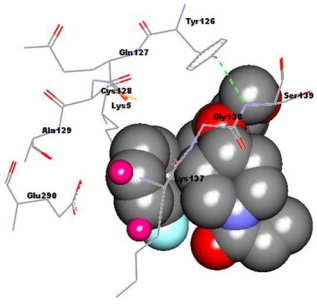	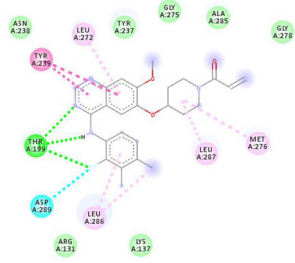	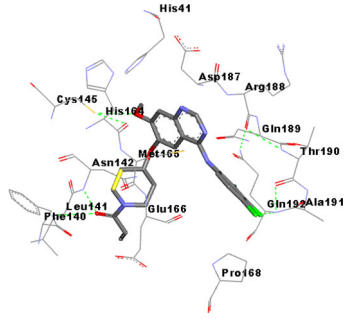

12.7. Best docking poses of WS phytoconstituents with Nsp-10/Nsp-16 complex from SARS-CoV-2 (PDB ID: 6W75) in comparison to the FDA approved standard reference drugs (Losartan and Hydroxychloroquine)

Withaferin A	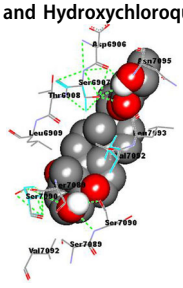	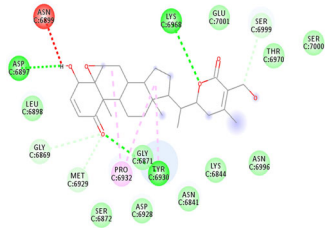	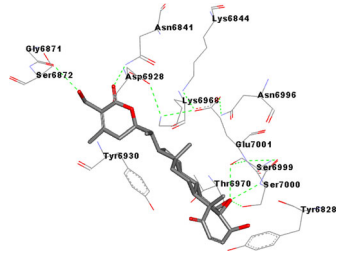
Withanolide A	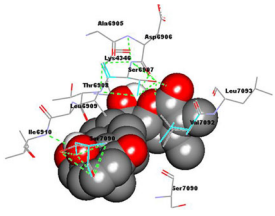	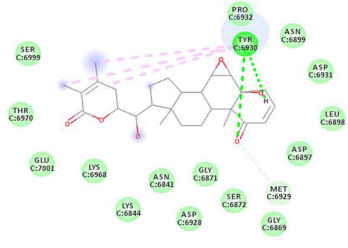	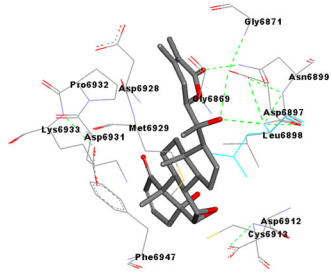

(*continued*)

Table 12. Continued.

Ligands	AutoDock v4.2.6	AutoDock vina	iGEMDOCK v2.1
Withanolide B	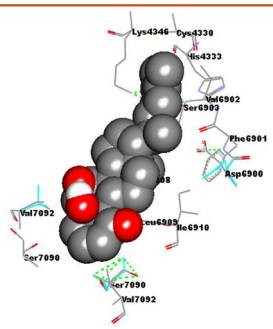	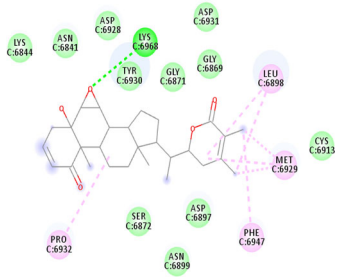	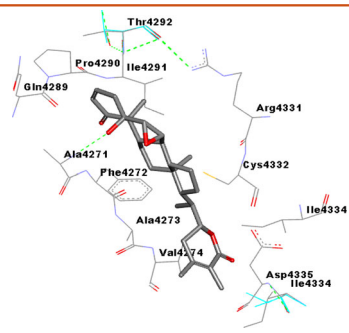
Withanolide D	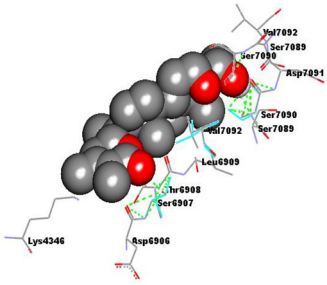	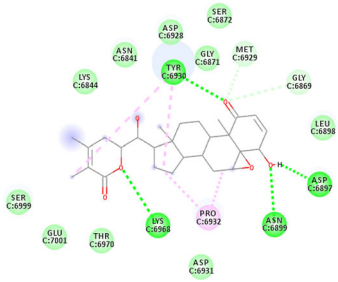	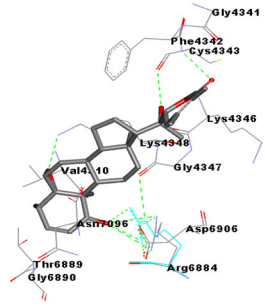
Withanolide E	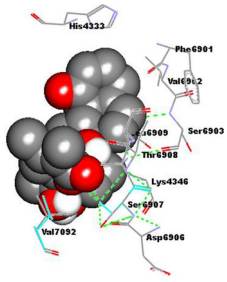	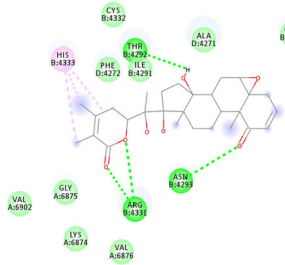	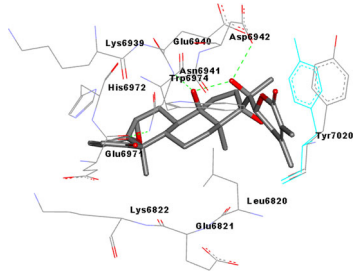
Withanone	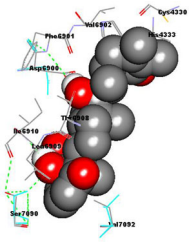	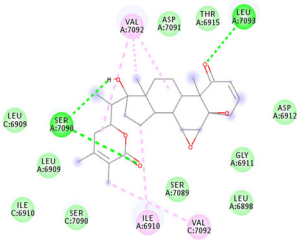	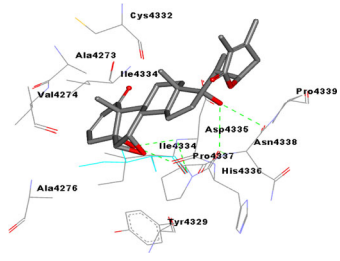
Viscosalactone B	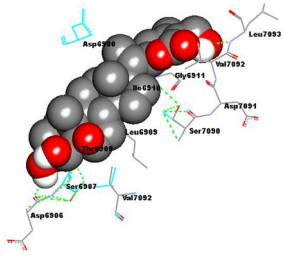	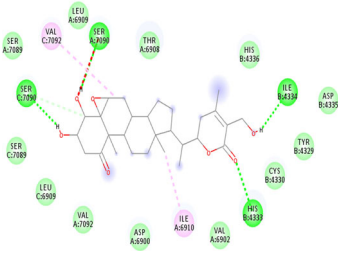	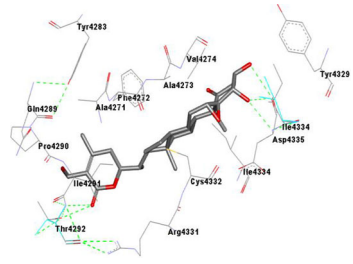
Anaferine	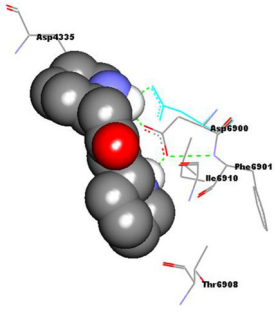	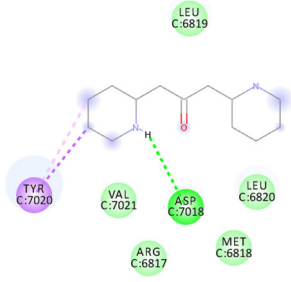	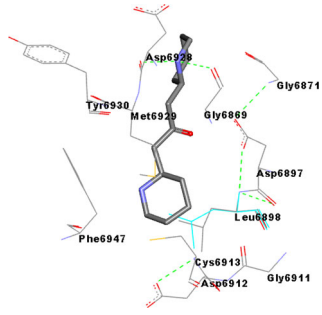

(*continued*)

Table 12. Continued.

Ligands	AutoDock v4.2.6	AutoDock vina	iGEMDOCK v2.1
Withasomnine	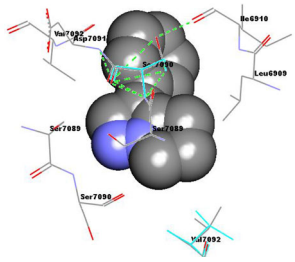	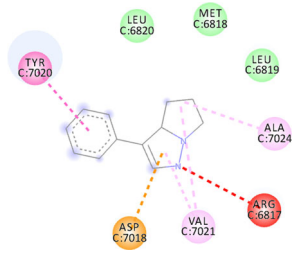	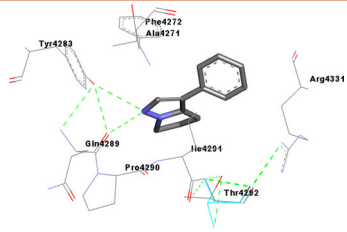
Losartan	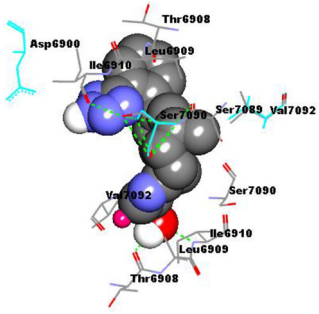	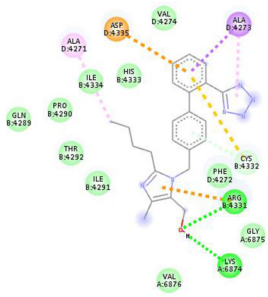	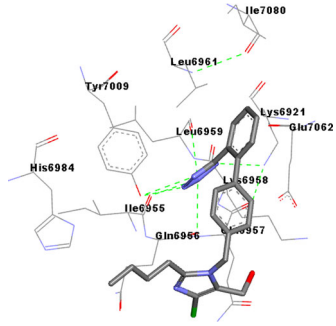
Hydroxychloroquine	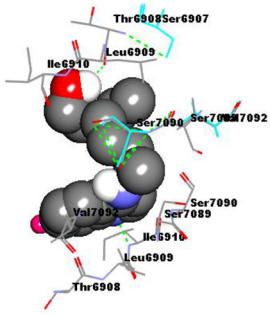	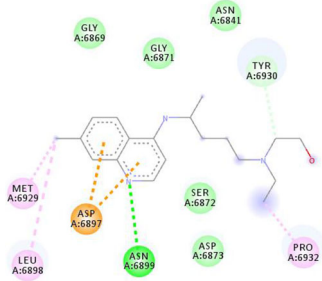	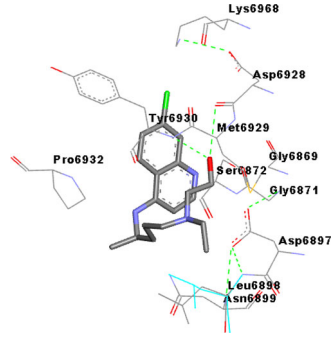

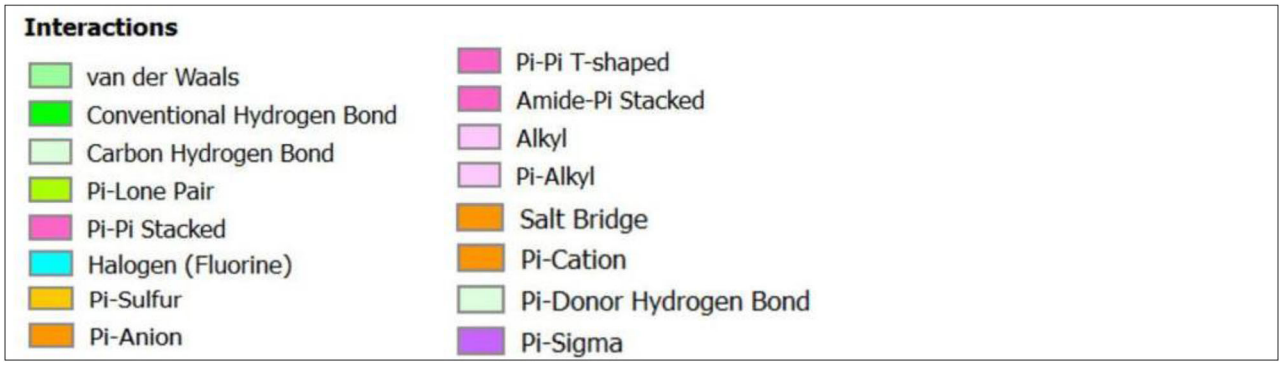

domain (RBD) bound with ACE2 have been provided as supplementary data files ST1, SFI, ST2 and SF2, respectively.

3.4. Bioavailability radar and score as parameters for analysis of pharmacokinetic properties of WS phytoconstituents

Pharmacokinetics and pharmacodynamics are two interlinked terms in drug development having a mutual influence on each other. Bioavailability radar offers a first glimpse into the pharmaceutical properties of a prospective drug candidate. By convention, the pink area represents the optimal biological range for each physiochemical property including lipophilicity (XLOGP3 range 0.7–5.0), size (MW range 150–500), polarity (TPSA range 20–130 $Å^2$), solubility (log $S \leq 6$), saturation (fraction of carbons in sp^3 hybridization ≤ 0.25), and flexibility (≤ 9). The Abbot Bioavailability Score62 is identical, but attempts to determine whether a compound is likely to have oral bioavailability score of at least 10% in rats and/or Caco-2 permeability (Martin, 2005). As is evident from Figure 2A

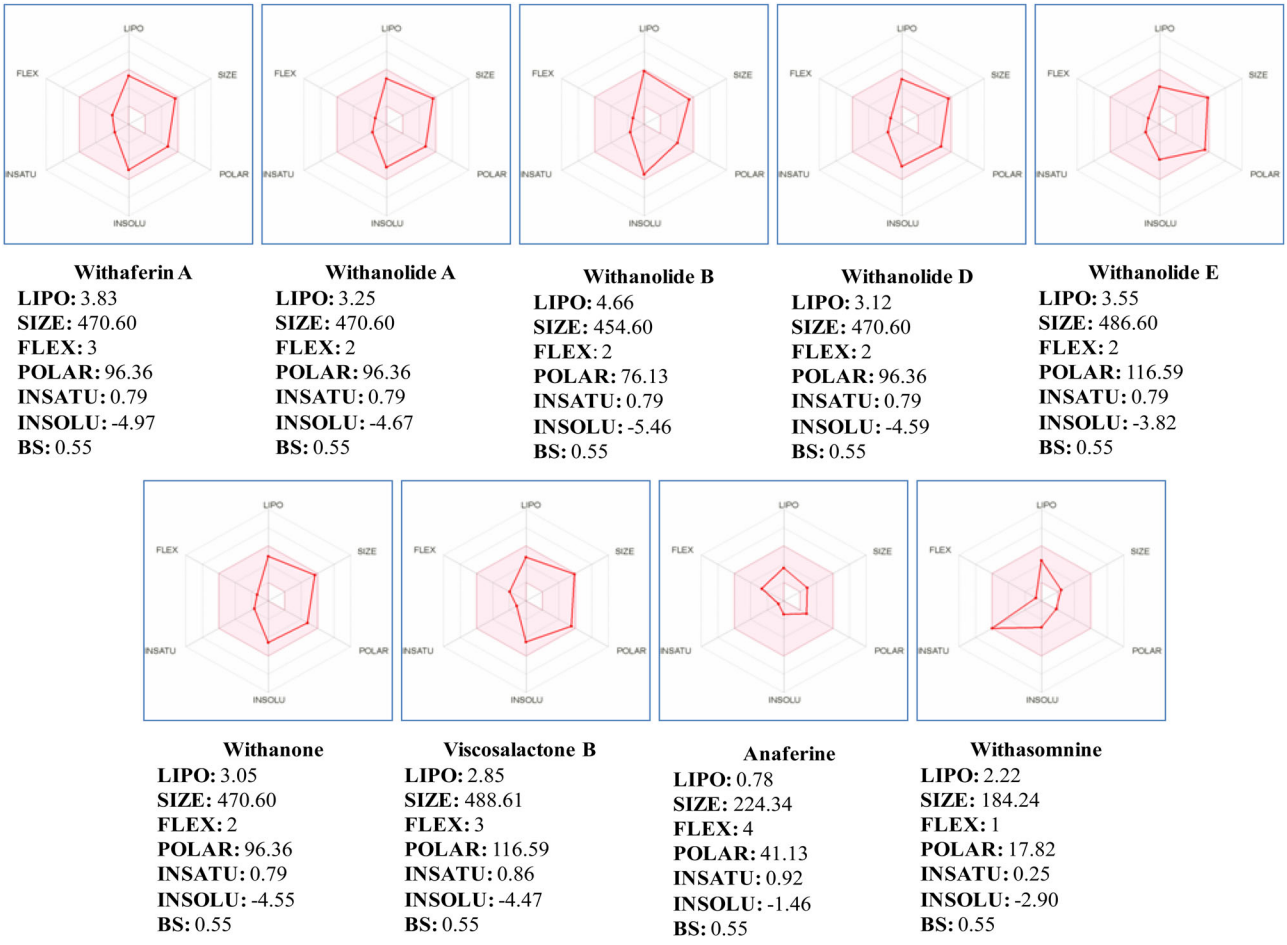

Figure 2. (A) Bioavailability radar and score prediction of WS phytoconstituents using SwissADME. (B) Bioavailability radar and score prediction of FDA–approved reference standard drugs using SwissADME.

and B, all withanolides from WS exhibited a significant bioavailability radar and score as comparable to the standard reference FDA-approved drugs.

3.5. Druglikeness and Bioactivity score (BAS) analysis

Biological targets of prospective drug candidates can be classified into ion channels, proteases, kinases, G-protein coupled receptors (GPCRs), nuclear receptors and enzymes. The BAS of WS phytoconstituents was determined using web-based software Molinspiration (www.molinspiration.com). As a general rule, it is known that if the BAS > 0.0, then the drug candidate is physiologically active; if it is in the range -5.0 to 0.0; then the drug candidate is moderately active, and if the BAS< -5.0, then the drug candidate is inactive.

It is evident from Table 13, that most of the WS phytoconstituents had positive values with respect to the following receptors.

3.5.1. As GPCR ligands

All WS phytoconstituents were active except withanolide E, anaferine and withasomnine which were predicted to be moderatively active. Most of the reference drugs also had positive values for GPCR except procainamide and arbidol which were predicted to be moderately active.

3.5.2. As ICMs

All WS phytoconstituents had positive values except withasomnine which was found to be moderately active. Standard reference drugs losartan, cinacalcet, hydroxychloroquine, oberadilol and poziotinib were all found to be active whereas procainamide and arbidol were found to be moderately active.

3.5.3. As KIs

All WS phytoconstituents displayed moderate activity except withasomnine that displayed significant activity. Standard reference drugs losartan, hydroxychloroquine and poziotinib were found to be active whereas procainamide, cinacalcet, arbidol and oberadilol were found to be moderately active.

3.5.4. As NRLs

Withaferin A, withanolides A, B, D and E, withanone and viscosalactone B possessed significant BAS scores whereas anaferine and withasomnine were found to be moderately active. All standard reference drugs were predicted to have moderate BAS scores as NRLs.

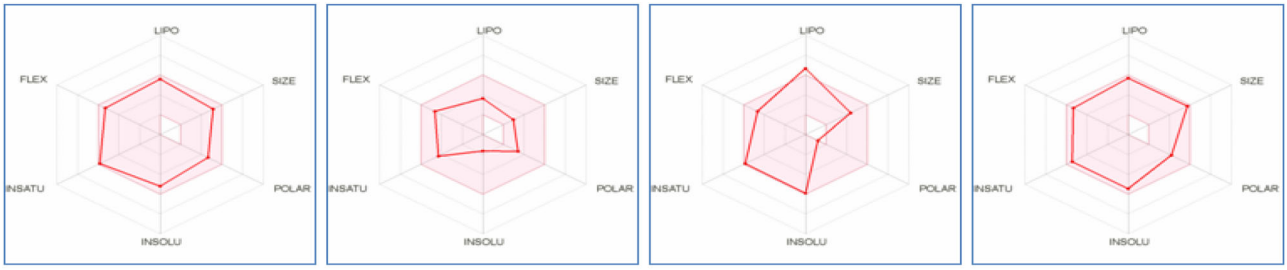

Losartan
LIPO: 4.29
SIZE: 422.91
FLEX: 8
POLAR: 92.51
INSATU: 0.27
INSOLU: -5.18
BS: 0.56

Procainamide
LIPO: 0.88
SIZE: 235.33
FLEX: 7
POLAR: 58.36
INSATU: 0.46
INSOLU: -1.65
BS: 0.55

Cinacalcet
LIPO: 6.14
SIZE: 357.41
FLEX: 7
POLAR: 12.03
INSATU: 0.27
INSOLU: -5.92
BS: 0.55

Arbidol
LIPO: 4.43
SIZE: 477.41
FLEX: 8
POLAR: 80.00
INSATU: 0.32
INSOLU: -5.45
BS: 0.55

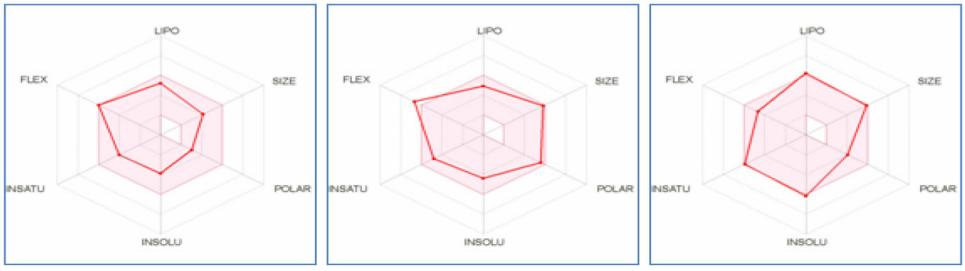

Hydroxychloroquine
LIPO: 3.58
SIZE: 335.87
FLEX: 9
POLAR: 48.39
INSATU: 0.50
INSOLU: -3.91
BS: 0.55

Oberadilol
LIPO: 3.06
SIZE: 483.99
FLEX: 10
POLAR: 118.77
INSATU: 0.40
INSOLU: -4.37
BS: 0.55

Poziotinib
LIPO: 5.36
SIZE: 491.34
FLEX: 7
POLAR: 76.58
INSATU: 0.26
INSOLU: -6.16
BS: 0.55

Figure 2. Continued.

3.5.5. As PIs

Withaferin A, withanolides A, B, D and E, withanone and viscosalactone B had positive BAS scores indicating their potential as protease inhibitors. On the other hand, anaferine and withasomnine were found to have moderate activity as protease inhibitors. Interestingly, most withanolides especially withanolide B and withanolide A showed potent binding to papain like protease of SARS-CoV-2 (PDB ID: 6W9C), SARS-CoV 3CL-pro main protease (PDB ID: IP9U) and SARS-CoV-2 Nsp10/Nsp-16 complex (PDB ID: 6W75) thus supporting their role as potential viral protease inhibitors. On the other hand, losartan, cinacalcet and hydroxychloroquine also displayed positive values as protease inhibitors whereas procainamide, arbidol, oberadilol and poziotinib displayed moderate potential as protease inhibitors.

3.5.6. As EIs

Most of the WS phytoconstituents including Withaferin A, withanolides A, B, D and E, withanone, viscosalactone B and anaferine had positive BAS scores indicating their potential as enzyme inhibitors whereas withasomnine displayed moderate potential. This observation was further validated by the fact that most of the phytoconstituents including Withaferin A, withanolides A, B, D and E, viscosalactone B and anaferine showed potent binding to human ACE2 receptor in the nanomolar range which was about 1000× times greater than the binding of known standard reference drugs arbidol and losartan (Table 4). This finding lends support for targeted use of withanolides from WS as SARS-CoV-2 entry blocking agents by virtue of their preferential binding to human ACE2, thereby blocking or inhibiting it. Losartan, cinacalcet, hydroxychloroquine, oberadilol and poziotinib also displayed significant potential as enzyme inhibitors whereas procainamide and arbidol displayed moderate potential.

Druglikeness of a compound can be predicted by comparing its structural features with those of marketed drugs. All WS phytoconstituents showed molar lipophilicity (cLog P) <5 thereby indicating good permeability across cell membranes (Figure 2A). Withaferin A, withanolide D, viscosalactone B and withasomnine had positive values of druglikeness which indicated that these compounds contain fragments that are present in marketed drugs. Out of the standard reference drugs, procainamide, hydroxychloroquine and oberadilol exhibited positive scores for druglikeness (Table 14).

Table 13. Bioactivity scores and Druglikeness of WS phytoconstituents *versus* FDA-approved standard reference drugs (Losartan, Procainamide, Cinacalcet, Arbidol, Hydroxychloroquine, Oberadilol, Poziotinib).

S. No.	Ligands	Parameters of bioactivity score					
		GPCR ligand	Ion channel modulator (ICM)	Kinase inhibitor (KI)	Nuclear receptor ligand (NRL)	Protease inhibitor (PI)	Enzyme inhibitor (EI)
1.	Withaferin A	0.07	0.14	−0.49	0.76	0.15	0.94
2.	Withanolide A	0.04	0.32	−0.43	0.71	0.15	0.86
3.	Withanolide B	0.07	0.24	−0.47	0.79	0.15	0.76
4.	Withanolide D	0.05	0.30	−0.50	0.73	0.16	1.07
5.	Withanolide E	−0.70	0.16	−0.50	0.61	0.06	0.89
6.	Withanone	0.00	0.27	−0.38	0.71	0.12	0.78
7.	Viscosalactone B	0.03	0.04	−0.51	0.78	0.19	0.84
8.	Anaferine	−0.08	0.17	−0.60	−0.58	−0.14	0.08
9.	Withasomnine	−0.49	−0.43	0.58	−0.10	−0.58	−0.17
10.	Losartan	1.06	0.16	0.03	0.01	0.33	0.44
11.	Procainamide	−0.09	0.01	−0.10	−0.70	−0.20	−0.04
12.	Cinacalcet	0.22	0.15	−0.0.8	0.00	0.17	0.02
13.	Arbidol	−0.19	−0.44	−0.39	−0.34	−0.46	−0.07
14.	Hydroxychloroquine	0.35	0.30	0.44	−0.12	0.12	0.15
15.	Oberadilol	0.04	−0.47	−0.43	−0.37	−0.02	0.02
16.	Poziotinib	0.04	−0.17	0.53	−0.35	−0.27	0.01

Rule: BAS >0: Active;
BAS −5.0–0.0: Moderately active, moderately active and inactive.
BAS ≤5.0: Inactive;

Table 14. Drug like properties of WS phytoconstituents *versus* FDA–approved standard reference drugs (Losartan, Procainamide, Cinacalcet, Arbidol, Hydroxychloroquine, Oberadilol, Poziotinib).

S. No.	Ligands	Druglikeness (DL)	clogS
1.	Withaferin A	1.69	−4.47
2.	Withanolide A	−0.63	−4.53
3.	Withanolide B	−1.04	−4.98
4.	Withanolide D	0.14	−4.53
5.	Withanolide E	−0.41	−4.03
6.	Withanone	−0.63	−4.53
7.	Viscosalactone B	1.83	−4.29
8.	Anaferine	−0.69	−2.48
9.	Withasomnine	4.16	−2.81
10.	Losartan	−6.63	−4.99
11.	Procainamide	7.96	−1.72
12.	Cinacalcet	−4.58	−5.65
13.	Arbidol	−1.16	−4.75
14.	Hydroxychloroquine	5.73	−3.55
15.	Oberadilol	3.49	−6.12
16.	Poziotinib	−4.70	−6.72

3.6. Toxicity risk assessment

In silico prediction of drug-like properties has now become a norm for pharmaceutical industries for investing in and classifying drug compounds and their product potential. The toxicity risk evaluation is an important consideration to prevent undesirable substances with adverse effects to undergo further drug screening (Balakrishnan et al., 2015). Potential drug candidates are analyzed for their toxicity parameters like tumorigenic, mutagenic, irritant and for their effects on the reproductive system. In the present study, toxicity risk assessment of WS phytoconstituents was calculated using OSIRIS data warrior. The software estimates the toxicity potential of the compounds based on similarities between the phytoconstituents being examined and the compounds present in its *in vitro* and *in vivo* database (Sander, 2001).

The obtained results have been presented in Table 15. As is evident from Table 15, none of the analyzed WS phytoconstituents had any mutagenic effects in contrast to standard reference drugs hydroxychloroquine and poziotinib which displayed high mutagenicity. Most of the WS phytoconstituents displayed little to no tumorigenicity in comparison to standard reference drugs cinacalcet and oberadilol which exhibited a high tendency for tumorigenicity and poziotinib which exhibited a mild tumorigenicity. The irritant and reproductive effects of the WS phytoconstituents were also predicted to be from negligible to none, in contrast to standard reference drugs procainamide which was predicted to possess high adverse effects and poziotinib that was predicted to have mild irritant and reproductive effects.

3.7. Ligand-based target prediction analysis

Similarity in structures of ligands or distribution of electrostatic potential may result in an identical effect leading to the probability of interaction with similar targets (Wirth & Sauer, 2011). These predictions also indicate how a drug candidate can be chemically altered in order to maximize its effect on a given target by comparing it to known ligands having similar structure. Thus, this prediction analysis can help harness natural ligands for use as therapeutic adducts. From the pie-chart representation, it is evident that most of the withanolides possessed broad-spectrum of bioactivity against several targets present in humans (Figure 3).

3.8. Identification of SOMs in WS phytoconstituents

Biotransformation refers to a biochemical modification process of xenobiotics inside the living system involving the utilization of special enzymes. In pharmaceutical industry, this term is equivalent to 'drug metabolism'. Drug metabolism influences drug-like properties of prospective drug molecules which may contribute to the production of metabolites with drastically altered pharmacological and toxicological

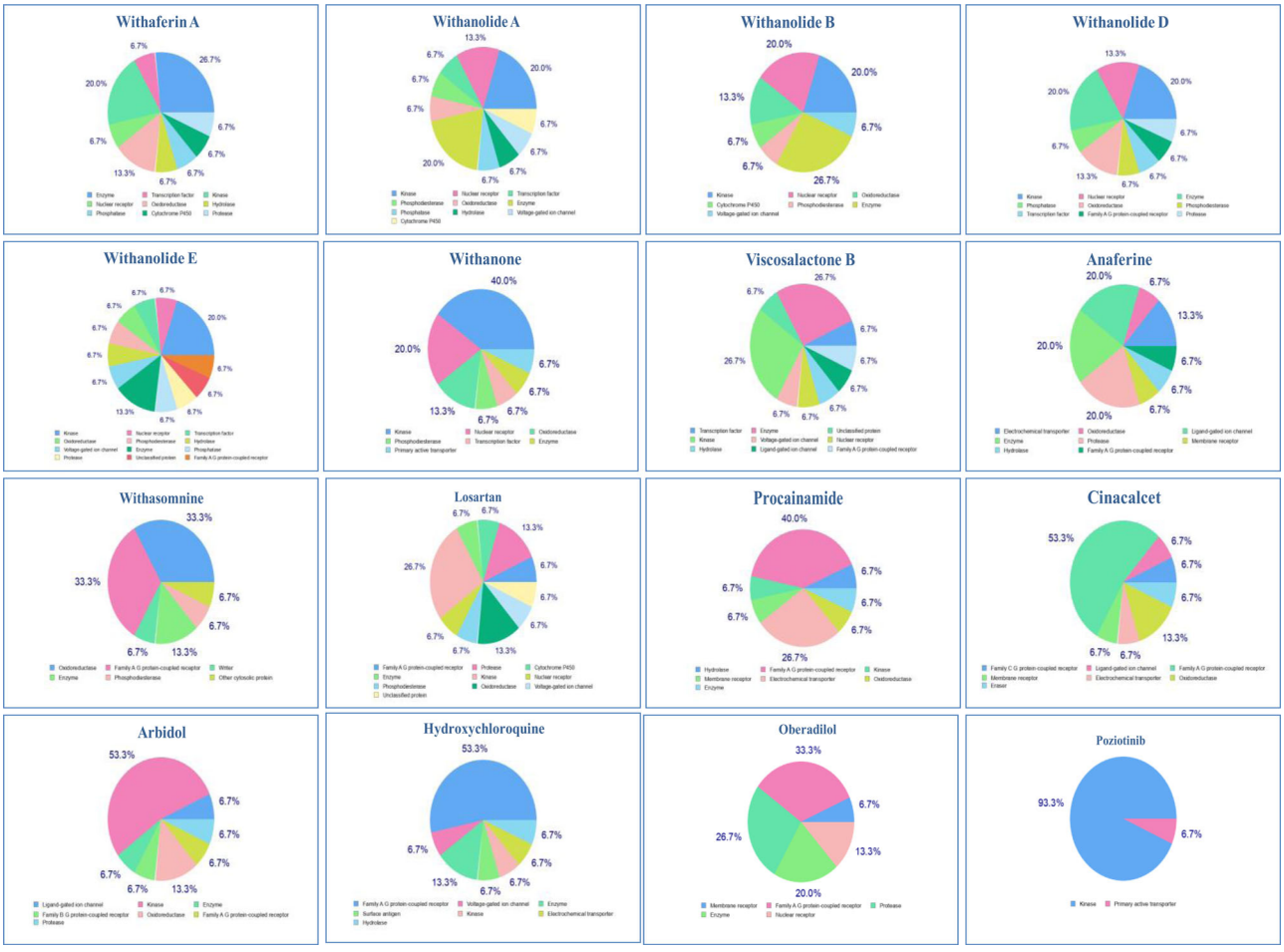

Figure 3. Ligand–based target prediction analysis of WS phytoconstituents *versus* FDA–approved standard reference drugs (Losartan, Procainamide, Cinacalcet, Arbidol, Hydroxychloroquine, Oberadilol, Poziotinib) using SwissTargetPrediction.

parameters. The recognition of SOMs containing specific atom(s) in the molecule which are oxidized by CYP isozymes, provides knowledge for the design and optimization of potent candidates in early stage. Cytochrome P450s are accountable for more than 90% of the pharmaceutical drugs to undergo phase I metabolism. Therefore, having prior knowledge about the metabolic liabilities of prospective drug candidates could have important ramifications in drug discovery process. The primary, secondary and tertiary predicted SOMs for selected WS phytoconstituents *versus* FDA-approved standard reference drugs have been shown in Figure 4. The figure is a graphical output for a combination of all nine isozymes of cytochrome P450. The results indicated that WS phytoconstituents and standard reference drugs were predicted to possess SOMs likely to undergo phase I metabolism.

3.9. Structure activity relationship (SAR)

WS is known to harbor a wide variety of secondary metabolites having low MWs *viz*. terpenoids, flavonoids, tannins, alkaloids and resins. Withanolides, alkaloids, flavonoids and tannins are the major chemical constituents that include compounds of diverse chemical structures (Dhar et al., 2015; Kumar et al., 2015). Of these, withanolides are attributed with diverse and widely known biological activities. In the present study, most of the predicted pharmacological activity against the chosen biological target(s) was found to be associated with two main withanolides, *viz*. withanolide A and B, as well as withanone, a WS phytoconstituent with structural similarity to withanolide D. Nearly 40 naturally occurring withanolides have been reported till date comprising of C-28 steroidal lactone triterpenoids assembled on an integral or reorganized ergostane structure, in which C-22 and C-26 are oxidized to form a six-membered lactone ring (Jain et al., 2012). The withanolide backbone is chemically classified as 22-hydroxy ergostane-26-oic acid 26, 22-lactone (Mirjalili et al., 2009). The withanolides consist of several oxygen atoms and are thought to be synthesized *via* oxidation of all carbon atoms in a steroid nucleus.

The parent configuration of withanolides and ergostane-type steroids is one C-8 or C-9 side chain with an either six or five membered lactone or lactol ring. A carbon-carbon bond or oxygen bridge is responsible in attaching the lactone ring with the carbocyclic part of the molecule (Mirjalili et al., 2009). Withanolides have a varying distribution in the fruits and vegetative parts of the plant such as leaves, roots and stem (Sangwan et al., 2008). However, withanolides are mainly localized in the leaves, in low concentrations

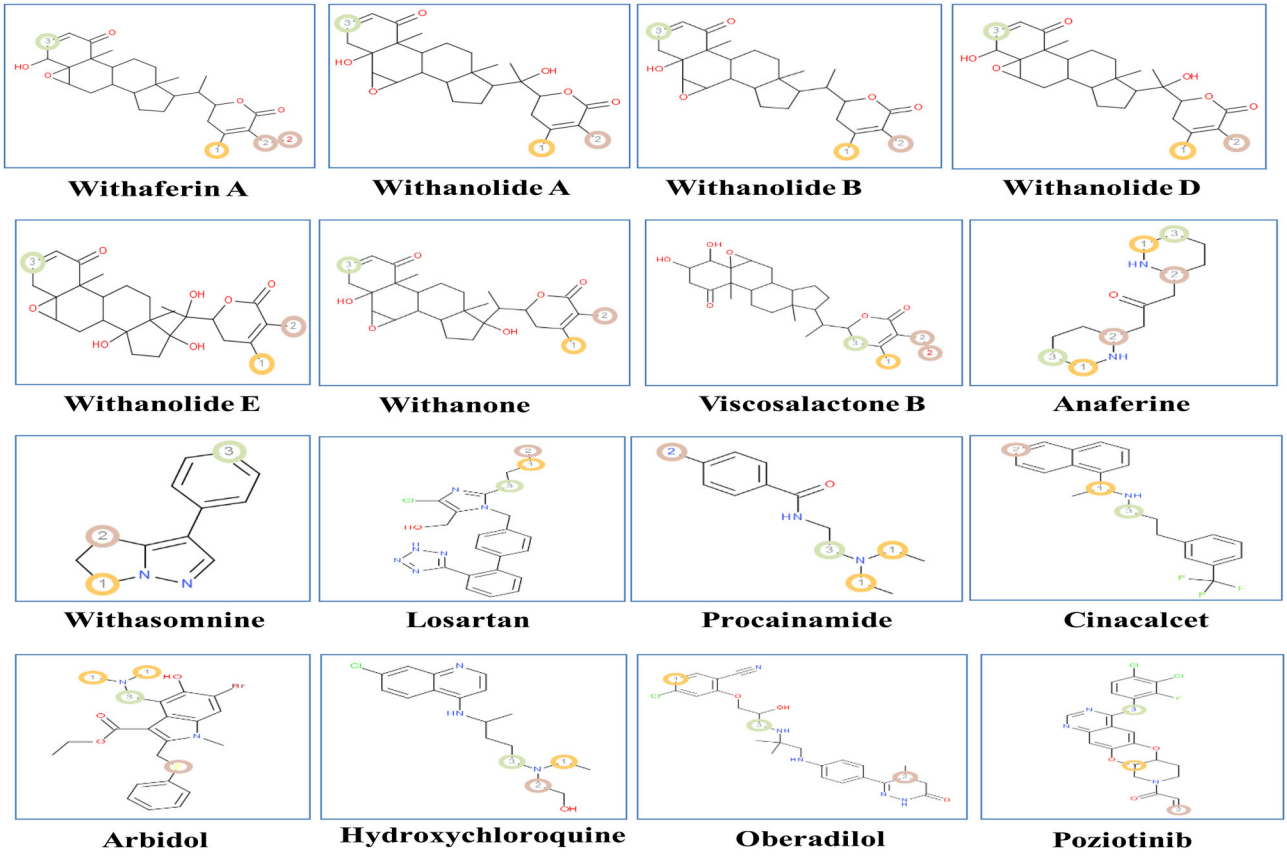

Figure 4. Prediction of cytochrome P450–mediated SOMs on WS phytoconstituents *versus* FDA–approved standard reference drugs (Losartan, Procainamide, Cinacalcet, Arbidol, Hydroxychloroquine, Oberadilol, Poziotinib) using RS–WebPredictor.

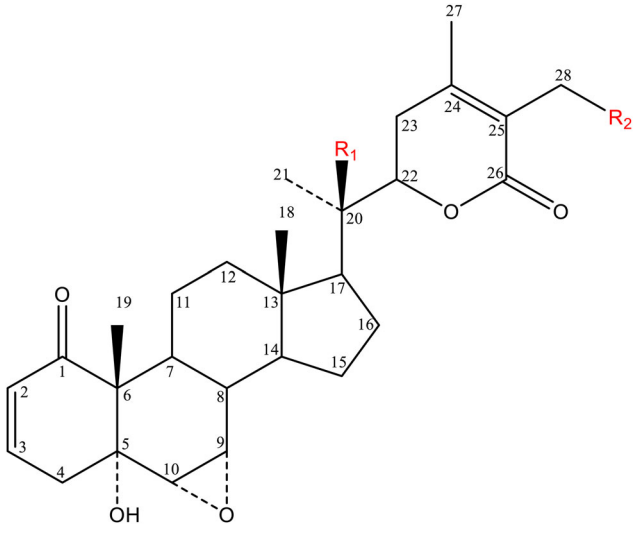

Figure 5. Structural differences in Withanolide A (R1 = OH, R2 = H); Withanolide B (R1 = H, R2 = H); Withanolide E (5β, 6β–epoxy) and Withanone (17α–OH, R1 = H, R2 = H).

(0.001–0.5% of dry weight) which is the main drawback for their use as drugs. Geographical, environmental and seasonal factors as well as growth conditions are also known to contribute to modulation of the content of withanolides (Dhar et al., 2013).

In the present study, the differential binding kinetics obtained for withanolide A ($C_{28}H_{38}O_6$), withanolide B ($C_{28}H_{38}O_5$), withanolide E ($C_{28}H_{38}O_7$) and withanone ($C_{28}H_{38}O_7$) might be attributed to the varying number of oxygen atoms in their structures which might affect hydrogen bonding within the binding site of the target protein(s). Another explanation for differential SAR obtained for the above withanolides might be due to various kinds of structural rearrangements (A or B) involving oxygen substituents like bond scission, new bond formation, ring aromatization, etc. which help in formation of novel structural variants and compounds with novel structures (Figure 5) often described as modified withanolides or ergostane type steroids (Misico et al., 2011). The structural rearrangement as seen in withanolide A and B might be responsible for a better complementary fit of the phytoconstituent in the binding pocket of the target protein(s).

3.10. Principle component analysis

PCA is one of the most familiar methods of multivariate analysis which attempts to model the total variance of originally formed data set with the unrelated principal components. Absorption rate, TPSA, MW, clog P, NOHNH, NON, number of rotatable bonds and Lipinski's violations were the various variable properties on which PCA was performed using linear correlation as shown in Figure 6A and 6B. PCA analysis was also performed on leadlikeness (Table 14; Figure 7) as well as

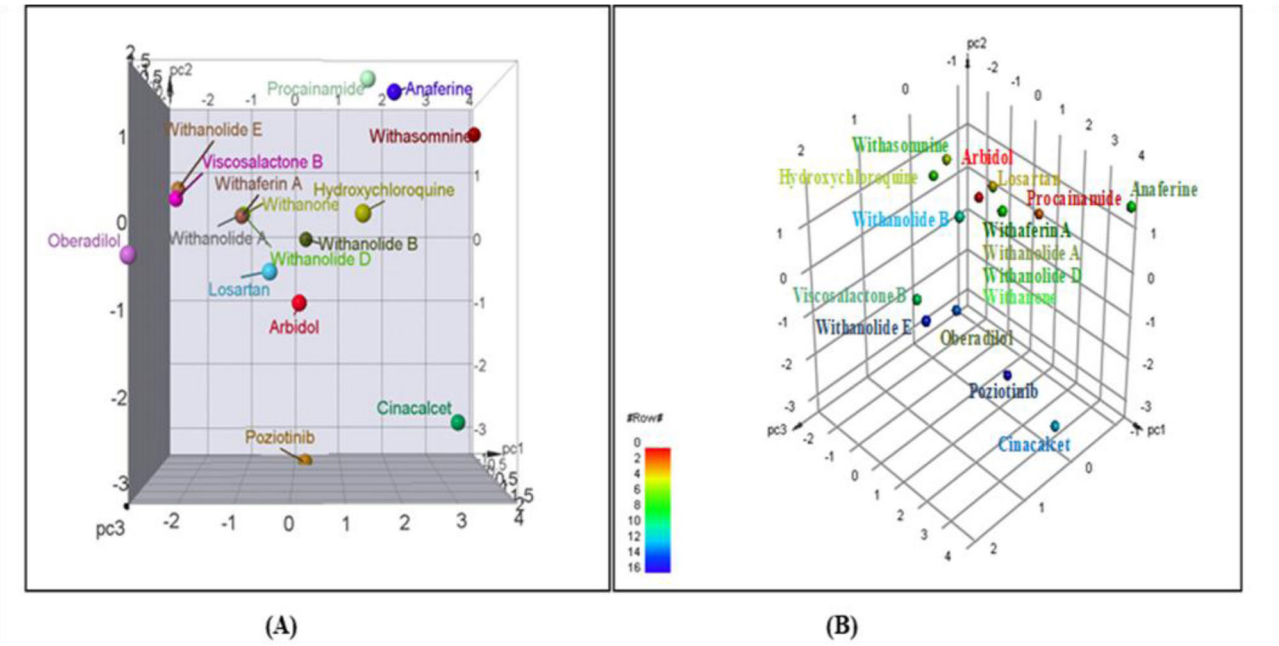

Figure 6. PCA of physiological properties of WS phytoconstituents *versus* FDA–approved standard reference drugs (Losartan, Procainamide, Cinacalcet, Arbidol, Hydroxychloroquine, Oberadilol, Poziotinib). (A) Scatter Plot (B) 3D Point Plot.

Table 15. Toxicity risk assessment of WS phytoconstituents *versus* FDA-approved standard reference drugs (Losartan, Procainamide, Cinacalcet, Arbidol, Hydroxychloroquine, Oberadilol, Poziotinib).

S. No.	Ligands	Mutagenic	Tumorigenic	Reproductive effective	Irritant
1.	Withaferin A	None	None	Mild	None
2.	Withanolide A	None	Mild	Mild	Mild
3.	Withanolide B	None	Mild	Mild	Mild
4.	Withanolide D	None	None	Mild	None
5.	Withanolide E	None	None	Mild	None
6.	Withanone	None	Mild	Mild	Mild
7.	Viscosalactone B	None	None	None	None
8.	Anaferine	None	None	None	None
9.	Withasomnine	None	None	None	None
10.	Losartan	None	None	None	None
11.	Procainamide	None	None	None	High
12.	Cinacalcet	None	High	None	None
13.	Arbidol	None	None	None	None
14.	Hydroxychloroquine	High	None	None	None
15.	Oberadilol	None	High	None	None
16.	Poziotinib	High	Mild	Mild	Mild

for bioactivity score parameters using linear correlation between the variables (Table 13; Figure 8)

As is evident from Figures 6–8, all WS phytoconstituents fall close in 3D to the standard reference drugs used in the present study, thereby denoting their 'drug-like' character. Tables 16, 17 and 18 represent the Bravais–Pearson (linear correlation) coefficients of WS phytoconstituents *versus* FDA-approved standard reference drugs.

3.11. Molecular dynamics simulation

Figures 9 and 10, respectively, depict molecular simulation analysis of SARS-CoV-2 spike receptor-binding domain (PDB ID: 6M0J) bound with withanolide A and SARS-CoV-2 papain-like protease (PDB ID: 6W9C) bound with withanolide B. Both MD simulations showed an acceptable stability profile at a temperature of 300 K. Root mean square deviation (RMSD) is one of the most important fundamental properties to establish protein stability and its conformation to experimental structure (Kuzmanic & Zagrovic, 2010; Laskowski et al., 1997). RMSD is a measure of the deviation of the 3D or tertiary structure of a protein and is applied in order to get an insight into the stability of the protein in a biological system during a MD simulation. SARS-CoV-2 spike receptor-binding domain-withanolide A complex displayed constant RMSDs (0.5–2.0 angstrom) of both protein side chains and Cα atoms from the initial structure (before equilibrium) throughout the 3 ns time scale (Figure 9.1). Similarly, SARS-CoV-2 papain-like protease-withanolide B complex also exhibited constant RMSDs (0.8–2.9 angstrom) of both protein side chains and Cα atoms from the initial structure throughout the 3 ns time scale (Figure 10.1). Figures 11.1–11.3 and 12.1–12.3, respectively depict MS dynamics analyses of SARS-CoV spike glycoprotein (PDB ID: 5WRG) with withanolide B and SARS-CoV-2 main protease (PDB ID: 6LU7) with withanolide A.

Vibrations around the equilibrium are not random, but depend on the local structure flexibility. In order to calculate the average fluctuation of all residues during simulations, the root mean square fluctuation (RMSF) of the Cα atoms of both target proteins were plotted from the primary structure of both proteins as a function of residue number (Kuzmanic & Zagrovic, 2010). The obtained patterns of RMSFs for both the proteins and ligands have been presented in Figures 11.1–11.3 and 12.1–12.3, respectively.

4. Discussion

The current outbreak of SARS-CoV-2, a life threatening zoonotic coronavirus has made us painfully realize that existing and available options for its treatment are limited.

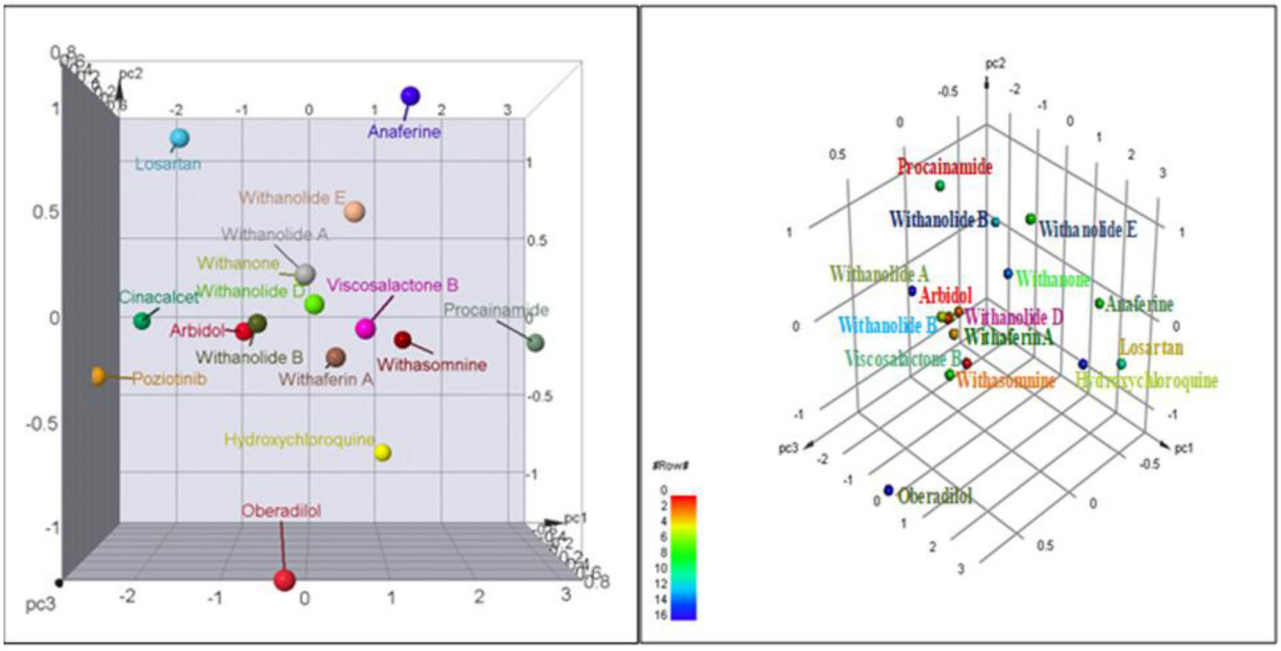

Figure 7. PCA of leadlikeness of WS phytoconstituents *versus* FDA–approved standard reference drugs (Losartan, Procainamide, Cinacalcet, Arbidol, Hydroxychloroquine, Oberadilol, Poziotinib). (A) Scatter Plot (B) 3D Point Plot.

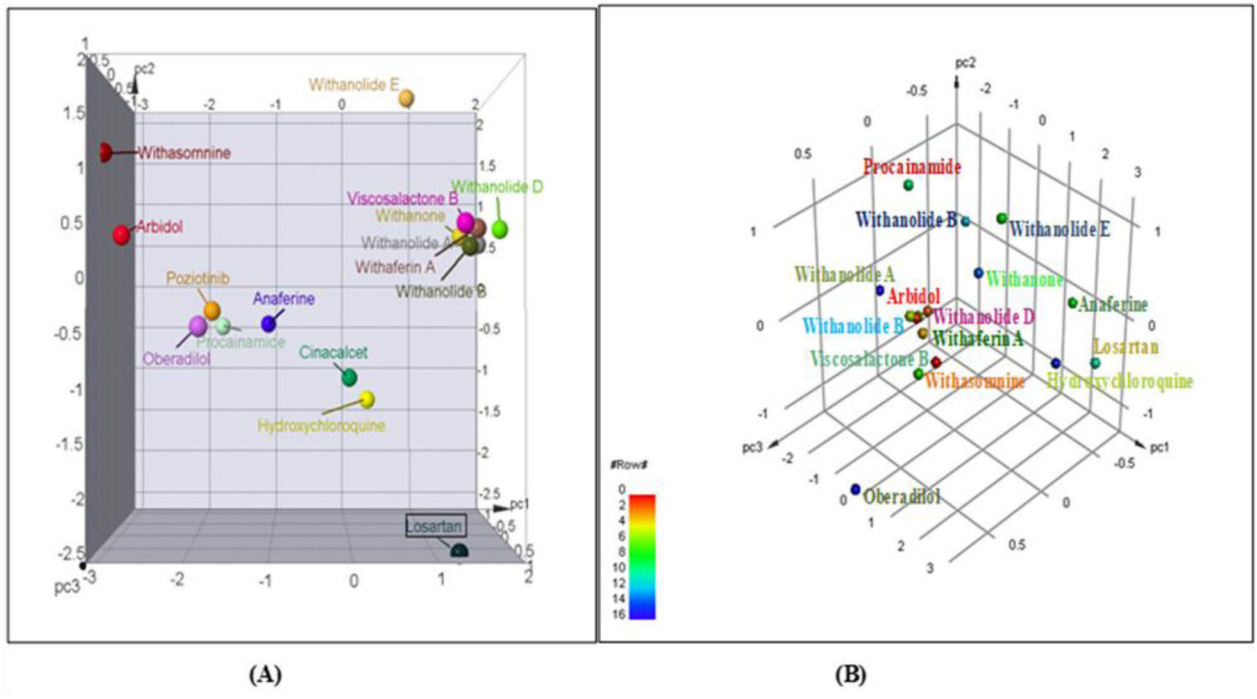

Figure 8. PCA of bioactivity score prediction of WS phytoconstituents *versus* FDA– approved standard reference drugs (Losartan, Procainamide, Cinacalcet, Arbidol, Hydroxychloroquine, Oberadilol, Poziotinib). (A) Scatter Plot (B) 3D Point Plot.

Although, several efforts were made to treat SARS in 2002 and MERS in 2013, none of the past or existing efforts to treat the ongoing pandemic of 2020 has been found to be fruitful till date. Existing therapeutic options include the use of repurposed/repositioned drugs for treatment of COVID-19 pandemic. Development of effective vaccine candidates is also underway but would take considerable time and effort to produce fruitful results as shown in Figure 13. Prospective therapeutic discovery against coronavirus can be subdivided into two groups depending on the target: one acting upon the virus and the other acting on the human innate immune system. The latter plays a significant

Table 16. Bravais–Pearson (linear correlation) coefficient of WS phytoconstituents *versus* FDA-approved standard reference drugs (Losartan, Procainamide, Cinacalcet, Arbidol, Hydroxychloroquine, Oberadilol, Poziotinib) for physicochemical properties.

Properties	1	2	3	4	5	6	7	8	9	10	11	12	13	14	15	16
% AB (NOHNH)	1	−0.719	−0.867	0.387	−0.807	0.0443	−1	0.274	0.99	−0.0259	0.037	−0.0781	0.0966	−0.0537	0.0186	5.38E−05
	2	−0.719	0.582	−0.357	0.399	0.243	0.719	−0.466	−0.779	0.214	0.45	−0.346	0.156	0.032	−0.0146	−1.39E−08
(NON)	3	−0.867	0.582	0.0762	0.938	−0.0124	0.867	0.11	−0.893	−0.397	−0.147	−0.119	−0.00919	−0.0307	0.0873	2.76E−09
LV	4	0.387	−0.357	0.0762	0.0607	0.182	−0.387	0.76	0.35	−0.822	−0.0907	−0.427	−0.103	−0.00279	−0.0306	1.09E−08
MW	5	−0.807	0.399	0.938	0.0607	0.012	0.807	0.278	−0.821	−0.491	−0.203	0.157	0.0848	−0.0985	−0.0469	5.89E−10
RB	6	0.0443	0.243	−0.0124	0.182	0.012	−0.0443	0.363	0.0185	−0.386	0.905	0.157	−0.0754	−0.0364	0.00653	4.45E−09
TPSA	7	−1	0.719	0.867	−0.387	0.807	−0.0443	−0.274	−0.99	0.0259	−0.0371	0.0782	−0.0964	0.0537	−0.0186	5.38E−05
clog Pc	8	0.274	−0.466	0.11	0.76	0.278	0.363	−0.274	0.264	−0.931	−0.0242	0.205	0.112	0.0929	0.00734	−1.71E−08
pc1	9	0.99	−0.779	−0.893	0.35	−0.821	0.0185	−0.99	0.264	9.62E−09	−8.89E−09	5.33E−09	−1.73E−08	6.60E−09	−5.23E−09	1.16E−08
pc2	10	−0.0259	0.214	−0.397	−0.822	−0.491	−0.386	0.0259	−0.931	9.62E−09	−5.16E−09	−9.75E−09	−1.46E−08	−1.70E−09	3.02E−10	−8.98E−10
pc3	11	0.037	0.45	−0.147	−0.0907	−0.203	0.905	0.157	−0.0371	−0.0242	−8.89E−09	−5.16E−09	1.02E−08	−8.09E−09	−2.00E−09	−2.34E−08	−1.94E−08
pc4	12	−0.0781	−0.346	−0.119	−0.427	0.157	0.0782	0.205	5.33E−09	−9.75E−09	1.02E−08		−7.30E−09	9.18E−09	−6.69E−09	5.02E−09
pc5	13	0.0966	0.156	−0.00919	−0.103	0.0848	−0.0754	0.112	−1.73E−08	−1.46E−08	−8.09E−09	−7.30E−09		4.55E−09	9.35E−09	2.03E−09
pc6	14	−0.0537	0.032	−0.0307	−0.00279	−0.0985	−0.0364	0.0929	6.60E−09	−1.70E−09	−2.00E−09	9.18E−09	4.55E−09		6.33E−09	−1.14E−08
pc7	15	0.0186	−0.0146	0.0873	−0.0306	−0.0469	0.00653	−0.0186	0.00734	−5.23E−09	3.02E−10	−2.34E−08	−6.69E−09	9.35E−09	6.33E−09		−1.39E−08
pc8	16	5.38E−05	−1.39E−08	2.76E−09	1.09E−08	5.89E−10	4.45E−09	5.38E−05	−1.71E−08	1.16E−08	−8.98E−10	−1.94E−08	5.02E−09	2.03E−09	−1.14E−08	−1.39E−08	

Table 17. Bravais–Pearson (linear correlation) coefficient of WS phytoconstituents *versus* FDA–approved standard reference drugs (Losartan, Procainamide, Cinacalcet, Arbidol, Hydroxychloroquine, Oberadilol, Poziotinib) for drug like properties and leadlikeness.

Properties	1	2	3	4	5	6
LL	1		−0.669	0.631	0.858	−0.51	−0.066
clog Pc	2	−0.669		−0.754	−0.912	−0.173	−0.372
clogS	3	0.631	−0.754		0.896	0.311	−0.316
pc1	4	0.858	−0.912	0.896		−1.95E−09	1.70E−09
pc2	5	−0.51	−0.173	0.311	−1.95E−09		8.57E−10
pc3	6	−0.066	−0.372	−0.316	1.70E−09	8.57E−10	

role in controlling the viral replication and secretion of cytokines are expected to improve the immune system functioning.

In our every tryst with nature, we always perceive and find more than what we seek. Ancient Vedic literature has described nature as the 'mother of all healings'. Nature is known to have its own antidote against all natural and mankind activity induced maladies such as COVID-19. The benefits of 'Ecotherapy' and 'healing power' of nature have led to the discovery of several miraculous systems of healing amongst which Ayurveda holds a significant position.

Withanolides are a group of at least 300 naturally occurring steroids built on an ergostane skeleton that are produced as secondary metabolites in several plant species. They are composed specifically of triterpenoids bearing around 28-carbon backbone (Cai et al., 2015). Given the importance of WS in Ayurveda as well as ethnopharmacology, majority of the studies reported in literature are confined to its antitumor and rejuvenating properties. There is scanty information available regarding the antiviral activity of WS. In the present paper, an attempt has been made to explore the antiviral potential of WS against COVID-19 using molecular and chemoinformatic tools and *in silico* methods.

Generally, an orally active drug candidate cannot have more than one violation of Lipinski's criteria otherwise it might compromise its bioavailability. Good drug candidates with MW $<$ 500 can be administered easily and are readily diffusible and absorbed. For optimal biological activity, the number of rotatable bonds should be $<$10, indicating a higher amount of molecular stability. Similarly, total polar surface area (TPSA) should coincide with hydrogen bonding of a molecule and characterize the delivery properties of the drug which should be $<$160 Å^2. For a high oral bioavailability, the absorption rate determined from TPSA should be $>$50% (Balakrishnan et al., 2014). Interestingly, none of the phytocomponents of WS exhibited Lipinski's violation, however, the standard drugs cinacalcet and poziotinib displayed 1 violation of Lipinski's rule of five (Table 2). In addition, the selected phytoconstituents exhibited no violations of Veber, Egan and Muegge filters thereby indicating their druglike character (Table 3).

Prior to selection of WS phytoconstituents, their ADMET properties were calculated using online database (admetSAR), which provides latest and most inclusive manually created data for various chemicals with known ADMET properties (Cheng et al., 2012). Interestingly, in the present study, most of the WS phytoconstituents exhibited positive results of ADME and none of the phytoconstituents were

Table 18. Bravais–Pearson (linear correlation) coefficient of WS phytoconstituents *versus* FDA–approved standard reference drugs (Losartan, Procainamide, Cinacalcet, Arbidol, Hydroxychloroquine, Oberadilol, Poziotinib) for bioactivity score prediction.

Properties		1	2	3	4	5	6	7	8	9	10
EI	1		0.0219	0.658	0.923	0.689	0.901	0.37	0.114	−0.0254	0.193
GPCR	2	0.0219		0.317	−0.0436	0.573	0.354	−0.894	0.229	−0.148	0.0199
ICM	3	0.658	0.317		0.543	0.762	0.849	−0.13	−0.501	−0.101	−0.0238
NRL	4	0.923	−0.0436	0.543		0.599	0.836	0.456	0.244	−0.106	−0.151
PI	5	0.689	0.573	0.762	0.599		0.905	−0.318	0.0426	0.276	−0.0383
pc1	6	0.901	0.354	0.849	0.836	0.905		1.08E−09	8.12E−09	−3.79E−09	1.67E−08
pc2	7	0.37	−0.894	−0.13	0.456	−0.318	1.08E−09		7.21E−09	1.03E−09	−4.17E−09
pc3	8	0.114	0.229	−0.501	0.244	0.0426	8.12E−09	7.21E−09		4.11E−09	3.79E−10
pc4	9	−0.0254	−0.148	−0.101	−0.106	0.276	−3.79E−09	1.03E−09	4.11E−09		9.73E−09
pc5	10	0.193	0.0199	−0.0238	−0.151	−0.0383	1.67E−08	−4.17E−09	3.79E−10	9.73E−09	

Table-1: MD simulation statistics

# Atoms	# Protein Residues	# Waters	Equilibration Time (ns)	Production Time (ns)
78793	194	25239	3.0	3.0

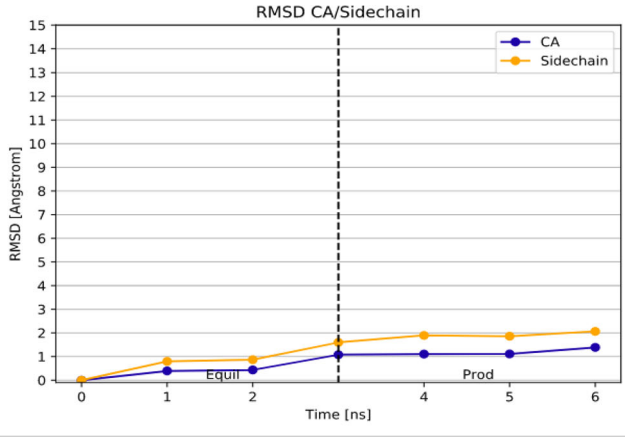

Fig 9.1

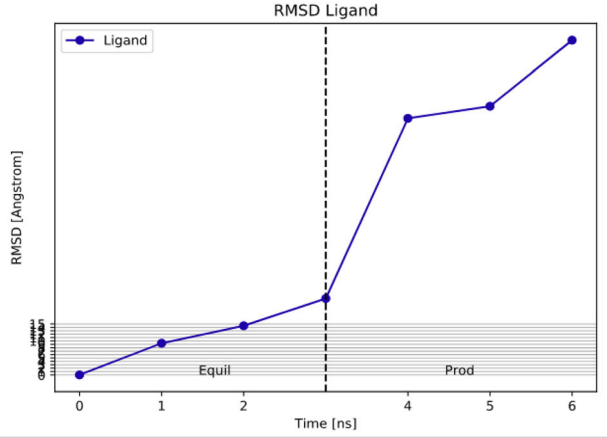

Fig 9.2

Figure 9. Molecular simulation of SARS–CoV–2 spike receptor–binding domain bound (6M0J) with withanolide A using Playmolecule open server (Table 1). Figures 9.1–9.2, Tables 2–4 here corresponds to the tables of MD simulation statistics. RMSD values were obtained as a function of time obtained at 300 K. Values were calculated with the use of Cα atoms. Figures 9.3–9.4. Average RMSF values obtained as a function of amino acid sequence numbers at 300 K. Values were calculated with the use of Cα atoms.

predicted to have any mutagenic effect. Further, in case of Caco-2 permeability, anaferine and withasomnine exhibited positive results indicating Caco-2 permeability. Positive results for Caco-2 indicate good permeability characteristics of compounds under evaluation since Caco-2 cells express a number of transporter and efflux proteins as well as Phase II conjugation enzymes for metabolic transformation of test substances (van Breemen & Li, 2005). Ames test is a short-term bacterial reverse mutation assay used for evaluating compounds for their ability to induce genetic damage and frame shift mutations (Ames et al., 1975; Mortelmans & Zeiger, 2000). Mutagenic effects bear a close connection to carcinogenesis (Xu et al., 2012). Interestingly, in the present study, none of the chosen WS phytoconstituents were predicted to have any mutagenic effect. The 3CL-pro of CoVs is necessary for the proteolytic maturation of the virus and a potential drug target to prevent infection from spreading by inhibiting the cleavage of viral proteins (Tian et al., 2015). Therefore, inhibition of such proteases which have a role in virus replication are often used as treatment strategies in antiviral drug therapeutics (Delaney, 2004). Human ACE2 expression in the airway epithelia appears to be critical as an entry receptor for SARS-CoV and SARS-CoV-2 (Morris et al., 1998). The transmembrane spike (S) glycoprotein present on the surface of coronaviruses facilitates their entry into the cell *via* ACE2 and is considered to be another prime target for antiviral agents against coronaviruses. These findings have implications for understanding disease pathogenesis

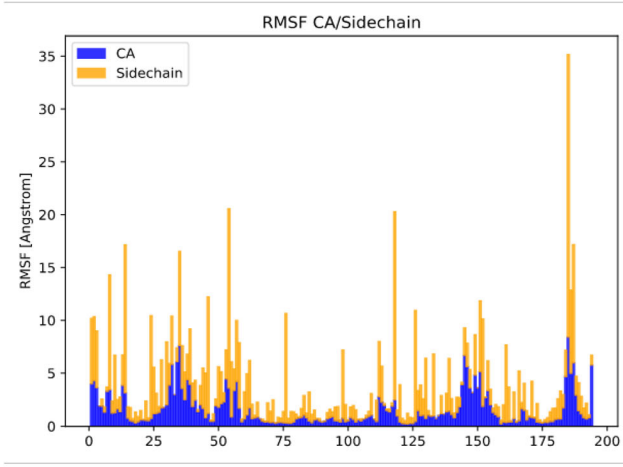

Fig 9.3

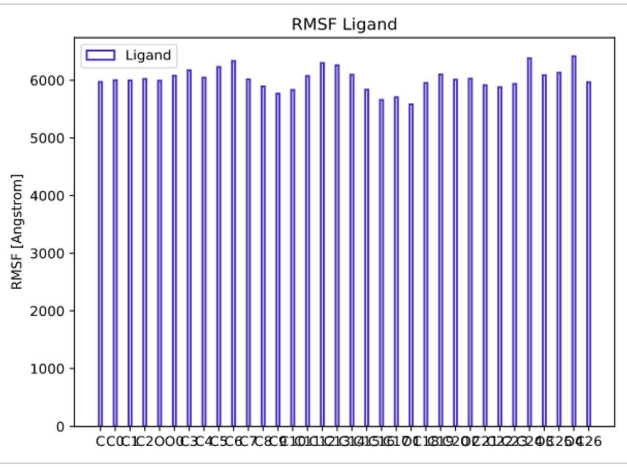

Fig 9.4

Table-2: Protein Clusters on RMSD

Cluster ID	Population (%)
3	33.33
2	23.33
1	23.33
5	13.33
4	6.67

Table-3: Protein Clusters on Contacts

Cluster ID	Population (%)
3	36.67
4	30.0
2	13.33
5	10.0
1	10.0

Table-4: Protein Clusters on Sec. Struct.

Cluster ID	Population (%)
3	33.33
2	26.67
5	23.33
4	10.0
1	6.67

Figure 9. Continued.

Table-1: MD simulation statistics

# Atoms	# Protein Residues	# Waters	Equilibration Time (ns)	Production Time (ns)
78268	313	24421	3.0	20.0

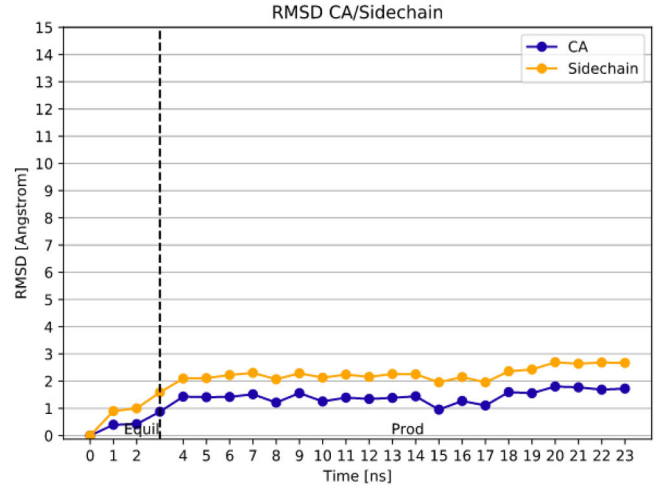

Fig 10.1

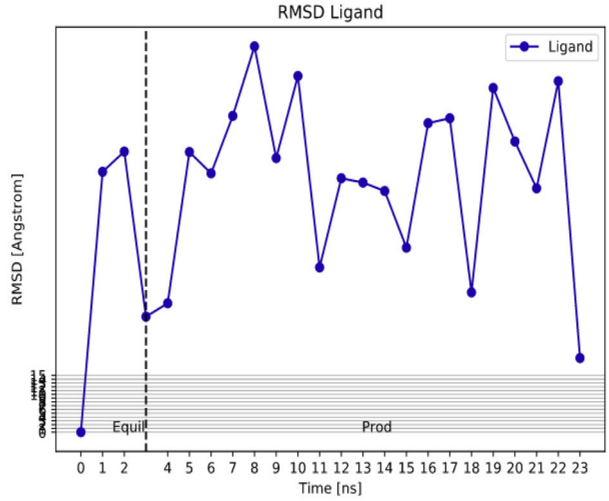

Fig 10.2

Figure 10. Molecular simulation of papain–like protease (6W9C–A chain) with withanolide B using Playmolecule open server. Figures 10.1–10.2, Tables 2–4 here corresponds to the tables of MD simulation statistics. RMSD values were obtained as a function of time obtained at 300 K. Values were calculated with the use of Cα atoms. Figures 10.3–10.4. Average RMSF values obtained as a function of amino acid sequence numbers at 300 K. Values were calculated with the use of Cα atoms.

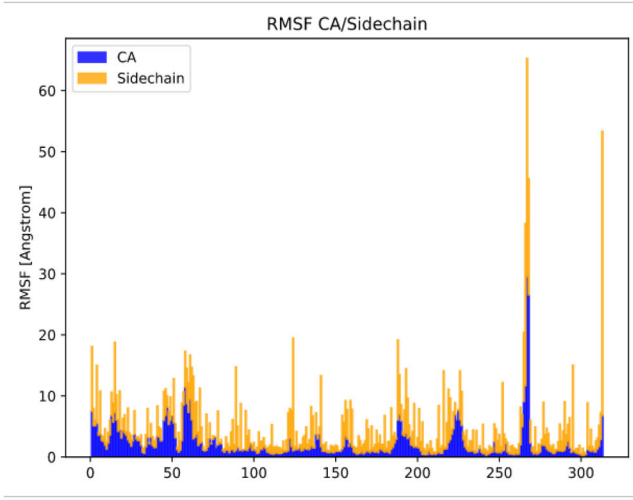

Fig 10.3

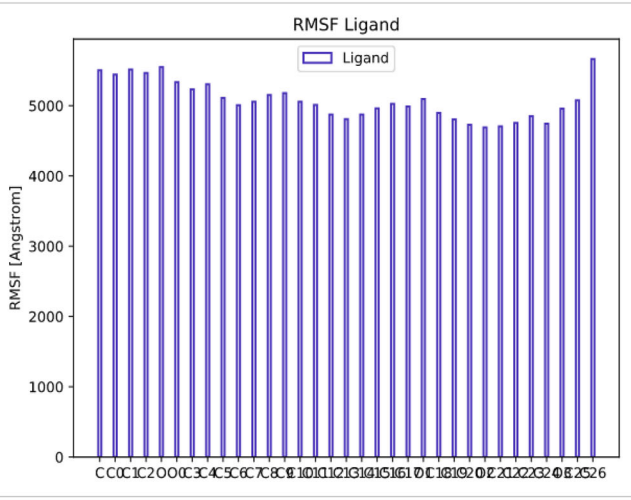

Fig 10.4

Protein Clusters Section

Table-2: Protein Clusters on RMSD

Cluster ID	Population (%)
1	14.5
6	11.0
10	10.0
3	8.5
13	8.0
9	7.5
7	7.0
14	6.5
12	6.5
5	6.5
4	5.0
11	3.5
8	3.0
2	2.5

Table-3: Protein Clusters on Contacts

Cluster ID	Population (%)
10	14.5
2	14.0
4	10.0
9	9.5
3	9.5
5	9.0
1	9.0
8	8.5
11	6.5
6	4.5
7	2.5
14	1.5
13	0.5
12	0.5

Table-4: Protein Clusters on Sec. Struct.

Cluster ID	Population (%)
5	12.5
2	11.5
1	8.5
11	8.0
9	8.0
7	7.5
14	7.0
10	6.5
6	6.5
13	6.0
12	6.0
4	5.0
3	4.0
8	3.0

Figure 10. Continued.

and opportunity to identify potential drug candidates for treatment.

Nelfinavir and lopinavir are viral protease inhibitors used against HIV infection but are reported to possess high cytotoxic effects. Lopinavir and ritonavir are viral protease inhibitors recommended for the treatment of SARS and MERS having similar mechanisms of action as nelfinavir and lopinavir. (Miyamoto and Kollman, 1992). To elucidate the binding affinity, docking studies of various withanolides found in WS were carried out on human ACE2 receptor, SARS-CoV and SARS-CoV-2 specific proteins. Among various phytoconstituents, withanolide A displayed strong binding affinity to SARS-CoV spike glycoprotein (BE: −9.78 kcal/mol, K_d: 67.23 nM), SARS-CoV-2 spike glycoprotein (BE: −7.18 kcal/mol, K_d: 5.48 μM), SARS-CoV 3CL-pro main protease (BE:-8.93 kcal/mol, K_d: 285.01 nM) and SARS-CoV-2 Nsp10/Nsp-16 complex (BE: −10.38 kcal/mol, K_d: 24.67 nM). On the basis of binding energy, withanolides A and B and withanone were found to be the most effective phytocomponents in WS. The present study reports for the first time the antiviral efficacy of medicinal herbs like *Withania somnifera* that form the crux of Ayurveda, the Indian traditional system of medicine as a

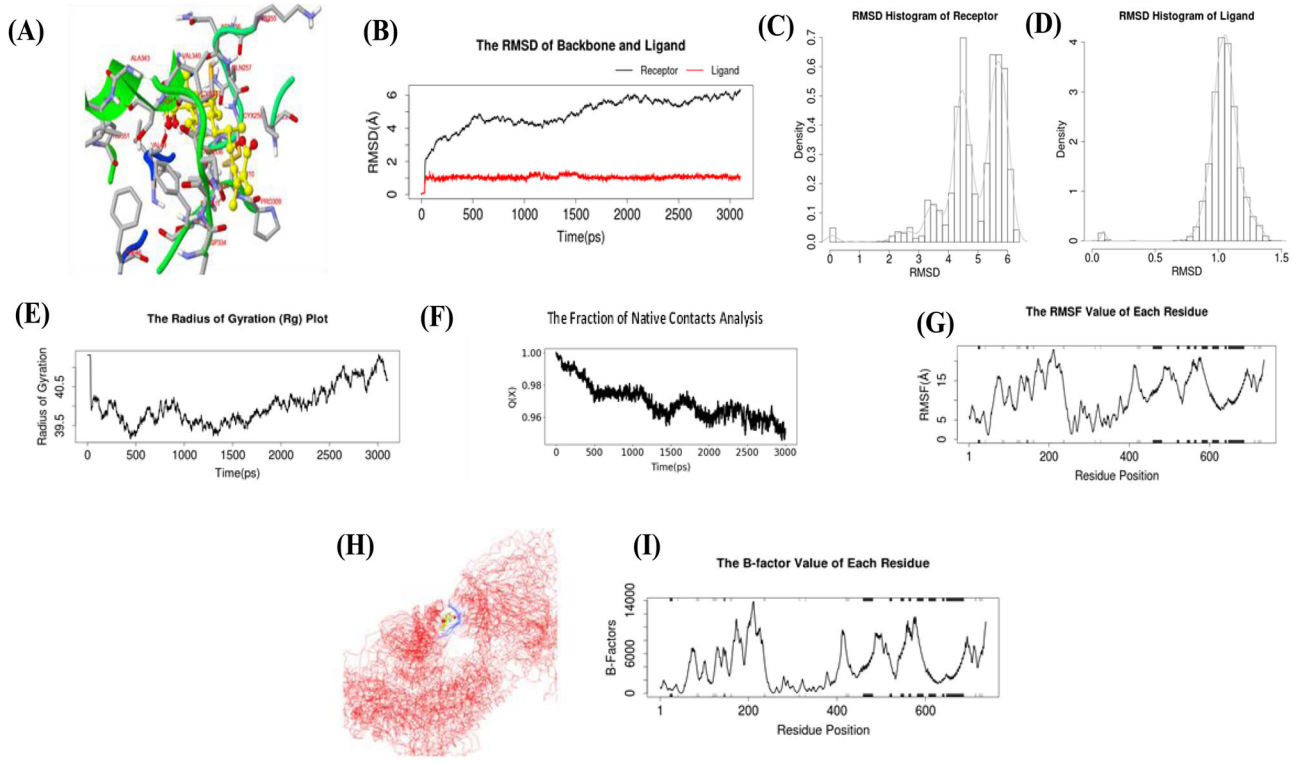

Figure 11.1. MD simulation of SARS–CoV spike glycoprotein (PDB ID: 5WRG) with withanolide B using LARMD online server. (A) Ligand–protein conformation, (B) RMSD of receptor and ligand (C) RMSD histogram of receptor (D) RMSD histogram of ligand (E) Radius of gyration—R_g value (F) Fraction of native contacts analysis of SARS-CoV–2 PL-pro (PDB ID: 6W9C) with withanolide B over a time frame of 4000 ps (4 ns) (G) RMSF value of each residue (H) B–factor value (changing from blue to red with increase in value) and (I) B–factor analysis of defined complex.

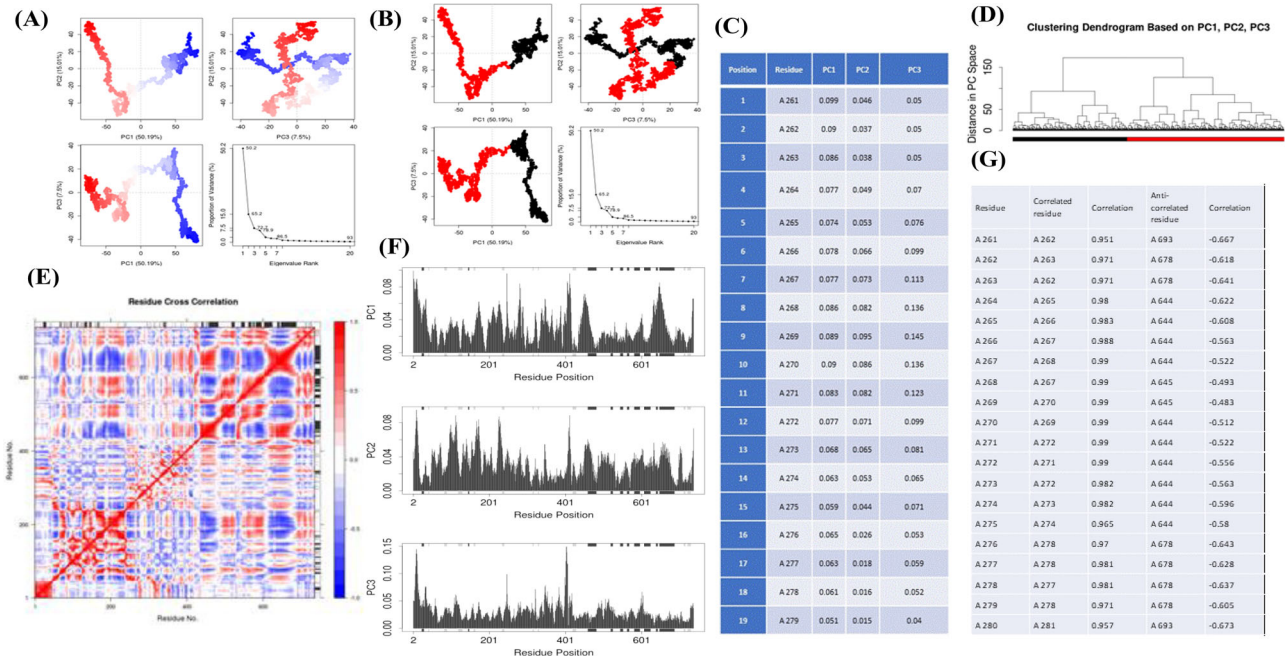

Position	Residue	PC1	PC2	PC3
1	A 261	0.099	0.046	0.05
2	A 262	0.09	0.037	0.05
3	A 263	0.086	0.038	0.05
4	A 264	0.077	0.049	0.07
5	A 265	0.074	0.053	0.076
6	A 266	0.078	0.066	0.099
7	A 267	0.077	0.073	0.113
8	A 268	0.086	0.082	0.136
9	A 269	0.089	0.095	0.145
10	A 270	0.09	0.086	0.136
11	A 271	0.083	0.082	0.123
12	A 272	0.077	0.071	0.099
13	A 273	0.068	0.065	0.081
14	A 274	0.063	0.053	0.065
15	A 275	0.059	0.044	0.071
16	A 276	0.065	0.026	0.053
17	A 277	0.063	0.018	0.059
18	A 278	0.061	0.016	0.052
19	A 279	0.051	0.015	0.04

Residue	Correlated residue	Correlation	Anti-correlated residue	Correlation
A 261	A 262	0.951	A 693	-0.667
A 262	A 263	0.971	A 678	-0.618
A 263	A 262	0.971	A 678	-0.641
A 264	A 265	0.98	A 644	-0.622
A 265	A 266	0.983	A 644	-0.608
A 266	A 267	0.988	A 644	-0.563
A 267	A 268	0.99	A 644	-0.522
A 268	A 267	0.99	A 645	-0.493
A 269	A 270	0.99	A 645	-0.483
A 270	A 269	0.99	A 644	-0.512
A 271	A 272	0.99	A 644	-0.522
A 272	A 271	0.99	A 644	-0.556
A 273	A 272	0.982	A 644	-0.563
A 274	A 273	0.982	A 644	-0.596
A 275	A 274	0.965	A 644	-0.58
A 276	A 278	0.97	A 678	-0.643
A 277	A 278	0.981	A 678	-0.628
A 278	A 277	0.981	A 678	-0.637
A 279	A 278	0.971	A 678	-0.605
A 280	A 281	0.957	A 693	-0.673

Figure 11.2. PCA of SARS–CoV spike glycoprotein (PDB ID: 5WRG) with withanolide B (A) PCA results for Trajectory (B) Simple clustering in PC subspace(C) Table data showing residue–wise loadings for PC1, PC2 and PC3 and residue number at each position (D) Clustering dendogram based on PC1, PC2 and PC3 (E) Dynamical residue cross–correlation map; the correlated residues are in blue, anti–correlated residues are in red; the pairwise residues with higher correlated coefficient ($>$0.8) and with higher anti–correlated coefficient ($\leq$0.4) are linked with light pink and light blue (Int_mod) (F) Residue–wise loadings for PC1, PC2 and PC3 (G) Table showing pairwise cross–correlation coefficients; higher correlated coefficient value is $>$0.8 and higher anti–correlated coefficient value is $\leq$0.4.

(A)

ELE	VDW	GAS	PBSOL	PBTOT	GBSOL	GBTOT	TS	deltaPB	deltaGB
-11.21	-57.38	-68.60	26.48	-42.12	20.22	-48.38	19.55	-22.57	-28.83

(C)

Acceptor	DonorH	Donor	Frames	Frac	AvgDist	AvgAng
A 308 : VAL@N	0 : UNN@H37	0 : UNN@O5	2	0.0006	3.3481	122.0165
A 306 : ARG@O	0 : UNN@H37	0 : UNN@O5	73	0.0235	3.2639	129.4816
A 308 : VAL@O	0 : UNN@H37	0 : UNN@O5	320	0.1032	3.1389	147.2763
0 : UNN@O1	A 602 : ASN@H	A 602 : ASN@N	1	0.0003	3.3708	164.1168
0 : UNN@O1	A 603 : CYS@H	A 603 : CYS@N	24	0.0077	3.4410	151.5285
0 : UNN@O3	A 521 : LYS@HZ2	A 521 : LYS@NZ	191	0.0616	3.2207	139.5150
0 : UNN@O3	A 521 : LYS@HZ1	A 521 : LYS@NZ	210	0.0677	3.2190	140.3313
0 : UNN@O1	A 521 : LYS@HZ2	A 521 : LYS@NZ	217	0.0700	3.2096	148.4242
0 : UNN@O1	A 521 : LYS@HZ1	A 521 : LYS@NZ	254	0.0819	3.1896	146.5975
0 : UNN@O3	A 521 : LYS@HZ3	A 521 : LYS@NZ	315	0.1016	3.2089	139.6684
0 : UNN@O1	A 521 : LYS@HZ3	A 521 : LYS@NZ	340	0.1097	3.2016	148.8572
0 : UNN@O2	A 524 : CYX@H	A 524 : CYX@N	522	0.1684	3.0522	128.5693
0 : UNN@O2	A 525 : VAL@H	A 525 : VAL@N	957	0.3087	3.3044	160.5783
0 : UNN@O5	A 308 : VAL@H	A 308 : VAL@N	1995	0.6435	3.2310	155.8190

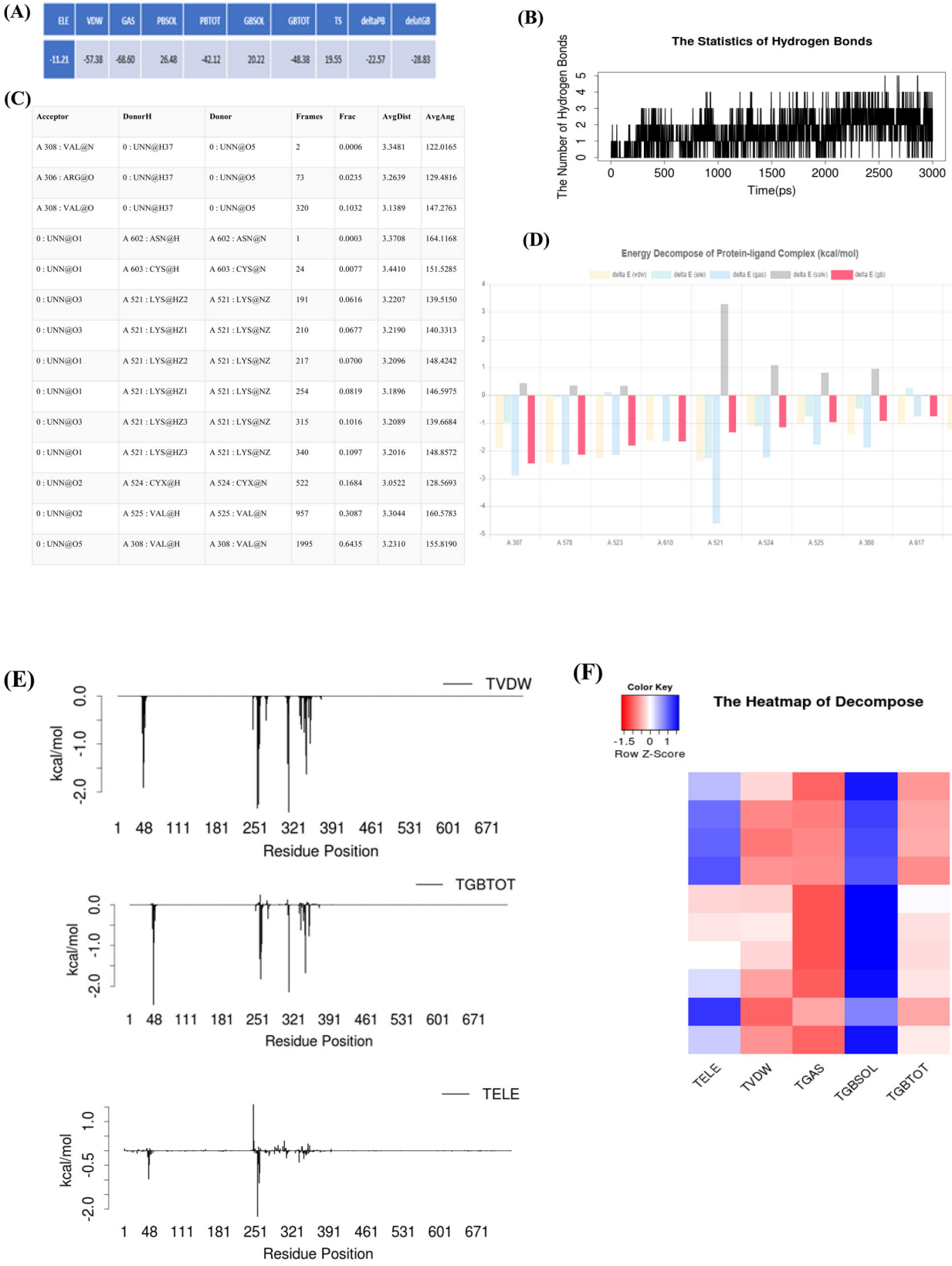

Figure 11.3. Energy, hydrogen bond analysis and decomposition analysis of SARS–CoV spike glycoprotein (PDB ID: 5WRG) with withanolide B (A) MM/PB(GB)SA result consists of electrostatic energy (ELE), van der Waals contribution (VDW), total gas phase energy (GAS), non–polar and polar contributions to solvation (PBSOL/GBSOL) (B,C) Statistics of hydrogen bonds (D) energy decompose of protein–ligand complex (Kcal/mol) (E) Graphical representation of decompose result (F) Showing the heatmap of decompose.

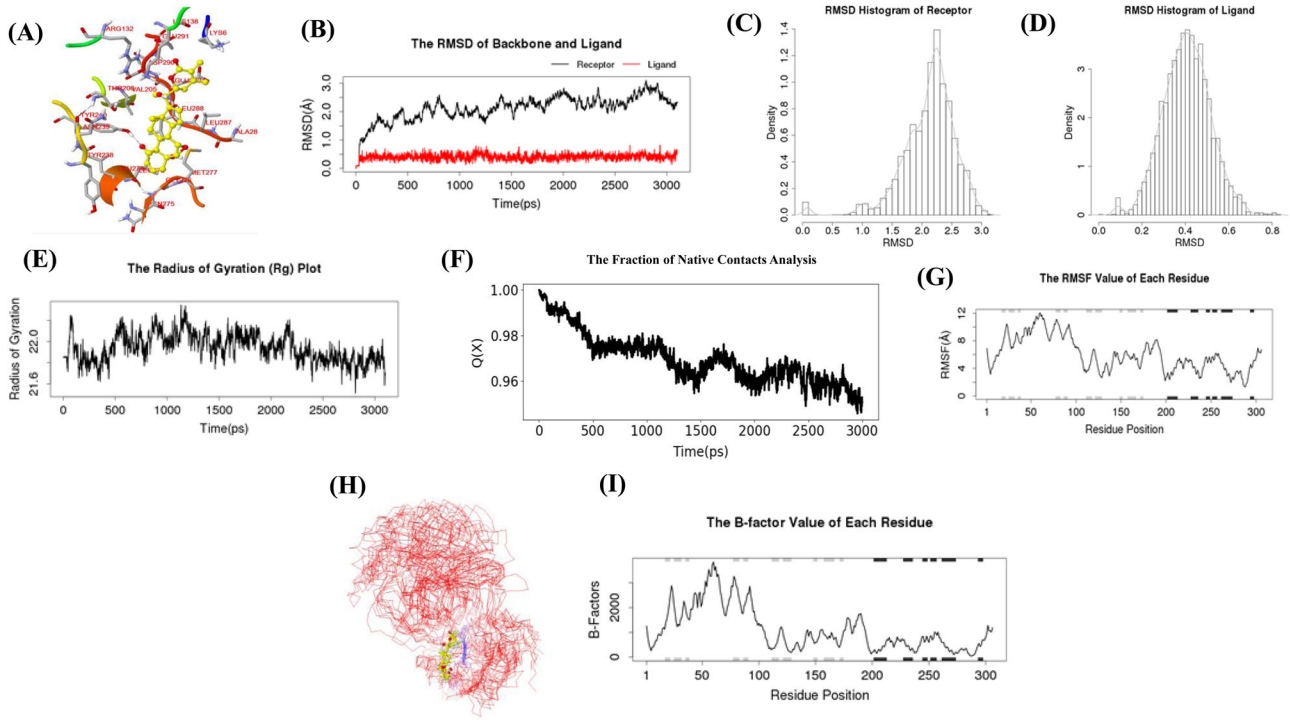

Figure 12.1. MD Simulation of SARS-CoV-2 main protease (PDB ID: 6LU7) with withanolide A using LARMD online server. (A) Ligand-protein conformation (B) RMSD of receptor and ligand (C) RMSD histogram of receptor (D) RMSD histogram of ligand (E) Radius of gyration- Rg value (F) Fraction of native contacts analysis of SARS-CoV-2 PL-pro (PDB ID: 6W9C) with withanolide A, over a time frame of 4000ps (4 ns) (G) RMSF value of each residue (H) B-factor value (changing from blue to red with increase in value) and (I) B-factor analysis of defined complex.

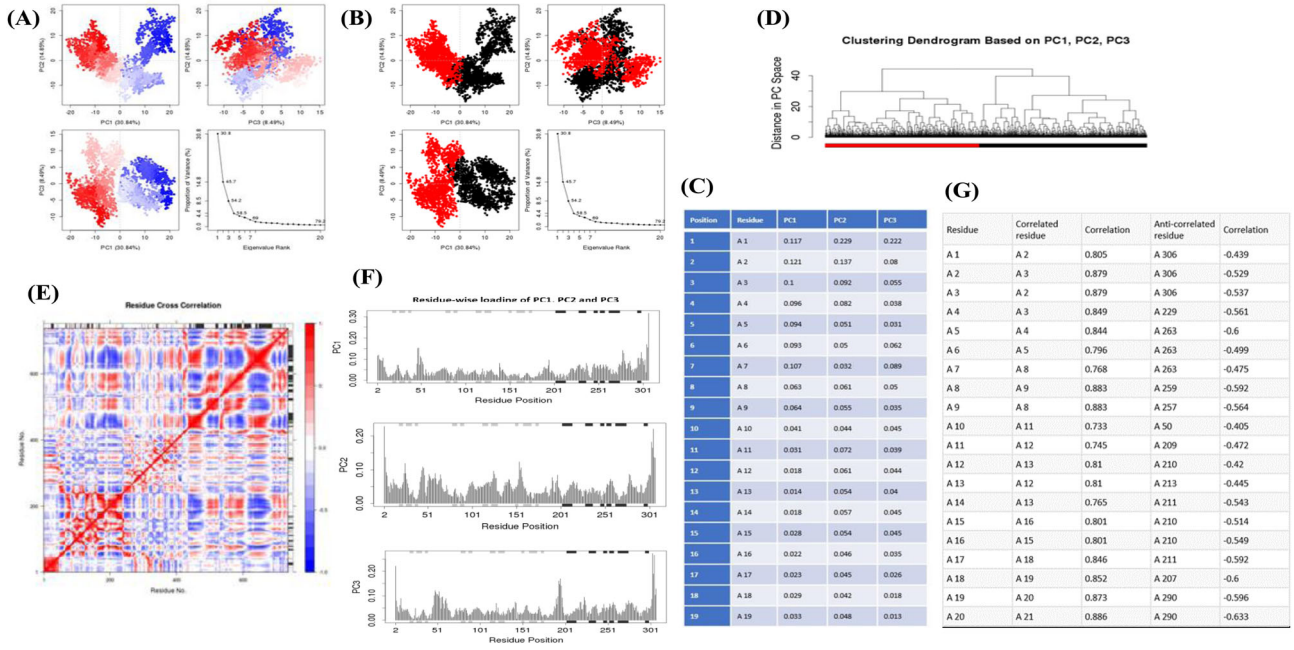

Position	Residue	PC1	PC2	PC3
1	A 1	0.117	0.229	0.222
2	A 2	0.121	0.137	0.08
3	A 3	0.1	0.092	0.055
4	A 4	0.096	0.082	0.038
5	A 5	0.094	0.051	0.031
6	A 6	0.093	0.05	0.062
7	A 7	0.107	0.032	0.089
8	A 8	0.063	0.061	0.05
9	A 9	0.064	0.055	0.035
10	A 10	0.041	0.044	0.045
11	A 11	0.031	0.072	0.039
12	A 12	0.018	0.061	0.044
13	A 13	0.014	0.054	0.04
14	A 14	0.018	0.057	0.045
15	A 15	0.028	0.054	0.045
16	A 16	0.022	0.046	0.035
17	A 17	0.023	0.045	0.026
18	A 18	0.029	0.042	0.018
19	A 19	0.033	0.048	0.013

Residue	Correlated residue	Correlation	Anti-correlated residue	Correlation
A 1	A 2	0.805	A 306	-0.439
A 2	A 3	0.879	A 306	-0.529
A 3	A 2	0.879	A 306	-0.537
A 4	A 3	0.849	A 229	-0.561
A 5	A 4	0.844	A 263	-0.6
A 6	A 5	0.796	A 263	-0.499
A 7	A 8	0.768	A 263	-0.475
A 8	A 9	0.883	A 259	-0.592
A 9	A 8	0.883	A 257	-0.564
A 10	A 11	0.733	A 50	-0.405
A 11	A 12	0.745	A 209	-0.472
A 12	A 13	0.81	A 210	-0.42
A 13	A 12	0.81	A 213	-0.445
A 14	A 13	0.765	A 211	-0.543
A 15	A 16	0.801	A 210	-0.514
A 16	A 15	0.801	A 210	-0.549
A 17	A 18	0.846	A 211	-0.592
A 18	A 19	0.852	A 207	-0.6
A 19	A 20	0.873	A 290	-0.596
A 20	A 21	0.886	A 290	-0.633

Figure 12.2. PCA of SARS-CoV-2 main protease (PDB ID: 6LU7) with withanolide A (A) PCA results for trajectory (B) Simple clustering in PC subspace(C) Table data showing residue-wise loadings for PC1, PC2 and PC3 and residue number at each position (D) Clustering dendogram based on PC1, PC2 and PC3 (E) Dynamical residue cross-correlation map; the correlated residues are in blue, anti-correlated residues are in red; the pairwise residues with higher correlated coefficient (>0.8) and with higher anti-correlated coefficient (≤0.4) are linked with light pink and light blue (Int_mod) (F) Residue-wise loadings for PC1, PC2 and PC3 (G) Table showing pairwise cross-correlation coefficients; higher correlated coefficient value is >0.8 and higher anti-correlated coefficient value is ≤0.4.

(A)

ELE	VDW	GAS	PBSOL	PBTOT	GBSOL	GBTOT	TS	deltaPB	delatGB
-8.76	-46.67	-55.43	29.43	-26.00	17.84	-37.59	16.61	-9.39	-20.98

(B)

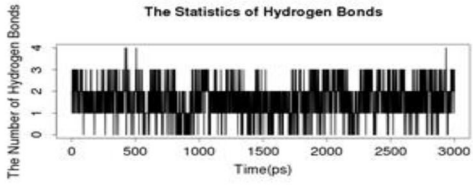

(C)

Acceptor	DonorH	Donor	Frames	Frac	AvgDist	AvgAng
A 287 : LEU@N	0 : UNN@H36	0 : UNN@O5	3	0.0010	3.3284	126.7758
A 289 : ASP@OD1	0 : UNN@H37	0 : UNN@O6	3	0.0010	3.1546	152.2037
A 289 : ASP@OD2	0 : UNN@H37	0 : UNN@O6	9	0.0029	3.2738	154.7389
A 290 : GLU@OE2	0 : UNN@H37	0 : UNN@O6	21	0.0068	3.2235	147.6793
A 137 : LYS@NZ	0 : UNN@H37	0 : UNN@O6	37	0.0119	3.2613	134.1959
A 131 : ARG@NH1	0 : UNN@H37	0 : UNN@O6	65	0.0210	3.2606	139.0129
A 131 : ARG@NH2	0 : UNN@H37	0 : UNN@O6	158	0.0510	3.2167	140.6968
A 199 : THR@OG1	0 : UNN@H37	0 : UNN@O6	377	0.1216	3.2261	143.1934
0 : UNN@O2	A 287 : LEU@H	A 287 : LEU@N	2	0.0006	3.4297	163.8241
0 : UNN@O3	A 131 : ARG@HH21	A 131 : ARG@NH2	3	0.0010	3.3148	125.2424
0 : UNN@O1	A 5 : LYS@HZ2	A 5 : LYS@NZ	7	0.0023	3.2226	133.8654
0 : UNN@O1	A 5 : LYS@HZ3	A 5 : LYS@NZ	8	0.0026	3.3174	139.5053
0 : UNN@O1	A 5 : LYS@HZ1	A 5 : LYS@NZ	12	0.0039	3.3013	136.6195
0 : UNN@O1	A 131 : ARG@HH11	A 131 : ARG@NH1	14	0.0045	3.2832	129.0420
0 : UNN@O6	A 199 : THR@HG1	A 199 : THR@OG1	15	0.0048	3.3192	136.2907
0 : UNN@O1	A 137 : LYS@HZ2	A 137 : LYS@NZ	27	0.0087	3.2731	148.5657
0 : UNN@O3	A 137 : LYS@HZ2	A 137 : LYS@NZ	41	0.0132	3.2815	150.1774
0 : UNN@O1	A 137 : LYS@HZ3	A 137 : LYS@NZ	44	0.0142	3.2876	140.7139
0 : UNN@O1	A 137 : LYS@HZ1	A 137 : LYS@NZ	44	0.0142	3.2603	140.4173
0 : UNN@O3	A 137 : LYS@HZ3	A 137 : LYS@NZ	48	0.0155	3.3197	142.2987
0 : UNN@O6	A 131 : ARG@HH21	A 131 : ARG@NH2	71	0.0229	3.2903	129.8963
0 : UNN@O3	A 137 : LYS@HZ1	A 137 : LYS@NZ	72	0.0232	3.2660	143.7889
0 : UNN@O5	A 287 : LEU@H	A 287 : LEU@N	125	0.0403	3.2917	149.8227
0 : UNN@O3	A 131 : ARG@HH22	A 131 : ARG@NH2	208	0.0671	3.2423	137.4954
0 : UNN@O1	A 131 : ARG@HH12	A 131 : ARG@NH1	228	0.0735	3.1600	135.4361
0 : UNN@O6	A 131 : ARG@HH12	A 131 : ARG@NH1	246	0.0794	3.2320	140.8624
0 : UNN@O1	A 131 : ARG@HH22	A 131 : ARG@NH2	260	0.0839	3.2122	137.8961
0 : UNN@O3	A 131 : ARG@HH12	A 131 : ARG@NH1	284	0.0916	3.2904	138.9531
0 : UNN@O6	A 137 : LYS@HZ1	A 137 : LYS@NZ	340	0.1097	3.1661	146.3794
0 : UNN@O6	A 137 : LYS@HZ2	A 137 : LYS@NZ	346	0.1116	3.1512	147.6441
0 : UNN@O6	A 137 : LYS@HZ3	A 137 : LYS@NZ	350	0.1129	3.1904	145.0681
0 : UNN@O6	A 131 : ARG@HH22	A 131 : ARG@NH2	735	0.2371	3.1978	139.9320
0 : UNN@O2	A 239 : TYR@HH	A 239 : TYR@OH	1624	0.5239	2.9957	156.0862

(D)

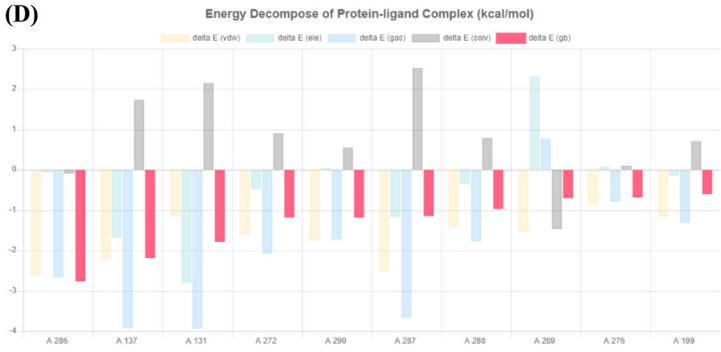

(E)

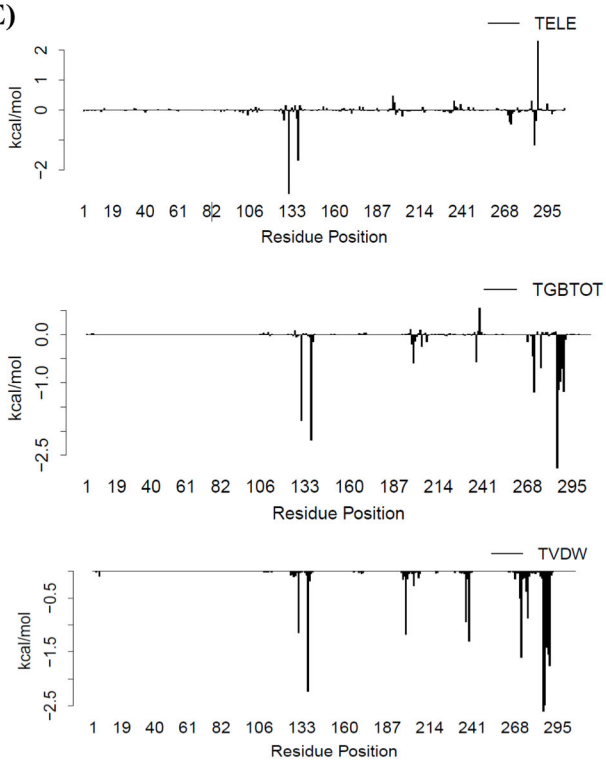

(F)

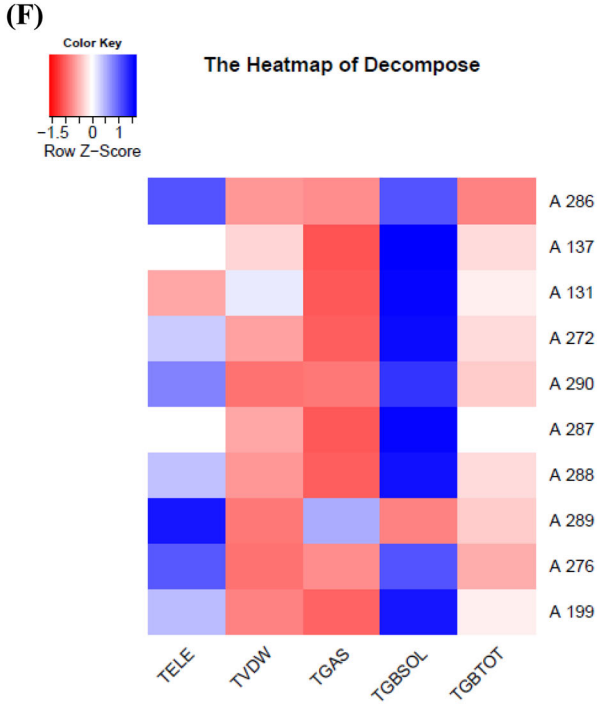

Figure 12.3. Energy, hydrogen bond analysis and decomposition analysis of SARS-CoV-2 main protease (PDB ID: 6LU7) with withanolide A. (A) MM/PB(GB)SA result consists of electrostatic energy (ELE), van der Waals contribution (VDW), total gas phase energy (GAS), non-polar and polar contributions to solvation (PBSOL/GBSOL) (B,C) Statistics of hydrogen bonds (D) Energy decompose of protein–ligand complex (Kcal/mol) (E) Graphical representation of decompose result (F) Showing the heatmap of decompose.

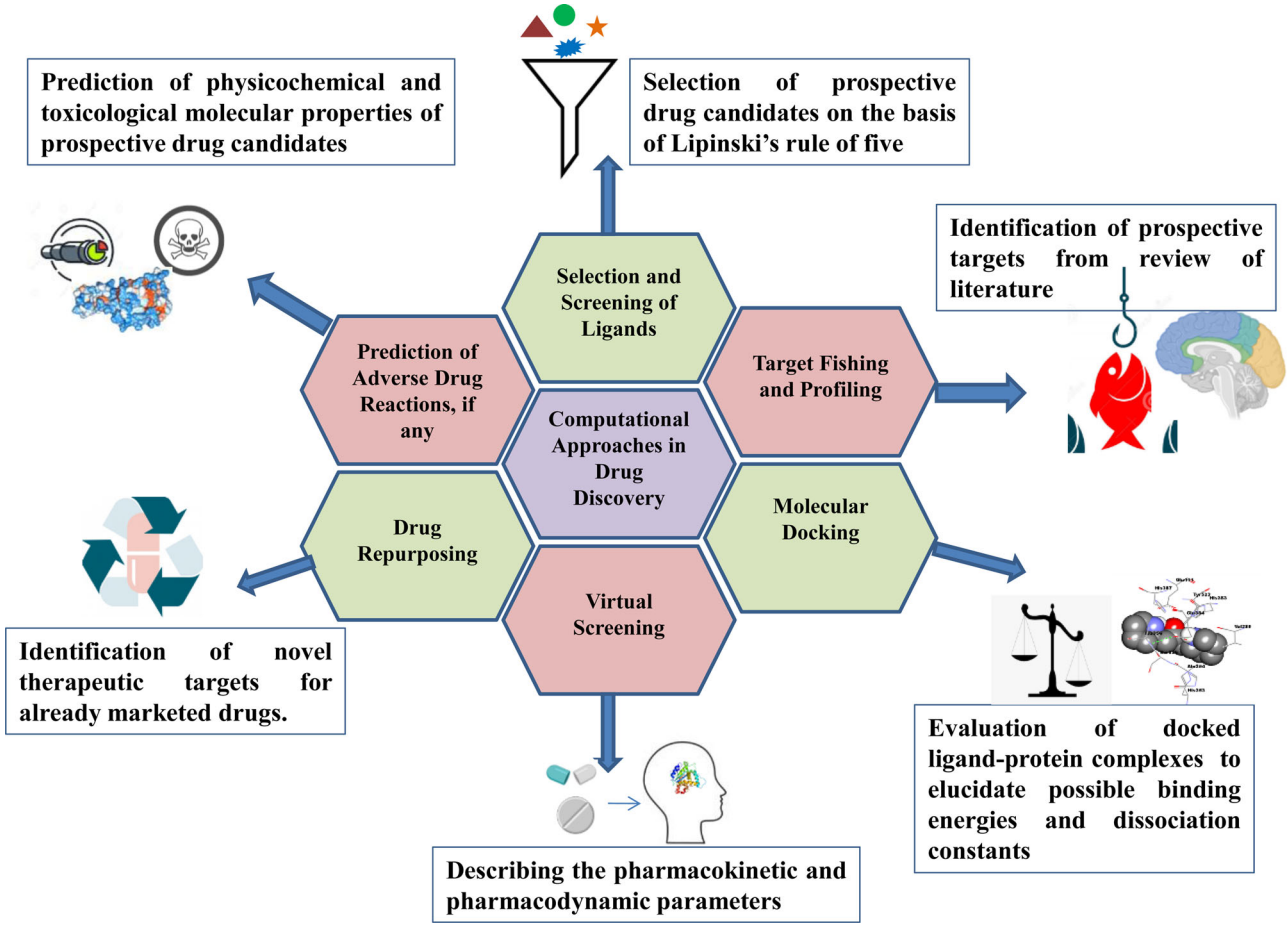

Figure 13. Stages in drug discovery and development.

viable alternative to chemosynthetic drugs for preventing/blocking entry of SARS-CoV-2 into host cells and also inhibiting viral main protease.

In conclusion, the most effective withanolides *viz*. withanolide A, withanolide B and withanone can be exploited and studied in future both *in vitro* and *in vivo* as prospective first choice antiviral agents for curbing COVID-19 infection. This preliminary study provides validation for plausible inhibitory potential of major withanolides found in WS.

Acknowledgements

The authors gratefully acknowledge Dr. Meraj Ahmad, Professor, Dept. of Sociology, University of Lucknow, Lucknow, India, for being the inspiration and motivation behind the present work in view of his exceptional work and contribution in the area of social sciences, social work, humanities and public health.

Disclosure statement

The authors declare that they have no competing interests.

ORCID

Aditi Srivastava http://orcid.org/0000-0003-3141-7311
Sahabjada Siddiqui http://orcid.org/0000-0003-0982-1465
Rumana Ahmad http://orcid.org/0000-0002-7535-4976
Sudhir Mehrotra http://orcid.org/0000-0001-7070-4554
Bilal Ahmad http://orcid.org/0000-0003-1680-5252
A. N. Srivastava http://orcid.org/0000-0001-9633-9903

References

Ahmad, R. (2019). Steroidal glycoalkaloids from *Solanum nigrum* target cytoskeletal proteins: An *in silico* analysis. Peer *Journal*, *7*, e6012. https://doi.org/10.7717/peerj.6012

Ames, B. N., McCann, J., & Yamasaki, E. (1975). Methods for detecting carcinogens and mutagens with the Salmonella/mammalian–microsome mutagenicity test. *Mutation Research/Environmental Mutagenesis & Related Subjects*, *31*(6), 347–363.

Anand, K., Ziebuhr, J., Wadhwani, P., Mesters, J. R., & Hilgenfeld, R. (2003). Coronavirus main proteinase (3CLpro) structure: Basis for design of anti-SARS drugs. *Science (New York, NY)*, *300*(5626), 1763–1767. https://doi.org/10.1126/science.1085658

Aniyery, R. B., Gupta, A., Singh, P., Khatri, C., & Pathak, A. (2015). Synthesis, characterization, biological activities and computational anticancer study of Dibutylbis [(2-isopropyl-5-ethylcyclohexyl) oxy] stannane. *Journal of Chemical & Pharmaceutical Science*, *8*, 957–963.

Arya, R., Das, A., Prashar, V., & Kumar, M. (2010). Potential inhibitors against papain-like protease of novel coronavirus (SARS-CoV-2) from FDA approved drugs. *ChemRxiv*. Preprint. https://doi.org/10.26434/chemrxiv.11860011.v2

Báez-Santos, Y. M., John, S. E., & Mesecar, A. D. (2015). The SARS-coronavirus papain-like protease: Structure, function and inhibition by designed antiviral compounds. *Antiviral Research*, *115*, 21–38. https://doi.org/10.1016/j.antiviral.2014.12.015

Bahar, I., Lezon, T. R., Bakan, A., & Shrivastava, I. H. (2010). Normal mode analysis of biomolecular structures: Functional mechanisms of

membrane proteins. *Chemical Reviews*, *110*(3), 1463–1497. https://doi.org/10.1021/cr900095e

Balakrishnan, N. A., Raj, J. S., & Kandakatla, N. A. (2015). *In silico* studies on new indazole derivatives as gsk-3 β inhibitors. *International Journal of Pharmacy & Pharmaceutical Sciences*, *7*, 295–299.

Balakrishnan, N., Raj, J. S., & Kandakatla, N. (2014). 2D/3D-QSAR, docking and optimization of 5-substituted-1h-indazole as inhibitors of GSK-3β. *International Journal of Pharmaceutical Science*, *6*(10), 413–420.

Belouzard, S., Chu, V. C., & Whittaker, G. R. (2009). Activation of the SARS coronavirus spike protein via sequential proteolytic cleavage at two distinct sites. *Proceedings of the National Academy of Sciences of the United States of America*, *106*(14), 5871–5876. https://doi.org/10.1073/pnas.0809524106

Bosch, B. J., van der Zee, R., de Haan, C. A., & Rottier, P. J. (2003). The coronavirus spike protein is a class I virus fusion protein: Structural and functional characterization of the fusion core complex. *Journal of Virology*, *77*(16), 8801–8811. https://doi.org/10.1128/jvi.77.16.8801-8811.2003

Burkard, C., Verheije, M. H., Wicht, O., van Kasteren, S. I., van Kuppeveld, F. J., Haagmans, B. L., Pelkmans, L., Rottier, P. J., Bosch, B. J., & de Haan, C. A. (2014). Coronavirus cell entry occurs through the endo-/lysosomal pathway in a proteolysis-dependent manner. *PLoS Pathogens*, *10*(11), e1004502.

Cai, Z., Zhang, G., Tang, B., Liu, Y., Fu, X., & Zhang, X. (2015). Promising anti-influenza properties of active constituent of *Withania somnifera* ayurvedic herb in targeting neuraminidase of H1N1 influenza: Computational study. *Cell Biochemistry & Biophysics*, *72*(3), 727–739. https://doi.org/10.1007/s12013-015-0524-9

Campillos, M., Kuhn, M., Gavin, A. C., Jensen, L. J., & Bork, P. (2008). Drug target identification using side-effect similarity. *Science (New York, NY)*, *321*(5886), 263–266. https://doi.org/10.1126/science.1158140

Chan, J. F. W., Chan, K.-H., Kao, R. Y. T., To, K. K. W., Zheng, B.-J., Li, C. P. Y., Li, P. T. W., Dai, J., Mok, F. K. Y., Chen, H., Hayden, F. G., & Yuen, K.-Y. (2013). Broad-spectrum antivirals for the emerging Middle East respiratory syndrome coronavirus. *The Journal of Infection*, *67*(6), 606–616. https://doi.org/10.1016/j.jinf.2013.09.029

Chen, Y., Liu, Q., & Guo, D. (2020). Emerging coronaviruses: Genome structure, replication, and pathogenesis. *Journal of Medical Virology*, *92*(4), 418–423. https://doi.org/10.1002/jmv.25681

Chen, Y. W., Yiu, C. P., & Wong, K. Y. (2020). Prediction of the SARS-CoV-2 (2019-nCoV) 3C-like protease (3CL pro) structure: Virtual screening reveals velpatasvir, ledipasvir, and other drug repurposing candidates. F1000 Research, *9*, 129.

Cheng, F., Li, W., Zhou, Y., Shen, J., Wu, Z., Liu, G., Lee, P. W., & Tang, Y. (2012). admetSAR: A comprehensive source and free tool for assessment of chemical ADMET properties. *J. Chem. Inf. Model.* 52(11), 3099–3105. https://doi.org/10.1021/ci300367a

Cheng, T., Li, Q., Zhou, Z., Wang, Y., & Bryant, S. H. (2012). Structure-based virtual screening for drug discovery: A problem-centric review. *The AAPS Journal*, *14*(1), 133–141. https://doi.org/10.1208/s12248-012-9322-0

Coronavirus Outbreak in India. https://www.covid19india.org/.

de Wilde, A. H., Jochmans, D., Posthuma, C. C., Zevenhoven-Dobbe, J. C., van Nieuwkoop, S., Bestebroer, T. M., van den Hoogen, B. G., Neyts, J., & Snijder, E. J. (2014). Screening of an FDA-approved compound library identifies four small-molecule inhibitors of Middle East respiratory syndrome coronavirus replication in cell culture. *Antimicrobial Agents & Chemotherapy*, *58*(8), 4875–4884. https://doi.org/10.1128/AAC.03011-14

Delaney, J. S. (2004). ESOL: Estimating aqueous solubility directly from molecular structure. *Journal of Chemical Information & Computer Sciences*, *44*(3), 1000–1005. https://doi.org/10.1021/ci034243x

Dhar, N., Rana, S., Bhat, W. W., Razdan, S., Pandith, S. A., Khan, S., Dutt, P., Dhar, R. S., Vaishnavi, S., Vishwakarma, R., & Lattoo, S. K. (2013). Dynamics of withanolide biosynthesis in relation to temporal expression pattern of metabolic genes in *Withania somnifera* (L.) Dunal: A comparative study in two morpho-chemovariants. *Molecular Biology Reports*, *40*(12), 7007–7016. https://doi.org/10.1007/s11033-013-2820-z

Dhar, N., Razdan, S., Rana, S., Bhat, W. W., Vishwakarma, R., & Lattoo, S. K. (2015). A decade of molecular understanding of withanolide biosynthesis and *in vitro* studies in *Withania somnifera* (L.) Dunal: Prospects and perspectives for pathway engineering. *Frontiers in Plant Sciences*, *6*, 1031. https://doi.org/10.3389/fpls.2015.01031

Donoghue, M., Hsieh, F., Baronas, E., Godbout, K., Gosselin, M., Stagliano, N., Donovan, M., Woolf, B., Robison, K., Jeyaseelan, R., Breitbart, R. E., & Acton, S. (2000). A novel angiotensin-converting enzyme-related carboxypeptidase (ACE2) converts angiotensin I to angiotensin 1–9. *Circulation Research*, *87*(5), E1. https://doi.org/10.1161/01.res.87.5.e1

Dyalla, J., Christopher, M. C., Harta, B. J., Venkataramanb, T., Michael, R., Holbrooka, J. K., Reed, F. J., Gene, G. O., Jr Peter, B. J., Laidlawd, M., & Lisa, M. J. (2014). Repurposing of clinically developed drugs for treatment of Middle East Respiratory Coronavirus Infection 2. *Infection*, *2*, 3.

Egan, W. J., Merz, K. M., & Baldwin, J. J. (2000). Prediction of drug absorption using multivariate statistics. *Journal of Medicinal Chemistry*, *43*(21), 3867–3877. https://doi.org/10.1021/jm000292e

Ertl, P., Rohde, B., & Selzer, P. (2000). Fast calculation of molecular polar surface area as a sum of fragment-based contributions and its application to the prediction of drug transport properties. *Journal of Medicinal Chemistry*, *43*(20), 3714–3717. https://doi.org/10.1021/jm000942e

Fouchier, R. A., Kuiken, T., Schutten, M., Van Amerongen, G., Van Doornum, G. J., Van Den Hoogen, B. G., Peiris, M., Lim, W., Stöhr, K., & Osterhaus, A. D. (2003). Aetiology: Koch's postulates fulfilled for SARS virus. Nature, *423*(6937), 240. https://doi.org/10.1038/423240a

Galvelis, R., Doerr, S., Damas, J. M., Harvey, M. J., & De Fabritiis, G. (2019). A scalable molecular force field parameterization method based on density functional theory and quantum-level machine learning. *Journal of Chemical Information & Modelling*, *59*(8), 3485–3493. https://doi.org/10.1021/acs.jcim.9b00439

Ghose, T. K. (1987). Measurement of cellulase activities. *Pure & Applied Chemistry*, *59*(2), 257–268.

Ghose, A., & Crippen, G. (1987). Atomic physicochemical parameters for three-dimensional-structure-directed quantitative structure-activity relationships. 2. Modeling dispersive and hydrophobic interactions. *Journal of Chemical Information & Computer Sciences*, *27*(1), 21–35. https://doi.org/10.1021/ci00053a005

Ghose, A. K., Viswanadhan, V. N., & Wendoloski, J. J. (1999). A knowledge-based approach in designing combinatorial or medicinal chemistry libraries for drug discovery. 1. A qualitative and quantitative characterization of known drug databases. *Journal of Combinatorial Chemistry*, *1*(1), 55–68. https://doi.org/10.1021/cc9800071

Glass, W. G., Subbarao, K., Murphy, B., & Murphy, P. M. (2004). Mechanisms of host defense following severe acute respiratory syndrome-coronavirus (SARS-CoV) pulmonary infection of mice. *Journal of Immunology (Baltimore, MD 1950))*, *173*(6), 4030–4039. https://doi.org/10.4049/jimmunol.173.6.4030

Guy, J. L., Jackson, R. M., Jensen, H. A., Hooper, N. M., & Turner, A. J. (2005). Identification of critical active-site residues in angiotensin-converting enzyme-2 (ACE2) by site-directed mutagenesis. *The FEBS Journal*, *272*(14), 3512–3520. https://doi.org/10.1111/j.1742-4658.2005.04756.x

Hamming, I., Timens, W., Bulthuis, M. L., Lely, A. T., Navis, G. J., & van Goor, H. (2004). Tissue distribution of ACE2 protein, the functional receptor for SARS coronavirus. A first step in understanding SARS pathogenesis. *The Journal of Pathology*, *203*(2), 631–637. https://doi.org/10.1002/path.1570

Harcourt, B. H., Jukneliene, D., Kanjanahaluethai, A., Bechill, J., Severson, K. M., Smith, C. M., Rota, P. A., & Baker, S. C. (2004). Identification of severe acute respiratory syndrome coronavirus replicase products and characterization of papain-like protease activity. *Journal of Virology*, *78*(24), 13600–13612. https://doi.org/10.1128/JVI.78.24.13600-13612.2004

Harmer, D., Gilbert, M., Borman, R., & Clark, K. L. (2002). Quantitative mRNA expression profiling of ACE 2, a novel homologue of angiotensin converting enzyme. *FEBS Letters*, *532*(1–2), 107–110.

Hogan, R. J., Gao, G., Rowe, T., Bell, P., Flieder, D., Paragas, J., Kobinger, G. P., Wivel, N. A., Crystal, R. G., Boyer, J., Feldmann, H., Voss, T. G., & Wilson, J. M. (2004). Resolution of primary severe acute respiratory syndrome-associated coronavirus infection requires Stat1. *Journal of*

Virology, *78*(20), 11416–11421. https://doi.org/10.1128/JVI.78.20.11416-11421.2004

Jain, R., Kachhwaha, S., & Kothari, S. L. (2012). Phytochemistry, pharmacology, and biotechnology of *Withania somnifera* and *Withania coagulans*: A review. *Journal of Medicinal Plants Research*, *6*(41), 5388–5399.

Khan, T., Ahmad, R., Azad, I., Raza, S., Joshi, S., & Khan, A. R. (2018). Computer-aided drug design and virtual screening of targeted combinatorial libraries of mixed-ligand transition metal complexes of 2-butanone thiosemicarbazone. *Computational Biology & Chemistry*, *75*, 178–195. https://doi.org/10.1016/j.compbiolchem.2018.05.008

Kirchdoerfer, R. N., Cottrell, C. A., Wang, N., Pallesen, J., Yassine, H. M., Turner, H. L., Corbett, K. S., Graham, B. S., McLellan, J. S., & Ward, A. B. (2016). Pre-fusion structure of a human coronavirus spike protein. Nature, *531*(7592), 118–121. https://doi.org/10.1038/nature17200

Kuiken, T., Fouchier, R. A., Schutten, M., Rimmelzwaan, G. F., van Amerongen, G., van Riel, D., Laman, J. D., de Jong, T., van Doornum, G., Lim, W., Ling, A. E., Chan, P. K., Tam, J. S., Zambon, M. C., Gopal, R., Drosten, C., van der Werf, S., Escriou, N., Manuguerra, J.-C., … Osterhaus, A. D. (2003). Osterhaus AD: Newly discovered coronavirus as the primary cause of severe acute respiratory syndrome. Lancet, *362*(9380), 263–270.

Kumar, V., Dey, A., Hadimani, M. B., Marcović, T., & Emerald, M. (2015). Chemistry and pharmacology of Withania somnifera: An update. *Tang*, 5(1), 1–3.

Kuzmanic, A., & Zagrovic, B. (2010). Determination of ensemble-average pairwise root mean-square deviation from experimental B-factors. *Biophysical Journal*, *98*(5), 861–871.

Laskowski, R. A., Hutchinson, E. G., Michie, A. D., Wallace, A. C., Jones, M. L., & Thornton, J. M. (1997). PDBsum: A web-based database of summaries and analyses of all PDB structures. *Trends in Biochemical Sciences*, *22*(12), 488–490.

Li, W., Zhang, C., Sui, J., Kuhn, J. H., Moore, M. J., Luo, S., Wong, S.-K., Huang, I.-C., Xu, K., Vasilieva, N., Murakami, A., He, Y., Marasco, W. A., Guan, Y., Choe, H., & Farzan, M. (2005). Receptor and viral determinants of SARS-coronavirus adaptation to human ACE2. *The EMBO Journal*, *24*(8), 1634–1643. https://doi.org/10.1038/sj.emboj.7600640

Lipinski, C. A., Lombardo, F., Dominy, B. W., & Feeney, P. J. (1997). Experimental and computational approaches to estimate solubility and permeability in drug discovery and development settings. *Advanced Drug Delivery Reviews*, *23*(1–3), 3–25.

Liu, X., Zhang, B., J. Z., Yang, H., & Rao, Z. (2020). The crystal structure of COVID-19 main protease in complex with an inhibitor N3. PDB.

Liu, S., Zheng, Q., & Wang, Z. (2020). Potential covalent drugs targeting the main protease of the SARS-CoV-2 coronavirus. Bioinformatics (*Oxford*, England*)*, *36*(11), 3295–3298.

Martin, Y. C. (2005). A bioavailability score. *Journal of Medicinal Chemistry*, *48*(9), 3164–3170.

Martina, B. E., Haagmans, B. L., Kuiken, T., Fouchier, R. A., Rimmelzwaan, G. F., Van Amerongen, G., Peiris, J. M., Lim, W., & Osterhaus, A. D. (2003). Virology: SARS virus infection of cats and ferrets. Nature, *425*(6961), 915. https://doi.org/10.1038/425915a

Martínez-Rosell, G., Giorgino, T., & De Fabritiis, G. (2017). PlayMolecule ProteinPrepare: A web application for protein preparation for molecular dynamics simulations. *Journal of Chemical Information & Modelling*, *57*(7), 1511–1516. https://doi.org/10.1021/acs.jcim.7b00190

McAuliffe, J., Vogel, L., Roberts, A., Fahle, G., Fischer, S., Shieh, W. J., Butler, E., Zaki, S., Claire, M. S., Murphy, B., & Subbarao, K. (2004). Replication of SARS coronavirus administered into the respiratory tract of African Green, rhesus and cynomolgus monkeys. Virology, *330*(1), 8–15. https://doi.org/10.1016/j.virol.2004.09.030

Mirjalili, M. H., Moyano, E., Bonfill, M., Cusido, R. M., & Palazón, J. (2009). Steroidal lactones from *Withania somnifera*, an ancient plant for novel medicine. *Molecules (Basel, Switzerland))*, *14*(7), 2373–2393. https://doi.org/10.3390/molecules14072373

Misico, R. I., Nicotra, V. E., Oberti, J. C., Barboza, G., Gil, R. R., & Burton, G. (2011). Withanolides and related steroids. In *Progress in the chemistry of organic natural products* (Vol. 94, pp. 127–229). Springer.

Misra, L., Mishra, P., Pandey, A., Sangwan, R. S., Sangwan, N. S., & Tuli, R. (2008). Withanolides from *Withania somnifera* roots. Phytochemistry, *69*(4), 1000–1004. https://doi.org/10.1016/j.phytochem.2007.10.024

Miyamoto, S., & Kollman, P. A. (1992). Settle: An analytical version of the SHAKE and RATTLE algorithm for rigid water models. *Journal of Computational Chemistry*, *13*(8), 952–962.

Morris, G. M., Goodsell, D. S., Halliday, R. S., Huey, R., Hart, W. E., Belew, R. K., & Olson, A. J. (1998). Automated docking using a Lamarckian genetic algorithm and an empirical binding free energy function. *Journal of Computational Chemistry*, *19*(14), 1639–1662.

Mortelmans, K., & Zeiger, E. (2000). The Ames Salmonella/microsome mutagenicity assay. *Mutation Research*, *455*(1–2), 29–60.

Muegge, I., Heald, S. L., & Brittelli, D. (2001). Simple selection criteria for drug-like chemical matter. *Journal of Medicinal Chemistry*, *44*(12), 1841–1846. https://doi.org/10.1021/jm015507e

Nebert, D. W., & Russell, D. W. (2002). Clinical importance of the cytochromes P450. *The Lancet*, *360*(9340), 1155–1162.

New drug target found for COVID-19. (2020). Argonne National Laboratory [Internet]. Anl.gov. [cited 1 June 2020]. https://www.anl.gov/article/new-drug-target-found-for-covid19

Oprea, T. I., Davis, A. M., Teague, S. J., & Leeson, P. D. (2001). Is there a difference between leads and drugs? A historical perspective. *Journal of Chemical Information & Computer Sciences*, *41*(5), 1308–1315. https://doi.org/10.1021/ci010366a

Proudfoot, A. E. (2002). Chemokine receptors: Multifaceted therapeutic targets. *Nature Reviews. Immunology*, *2*(2), 106–115. https://doi.org/10.1038/nri722

Richman, D. D., Whitley, R. J., & Hayden, F. G. (2016). *Clinical virology*. John Wiley & Sons.

Roberts, A., Vogel, L., Guarner, J., Hayes, N., Murphy, B., Zaki, S., & Subbarao, K. (2005). Severe acute respiratory syndrome coronavirus infection of golden Syrian hamsters. *Journal of Virology*, *79*(1), 503–511. https://doi.org/10.1128/JVI.79.1.503-511.2005

Rowe, T., Gao, G., Hogan, R. J., Crystal, R. G., Voss, T. G., Grant, R. L., Bell, P., Kobinger, G. P., Wivel, N. A., & Wilson, J. M. (2004). Macaque model for severe acute respiratory syndrome. *Journal of Virology*, *78*(20), 11401–11404. https://doi.org/10.1128/JVI.78.20.11401-11404.2004

Sander, T. (2001). OSIRIS property explorer. Organic Chemistry Portal.

Sangwan, R., Chaurasiya, N., Lal, P., Misra, L., Tuli, R., & Sangwan, N. (2008). Withanolide A is inherently *de novo* biosynthesized in roots of the medicinal plant Ashwagandha (*Withania somnifera*). *Physiologia Plantarum*, *133*(2), 278–287. https://doi.org/10.1111/j.1399-3054.2008.01076.x

Teague, S. J., Davis, A. M., Leeson, P. D., & Oprea, T. (1999). The design of leadlike combinatorial libraries. *Angewandte Chemie International Edition*, *38*(24), 3743–3748.

Tian, S., Wang, J., Li, Y., Li, D., Xu, L., & Hou, T. (2015). The application of *in silico* drug-likeness predictions in pharmaceutical research. *Advanced Drug Delivery Reviews*, *86*, 2–10. https://doi.org/10.1016/j.addr.2015.01.009

Tortorici, M. A., & Veesler, D. (2019). Structural insights into coronavirus entry. *Advances in Virus Research*, *105*, 93–116. https://doi.org/10.1016/bs.aivir.2019.08.002

Trott, O., & Olson, A. J. (2010). AutoDock Vina: Improving the speed and accuracy of docking with a new scoring function, efficient optimization, and multithreading. *Journal of Computational Chemistry*, *31*(2), 455–461. https://doi.org/10.1002/jcc.21334

van Breemen, R. B., & Li, Y. (2005). Caco-2 cell permeability assays to measure drug absorption. *Expert Opinion on Drug Metabolism & Toxicology*, *1*(2), 175–185. https://doi.org/10.1517/17425255.1.2.175

Varshney, A., Balkrishna, A., & Singh, J. (2020).Withanone from Withania somnifera may inhibit novel coronavirus (COVID-19) entry by disrupting interactions between viral s-protein receptor binding domain and host ACE2 receptor. *Virology*. https://doi.org/10.21203/rs.3.rs-17806/v1

Veber, D. F., Johnson, S. R., Cheng, H. Y., Smith, B. R., Ward, K. W., & Kopple, K. D. (2002). Molecular properties that influence the oral bioavailability of drug candidates. *Journal of Medicinal Chemistry*, *45*(12), 2615–2623. https://doi.org/10.1021/jm020017n

Viswanadhan, V. N., Denckla, B., & Weinstein, J. N. (1991). New joint prediction algorithm (Q7-JASEP) improves the prediction of protein secondary structure. Biochemistry, *30*(46), 11164–11172. https://doi.org/10.1021/bi00110a021

Viswanadhan, V. N., Ghose, A. K., & Weinstein, J. N. (1990). Mapping the binding site of the nucleoside transporter protein: A 3D-QSAR study. *Biochimica et Biophysica Acta (BBA)-Protein Structure & Molecular Enzymology*, *1039*(3), 356–366.

Wang, Z., Chen, X., Lu, Y., Chen, F., & Zhang, W. (2020). Clinical characteristics and therapeutic procedure for four cases with 2019 novel coronavirus pneumonia receiving combined Chinese and Western medicine treatment. *BioScience Trends*, *14*(1), 64–68.

Wirth, M., & Sauer, W. H. (2011). Bioactive molecules: perfectly shaped for their target? *Molecular Informatics*, *30*(8), 677–688. https://doi.org/10.1002/minf.201100034

Worldometer. (2020). https://www.worldometers.info/coronavirus/.

Wu, C., Liu, Y., Yang, Y., Zhang, P., Zhong, W., Wang, Y., Wang, Q., Xu, Y., Li, M., Li, X., & Zheng, M. (2020). Analysis of therapeutic targets for SARS-CoV-2 and discovery of potential drugs by computational methods. *Acta* Pharm Sin B. 10(5), 766-788.

Xu, C., Cheng, F., Chen, L., Du, Z., Li, W., Liu, G., Lee, P. W., & Tang, Y. (2012). *In silico* prediction of chemical Ames mutagenicity. *Journal of Chemical Information & Modeling*, *52*(11), 2840–2847. https://doi.org/10.1021/ci300400a

Yang, J. M., & Chen, C. C. (2004). GEMDOCK: A generic evolutionary method for molecular docking. Proteins, *55*(2), 288–304. https://doi.org/10.1002/prot.20035

Yang, J. F., Wang, F., Chen, Y. Z., Hao, G. F., & Yang, G. F. (2019). LARMD: Integration of bioinformatic resources to profile ligand-driven protein dynamics with a case on the activation of estrogen receptor. *Briefings in Bioinformatics*. bbz141. https://doi.org/10.1093/bib/bbz141

Zaretzki, J., Bergeron, C., Huang, T. W., Rydberg, P., Swamidass, S. J., & Breneman, C. M. (2013). RS-WebPredictor: A server for predicting CYP-mediated sites of metabolism on drug-like molecules. *Bioinformatics (Oxford, England))*, *29*(4), 497–498. https://doi.org/10.1093/bioinformatics/bts705

Zhang, L., Lin, D., Sun, X., Curth, U., Drosten, C., Sauerhering, L., Becker, S., Rox, K., & Hilgenfeld, R. (2020). Crystal structure of SARS-CoV-2 main protease provides a basis for design of improved α-ketoamide inhibitors. *Science*, *368*(6489), 409–412.

Zhou, P., Yang, X.-L., Wang, X.-G., Hu, B., Zhang, L., Zhang, W., Si, H.-R., Zhu, Y., Li, B., Huang, C.-L., Chen, H.-D., Chen, J., Luo, Y., Guo, H., Jiang, R.-D., Liu, M.-Q., Chen, Y., Shen, X.-R., Wang, X., … Shi, Z.-L. (2020). A pneumonia outbreak associated with a new coronavirus of probable bat origin. Nature, *579*(7798), 270–273. https://doi.org/10.1038/s41586-020-2012-7

Ziebuhr, J., Snijder, E. J., & Gorbalenya, A. E. (2000). Virus-encoded proteinases and proteolytic processing in the Nidovirales. *The Journal of General Virology*, *81*(Pt 4), 853–879. https://doi.org/10.1099/0022-1317-81-4-853

Zumla, A., Chan, J., Azhar, E., Hui, D., & Yuen, K. (2016). Coronaviruses – drug discovery and therapeutic options. *Nature Reviews: Drug Discovery*, *15*(5), 327–347. https://doi.org/10.1038/nrd.2015.37